

Electronic Thesis and Dissertation Repository

1-9-2015 12:00 AM

A Self-Potential for Monitoring Self-Sustaining Treatment for Active Remediation (STAR)

Mehrnoosh Ebrahimzadeh, *The University of Western Ontario*

Supervisor: Dr Jason Gerhard, *The University of Western Ontario*

A thesis submitted in partial fulfillment of the requirements for the Master of Engineering Science degree in Civil and Environmental Engineering

© Mehrnoosh Ebrahimzadeh 2015

Follow this and additional works at: <https://ir.lib.uwo.ca/etd>



Part of the [Environmental Engineering Commons](#)

Recommended Citation

Ebrahimzadeh, Mehrnoosh, "A Self-Potential for Monitoring Self-Sustaining Treatment for Active Remediation (STAR)" (2015). *Electronic Thesis and Dissertation Repository*. 2643.
<https://ir.lib.uwo.ca/etd/2643>

This Dissertation/Thesis is brought to you for free and open access by Scholarship@Western. It has been accepted for inclusion in Electronic Thesis and Dissertation Repository by an authorized administrator of Scholarship@Western. For more information, please contact wlsadmin@uwo.ca.

A SELF-POTENTIAL FOR MONITORING SELF-SUSTAINING TREATMENT
FOR ACTIVE REMEDIATION (STAR)
(Thesis format: Integrated Article)

by

Mehrnoosh Ebrahimzadeh

Graduate Program in Engineering Science

Department of Civil and Environmental Engineering

A thesis submitted in partial fulfillment
of the requirements for the degree of
Master of Engineering Science

The School of Graduate and Postdoctoral Studies
The University of Western Ontario
London, Ontario, Canada
January, 2015

© Mehrnoosh Ebrahimzadeh 2015

Abstract

Self-sustaining Treatment for Active Remediation (STAR) is a novel soil remediation approach for Non-Aqueous Phase liquids (NAPLs) embedded in a porous medium. STAR is based on liquid smoldering combustion which destroys NAPLs while simultaneously generating heat due to the exothermic oxidation reaction. The technique is currently in use in several field pilot tests and a full-scale site remediation. Propagation of the smoldering front is monitored in the field by temperature data obtained from a thermocouple network, with limited resolution. Geophysical techniques, such as Self-Potential (SP), have potential as a non-destructive means for monitoring remediation processes. The SP method measures natural currents flowing in the ground generated by thermoelectric or electrokinetic processes. The objective of this work is to evaluate the potential of the SP technique for monitoring STAR.

First, a series of sandbox experiments were conducted to investigate the magnitude of thermoelectric coupling coefficient for different sand sizes, water content and non- star heat sources. Results showed that a negative voltage anomaly is expected at the surface in the presence of a subsurface heat source and the magnitude of the anomaly is sensitive to water content and grain size. Next, SP measurements were conducted during several laboratory STAR tests examining the response as a function of both space and time. A significant SP anomaly was observed during the smoldering period. Moreover, the magnitude of the SP anomaly measured on the surface was demonstrated to be a function of the separation distance between the reaction front and the SP electrode position. R-squared for a linear regression of measured SP and the distance was 0.83, indicating that the majority of voltage anomaly had contribution to distance of the electrode to the smoldering front. Overall, this research demonstrated that the SP technique has significant potential as a non-invasive monitoring tool for STAR.

Keywords

site remediation, smoldering, STAR, non-aqueous phase liquids, monitoring, geophysics, self-potential.

Co-Authorship Statement

This thesis was written in accordance with regulations and guidelines for integrated-article format by the Faculty of Graduate and Postdoctoral Studies at the University of Western Ontario. All the experiments and relevant data was collected, analyzed and interpreted by the candidate under the supervision and guidance of Dr. Jason I. Gerhard.

Chapter 3 was drafted for future submission to a peer-reviewed journal. The proposed title is: Self-Potential for Monitoring Self-sustaining Treatment for Active Remediation (STAR)

by Mehrnoosh Ebrahimzadeh, Jason I. Gerhard, and Panagiotis Tsourlos

Contributions:

Mehrnoosh Ebrahimzadeh: designed and performed all the experiments, analysis and interpretation of experimental results and wrote draft of the chapter.

Jason I. Gerhard: initiated the research topic, assisted design of laboratory experiments, supervised experiments, assisted in data interpretation, reviewed/revised the draft chapter, and provided all funding for the equipment and lead author.

Panagiotis Tsourlos: initiated the research topic, assisted in data interpretation, and reviewed/revised the draft chapter.

Acknowledgments

I would like to express my deepest gratitude to my supervisor Dr. Jason Gerhard for his tremendous guidance, enthusiasm and continuous support. The completion of this dissertation would not have been possible without his incomparable assistance and invaluable effort.

I gratefully thank Dr. Panagiotis Tsourlos for sharing his extensive knowledge with me throughout this project. I would like to thank STAR group for sharing their laboratory expertise with me. I would also thank all my colleagues in RESTORE group for their support and cooperation. It was a great pleasure for me to work with them.

I am extremely grateful to all my incredible friends, especially Alireza, Hadi, Sahar and Shima for their constant support. I am very lucky to have many people who have always cared about me. I would like to thank my beloved brother and sister, Kianoosh and Nooshin, I am really happy to have them in my life. Finally, I would like to thank my lovely parents, Marzieh and Feridoun for their continuous love, encouragement and support as everything I have accomplished would not have been possible without them.

Table of Contents

Abstract	ii
Co-Authorship Statement.....	iii
Acknowledgments.....	iv
Table of Contents	v
List of Tables	vii
List of Figures	viii
List of Appendices	xii
List of Abbreviations, Symbols, Nomenclature.....	xiii
Chapter 1	1
1 Introduction	1
1.1 Problem Overview	1
1.2 Research Objectives.....	3
1.3 Thesis Outline	3
1.4 References.....	4
Chapter 2.....	6
2 Literature Review.....	6
2.1 Introduction.....	6
2.2 Available Remediation Techniques for NAPLs	7
2.3 Smoldering Combustion for NAPL Remediation.....	9
2.4 Self-potential Technique.....	14
2.4.1 Origin of the Self-potential	18
2.4.2 Self-Potential Anomalies on Volcanoes and Geothermal Regions.....	32
2.5 Summary and Gaps	34

2.6 References.....	35
Chapter 3.....	45
3 Self-Potential Technique for Monitoring Self-sustaining Treatment for Active Remediation (STAR)	45
3.1 Introduction.....	45
3.2 Materials and Methodology	49
3.3 Results and Discussion	57
3.3.1 Thermoelectric Coupling Coefficient Measurements.....	57
3.3.2 Self-potential Anomaly Associated with Smoldering.....	61
3.4 Summary and Conclusions	72
3.5 References.....	74
Chapter 4.....	77
4 Summary and Recommendations.....	77
4.1 Summary and Conclusions	77
4.2 Recommendations for Future Work.....	78
Appendices.....	80
Appendix A. Background Self-potential Measurement Methodology	80
Appendix B. Experimental Setup: Parameter Selection	82
Appendix C. Experimental Setup: Packing Procedure	85
Appendix D. Smoothing of Self-potential Data.....	86
Appendix E. Streaming Potential Associated with Blowing Air in STAR.....	87
Appendix F. Temperature Profiles.....	89
Appendix G. Self–Potential Anomaly Associated with Heating	94
Appendix H. Self–potential Anomaly Associated with Smoldering Using Convective Heater	95
Curriculum Vitae	97

List of Tables

Table 2.1. Temperature Coefficients of SP Electrodes (Petiau & Dupis 1980).	16
Table 2.2. Coupled Forces and Fluxes (Minsley 2007)	19
Table 3.1. Reported C_{TE} in The Literature.....	48
Table 3.2. Physical Properties of Canola Oil.....	49
Table 3.3. Experiments for Measuring Thermoelectric Coupling Coefficient.	50
Table 3.4. Performed Experiments for Monitoring STAR by Self-Potential Technique. 55	

List of Figures

Figure 2.1. Cross section of experimental setup for small scale proof of concept experiment to assess potential of combustion as NAPL remediation technique (Pironi et al., 2009).	11
Figure 2.2. (a) Average smolder velocity as function of the inlet air flux. (b) Observed peak temperature along the sample for different air flux (Pironi et al., 2009).	12
Figure 2.3. Temperature history data from the base case experiment conducted by Switzer et al. (2009).	14
Figure 2.4. Sketch of non-polarizing Ag/ AgCl electrode (Minsley 2007).	16
Figure 2.5. Sketch of silica surface in pH condition of 3-8, surface group is mostly consisting of siloxane, silanol and silicic acid group. E.D.L denotes the electrical diffuse layer (Kim & Lawler 2005).	20
Figure 2.6. Zeta potential as function of temperature and salinity (Revil et al., 1999). ...	21
Figure 2.7. Streaming potential coupling coefficient vs. water saturation (Revil et al., 2007).	23
Figure 2.8. Experimental sketch for measuring thermoelectric coupling coefficient in a rock sample (Yamashita 1961).	25
Figure 2.9. Thermoelectric self-potential generated by spherical body of elevated temperature (Nourbehecht 1959; Corwin & Hoover 1979).	25
Figure 2.11. Measured thermoelectric coefficients vs salinity (Leinov et al., 2010).	29
Figure 2.12. Self-potential generating mechanism over an ore body (Sato & Mooney 1960).	31
Figure 2.13. Comparison between self-potential measurements at the surface and PCE concentration in the wells in Savannah River site (Minsley et al., 2007).	32

Figure 2.14. Positive self-potential generating mechanism above the lava flows (Barde-Cabusson et al., 2009).....	34
Figure 3.1. Experimental setup for measuring thermoelectric coupling coefficient in Heating1 – Heating4. (a) Apparatus plan view showing the position of reference electrode and SP measuring stations (E1-E9) and sand surface temperature measuring stations (TS1-TS9) (b) Apparatus cross-section showing the position of the heat source and depth temperature measuring stations (T1-T9).....	53
Figure 3.2. Geometry of the sandbox. Sand box is filled with fine silica sand and deionized water (30% water content). Non-polarizing Cu/CuSO ₄ electrodes are located at the surface of the sand for voltage measurements. A cylinder of contaminated sand (coarse sand- canola oil) is located in the middle of the fine sand.	54
Figure 3.3. Plan view of experimental setup for Smoldering1 – Smoldering5.....	55
Figure 3.4. SP data sample which shows the fluctuating around an average value for background voltage.....	57
Figure 3.5. (a) Distribution of temperature at depth of 20 cm (b) SP at top of the tank after introducing the heat source (t=15 min).....	59
Figure 3.6. (a) SP distribution at top of the tank after introducing the heat source at time 15 and 22 minutes in Heating1. (b) Thermoelectric coupling coefficient calculation using SP measurements exactly above the heat source.	60
Figure 3.7. Measured C_{TE} for different sand sizes, water contents and heat sources.....	61
Figure 3.8. Temperature time histories for thermocouples in center of oil/sand cylinder for Smoldering1.	63
Figure 3.9. (a) A snapshot of the measured voltage difference in the smoldering period at the surface in Smoldering1. Two moving electrodes moved along profiles and collect data during the smoldering period. (b) Temperature distribution at the surface during the smoldering period. (c) A snapshot of the voltage difference in the smoldering period at	

the surface corrected for the temperature effect. SP measuring stations are shown by dots.	65
Figure 3.10. Measured SP anomaly over time during STAR test for Smoldering2 and Smoldering3 (not corrected for the temperature effect). Measuring electrode distance from the center of the smoldering region was 9 cm in the plan view. Phase II, III and IV are corresponded to the heating, smoldering and recovery periods respectively.	67
Figure 3.11. Measured SP over time for 5 different distances from the contaminated region being smouldered, compiled from 3 different experiments with otherwise similar conditions (not corrected for the temperature effect).	68
Figure 3.12. Measured temperature over time for 5 measuring SP stations in Smoldering2 – Smoldering5.	69
Figure 3.13. Measured SP over time corrected for temperature effect for 5 different distances from the contaminated region being smoldered, compiled from 3 different experiments with otherwise similar conditions.	69
Figure 3.14. Voltage difference over front-electrode separation distance (cm) for Smoldering4 (E1 and E2) and Smoldering5 (E1 and E2).	71
Figure 3.15. Voltage difference corrected for temperature effect over front-electrode separation distance (cm) for Smoldering4 (E1 and E2) and Smoldering5 (E1 and E2). ..	72
Figure A.1. Voltage measurement using moving electrode.	80
Figure A.2. Background voltage measurements for three experiments.	81
Figure B.1. Effect of water content in smoldering propagation, 15% water content.	83
Figure B.2. Effect of water content in smoldering propagation, 30% water content.	84
Figure C.1. (a) Clay trays for protecting the sand box from high smoldering temperature. (b) Position of the heater and air diffuser in the fine sand. (c) Coarse sand/canola oil cylinder emplaced in fine sand. (d) Non-polarizing electrode placed at the surface of the	

sand. (e) The pathway of coarse sand along the wall of the box. (f) Cleaned coarse sand after smoldering.	85
Figure D.1. Raw and smoothed SP data over time.	86
Figure E.1. (a) Electrode position in plan view. (b) Voltage differences against time associated with blowing air; experimental setup is exactly identical to STAR test.	88
Figure F.1. SP data (not corrected for the temperature effect) over time vs temperature histories for TC1-TC15 in Smoldering2; Electrode position is corresponded to 9 cm distance from center of oil/sand cylinder in plan view.	89
Figure F.2. SP data (not corrected for the temperature effect) over time vs temperature histories for TC1-TC15 in Smoldering3; Electrode position is corresponded to 9 cm distance from center of oil/sand cylinder in plan view.	90
Figure F.3. SP data (not corrected for the temperature effect) over time for E1 and E2 vs temperature histories for TC1-TC15 in Smoldering4; E1 is corresponded to 12 cm and E2 to 16 cm distance from center of oil/sand cylinder in plan view.	91
Figure F.4. SP data (not corrected for the temperature effect) over time for E1 and E2 vs temperature histories for TC1-TC15 in Smoldering5; E1 is corresponded to 23 cm and E2 to 25 cm distance from center of oil/sand cylinder in plan view.	92
Figure F.5. Surface temperature and corrected SP data for temperature effect over time for smoldering3.	93
Figure G.1. SP data over time associated with heating for E1, E2 and E3 vs. temperature of the heat source over time.	94
Figure H.1. SP data over time vs temperature histories over time for TC1-TC6.	95
Figure H.2. SP over time vs. SP corrected for temperature effect over time.	96

List of Appendices

Appendix A. Background Self-potential Measurement Methodology	80
Appendix B. Experimental Setup: Parameter Selection	82
Appendix C. Experimental Setup: Packing Procedure	85
Appendix D. Smoothing of Self-potential Data.....	86
Appendix E. Streaming Potential Associated with Blowing Air in STAR.....	87
Appendix F. Temperature Profiles.....	89
Appendix G. Self-Potential Anomaly Associated with Heating	94
Appendix H. Self-potential Anomaly Associated with Smoldering Using Convective Heater	95

List of Abbreviations, Symbols, Nomenclature

Abbreviations

DCA	Dichloroethane
DCE	Dichloroethylene
DNAPLs	Denser than water Non-aqueous phase Liquids
ERH	Electrical resistance heating
ISC	In-situ combustion
LNAPLs	Lighter than water Non-aqueous phase Liquids
NAPLs	Non-Aqueous Phase Liquids
PCB	polychlorinated biphenyl
REV	Representative elementary volume
SP	Self-Potential
STAR	Self-sustaining Treatment for Active Remediation
SVE	Soil Vapor Extraction
TCE	Trichloroethene
TCH	Thermal Conductive Heating Technique

Symbols

C	Concentration (mol.m^{-3})
C_k	Electrokinetic coupling coefficient (mV/Pa)
C_{TE}	Thermoelectric coupling coefficient ($\text{mV}/^\circ\text{C}$)
e	Elementary charge (C)
E	Electrical field (V.m^{-1})
F	Faraday's constant ($96,500 \text{ C.mol}^{-1}$)
I	Electric current density (A.m^{-2})
j	Current density (A.m^{-2})
j_c	Streaming current (A.m^{-2})
j_d	Diffusion current (A.m^{-2})

J_E	fluid volume flux ($m^3/(m^2 \cdot s)$)
J_s	Source current density ($A \cdot m^{-2}$)
j_t	Current due to temperature gradient ($A \cdot m^{-2}$)
k	Permeability (m^2 or Darcy)
L_T	Phenomenological cross coupling coefficient
$P_n(x)$	Legendre polynomials
Q_{\pm}	Heat flux (W/m^2)
Q_H	Heat source ($W \cdot m^{-3}$)
R	Gas constant ($8.314 J \cdot mol^{-1} \cdot K^{-1}$)
T	Temperature ($^{\circ}C$ or K)
$T_{(+)}$	Macroscopic Hittorf transport number
u	Ionic mobility ($m^2 \cdot V^{-1} \cdot s^{-1}$)
z	Ionic charge (C)
∇P	Pore pressure gradient (Pa)
$\nabla \tilde{\mu}_{(\pm)}^f$	Ionic electrochemical potential gradient in the electrolyte (J/mol)
ξ	Zeta potential (V)
η	Pore fluid viscosity (m^2/s)
κ	Thermal conductivity ($W/(m \cdot K)$)
π	Peltier coefficients ($\mu V/K$)
σ	Electric conductivity (S/m)
ϕ	Porosity (dimensionless)
ψ	Electrical potential (V)

Chapter 1

1 Introduction

1.1 Problem Overview

Non-Aqueous Phase Liquids (NAPLs) are one of the most problematic subsurface contaminants. They have been used widely in manufacturing industries for several decades and many sites have been contaminated due to accidental release or improper disposal (Kavanaugh et al., 2003). NAPLs are either lighter than water (LNAPLs) including gasoline, jet fuel, fuel oil and diesel or denser than water (DNAPLs) including creosote, crude oil, coal tar, polychlorinated biphenyl (PCB) oils and chlorinated solvents. A DNAPL's behavior in the subsurface (e.g., degree of lateral spreading and infiltration rates) is controlled by the physical properties of contaminant and the porous medium (Kueper & Gerhard 1995). Typically a DNAPL source zone can exhibit a complex distribution of residual (trapped DNAPL blobs) or pools (potentially mobile higher saturation regions) (Gerhard et al., 2007). NAPLs can act as long-term sources of groundwater and soil contamination due to their physical and chemical properties. Due to low absolute solubilities, they dissolve very slowly; however, these solubilities are high relative to drinking water criteria (Pankow & Cherry 1996). Thus, even a small amount of NAPL can result in groundwater that is considered highly contaminated. In Canada, there are 20,000-30,000 contaminated sites where soil, groundwater or surface water shows contaminant concentrations exceeding the environmental criteria (Sousa 2001).

Sites contaminated by complex, long-chain NAPLs such as heavy oils, coal tar and PCB oils cannot be remediated easily because most of these compounds are resistant to degradation by currently available physical, biological and chemical remediation approaches. Site excavation and disposal to hazardous waste landfills, one of the few available remediation techniques for these NAPLs, is significantly expensive (Switzer et al., 2009).

To address this problem, Pironi et al. (2009) and Switzer et al. (2009) introduced a novel remediation technique based on smoldering combustion of a liquid hydrocarbon

embedded in a porous medium. Most of the NAPLs are combustible and generate considerable amounts of heat during the combustion process (Pironi et al., 2011). Combustion of NAPLs is an exothermic oxidation reaction which generates carbon-dioxide, water and heat. When oxygen is available, complete destruction of the contaminant (i.e., fuel) can be achieved (Ohlemiller 2002). A beneficial feature of the process is its self-sustainability, which means external energy input is not required to progress the reaction after ignition (Switzer et al., 2009). Smoldering combustion has demonstrated its high potential as a NAPL remediation technique in proof-of-concept laboratory experiments conducted by Switzer et al. (2009) across a range of experimental conditions.

The remediation technique has been commercialized as Self-sustaining Treatment for Active Remediation (STAR; www.savronsolutions.com).

Numerous STAR field pilot tests have been completed and the first full scale field application is underway at a coal tar site in the United States. Progress of the smoldering combustion process in the field is primarily monitored by networks of thermocouples that monitor temperature propagation. These provide relatively sparse data that requires interpolation to infer the overall evolution of the remediation process (Scholes 2013). It is possible that non-intrusive, geophysical techniques could be utilized for monitoring STAR in an economic manner.

The self-potential (SP) technique is a passive geophysical method that is based on measuring the spontaneous voltage differences in the ground generated by electrokinetic, thermoelectric or electrochemical effects (Nourbehecht 1959; Reynolds 1997). SP anomalies, associated with elevated temperature and hydrothermal fluid movement pathways, have been used to map geothermal and volcanic sources (Corwin & Hoover 1979a; Zlotnicki & Nishida 2003). Dorfman et al. (1977) utilized the SP method for tracking the position of the heat front during an oil recovery flood in an oil reservoir. Recently, the SP method has been used as part of a strategy to locate the position of the burning front in a coal seam fire between 10 and 15 m below the surface (Karaoulis et al., 2014; Revil et al., 2013). It is clear that the SP method has the potential for mapping

processes associated with heat sources in the subsurface; however, there are few available studies on thermoelectric effects in porous media or the use of SP in near surface, environmental applications.

1.2 Research Objectives

The overall goal of this research is to explore the potential of SP as a non-invasive tool for monitoring smoldering combustion for NAPL remediation. The main objective of this research is to evaluate, for the first time, if an SP anomaly is produced by a smoldering combustion front. If so, then it is important to understand the nature of the generated voltage associated with STAR. All experiments were performed in the laboratory at the bench scale. A first series of experiments was performed to explore the magnitude and polarity of the SP anomaly in the presence of a heat source in a porous medium over a range of experimental conditions (various heat sources, water contents and sand types). A second series of experiments was conducted to evaluate the process under STAR conditions, including air injection and smoldering front propagation. Overall, this study represents the first proof-of-concept for SP tracking of STAR remediation.

1.3 Thesis Outline

This thesis is written in “Integrated Article Format”. The following is a brief description for each chapter:

- Chapter 2 summarizes the relevant literature, including NAPL thermal remediation techniques, STAR, and the SP technique and its application.
- Chapter 3 presents multiple experiments conducted to measure SP data for smoldering combustion. This chapter is written as manuscript that is expected to be submitted to a refereed journal.
- Chapter 4 summarizes the conclusions of this research and presents recommendations for future work.
- The appendices provide supplemental information regarding experimental design, experimental procedures, and provide all of the experimental data not included in Chapter 3.

1.4 References

- Corwin, R. F., & Hoover, D. B. (1979). The self-potential method in geothermal exploration. *Geophysics*, *44*(2), 226–245.
- Dorfman, N. H., Oskay, M. M., & Gaddis, M. P. (1977). Self-Potential Profiling: A New Technique for Determination of Heat Movement in a Thermal Oil Recovery Flood. *Presented at the SPE Annual Fall Technical Conference and Exhibition: American Institute of Mining, Metallurgical, and Petroleum Engineers*. Denver.
- Gerhard, J. I., Pang, T., & Kueper, B. H. (2007). Time scales of DNAPL migration in sandy aquifers examined via numerical simulation. *Ground Water*, *45*(2), 147–57.
- Karaoulis, M., Revil, A., & Mao, D. (2014). Localization of a coal seam fire using combined self-potential and resistivity data. *International Journal of Coal Geology*, *128-129*, 109–118.
- Kueper, B. H., & Gerhard, J. I. (1995). Variability of point source infiltration rates for two-phase flow in heterogeneous porous media. *Water Resources Research*, *31*, 2971–2980.
- Nourbehecht, B. (1959). *Irreversible thermodynamic effects in inhomogeneous media and their applications in certain geoelectric problems*. Massachusetts Institute of Technology.
- Ohlemiller, T. J. (2002). Chapter 9: Smoldering Combustion. In *SFPE Handbook of Fire Protection Engineering* (pp. 200–210).
- Pankow, J. F., & Cherry, J. A. (1996). *Dense chlorinated solvents and other DNAPLs ground water*. Portland (Oregon): Waterloo Press.
- Pironi, P., Switzer, C., Gerhard, J. I., Rein, G., & Torero, J. L. (2011). Self-sustaining smoldering combustion for NAPL remediation: laboratory evaluation of process sensitivity to key parameters. *Environmental Science & Technology*, *45*(7), 2980–2986.
- Pironi, P., Switzer, C., Rein, G., Fuentes, A., Gerhard, J. I., & Torero, J. L. (2009). Small-scale forward smoldering experiments for remediation of coal tar in inert media. *Proceedings of the Combustion Institute*, *32*(2), 1957–1964.
- Revil, A., Karaoulis, M., Srivastava, S., & Byrdina, S. (2013). Case History Thermoelectric self-potential and resistivity data localize the burning front of underground coal fires. *Geophysics*, *78*(5), 259–273.
- Reynolds, J. M. (1997). *An introduction to Applied and Environmental Geophysics* (pp. 191–521). John Wiley & Sons Ltd.

- Scholes, G. C. (2013). *Ignition method development and first field demonstration of In Situ smouldering remediation*. University of Western Ontario.
- Sousa, C. D. (2001). Contaminated sites: The Canadian situation in an international context. *Journal of Environmental Management*, 62(2), 131–154.
- Switzer, C., Pironi, P., Gerhard, J. I., Rein, G., & Torero, J. L. (2009). Self-Sustaining Smoldering Combustion: A Novel Remediation Process for Non-Aqueous-Phase Liquids in Porous Media. *Environmental Science & Technology*, 43(15), 5871–5877.
- Zlotnicki, J., & Nishida, Y. (2003). Review on morphological insights of self-potential anomalies on volcanoes. *Surveys in Geophysics*, 24, 291–338.

Chapter 2

2 Literature Review

2.1 Introduction

Non-aqueous phase liquids (NAPLs) are organic compounds and one of the most common sources of contamination throughout the industrialized world. Long-term exposure to them may cause serious human health problems and pose risks to the environment. NAPLs are divided into two categories: LNAPLs, which are lighter than water (e.g., diesel, jet oil, fuel oil and gasoline), and DNAPLs, which are denser than water (e.g., crude oil, creosote, chlorinated solvents, PCB oils and coal tar). DNAPLs can accumulate below the water table and act as a long-term source of groundwater contamination due to their physical properties, which includes low viscosity, low interfacial tension with water and low degradabilities (Pankow & Cherry 1996). In Canada, about 25% of urban areas are contaminated due to industrial activities (Sousa 2001). Current remediation strategies, such as thermal, biological or chemical remediation techniques, are not successful in remediating complex, long-chain NAPLs with low-volatility (e.g., PCB oils, coal tar and heavy petrochemicals) (Switzer et al., 2009). Furthermore, most remediation techniques are significantly expensive, time-consuming or ineffective in resolving NAPL contaminations. Recently, smoldering combustion has been introduced as a promising remediation technique for soils contaminated by NAPLs (Pironi et al., 2009; Switzer et al., 2009). Self-sustaining treatment for active remediation (STAR) is based on smoldering combustion of NAPLs in contaminated porous media that leads to the destruction of NAPLs while simultaneously generating heat.

The self-potential technique (SP) is a passive geophysical method that measures naturally occurring voltage differences in the earth due to thermoelectric or electrokinetic effects (Revil & Jardani 2013). The significant potential of SP technique for tracking the burning front in coal-seam fire has been proved by Revil et al. (2013) and Karaoulis et al. (2014). The SP technique is widely used in delineation heat source characteristics in volcanic and geothermal areas (Corwin & Hoover 1979b; Zlotnicki & Nishida 2003). The position of the burning front has been tracked successfully in coal-seam fires (Revil et al., 2013) and

thermal oil recovery flood using the SP technique (Dorfman et al., 1977). The thermoelectric SP technique measures generated electrical potential due to the presence of a heat source in the ground (Revil 1999). In this chapter, the relevant literature is summarized to provide context for developing an experimental setup for monitoring STAR and tracking the smoldering front using the SP technique.

2.2 Available Remediation Techniques for NAPLs

Varieties of in-situ and ex-situ remediation technologies are available to treat contaminated soil. Remediation techniques consist of chemical, physical, thermal or biological processes that treat soil by degrading, removing or immobilizing the contaminant. Thermal remediation techniques are briefly reviewed here due to their conceptual similarity of some processes with the smoldering techniques for NAPL remediation and also because this research is focused on tracking temperature gradient positions in remediation techniques.

Thermal treatment technologies consist of applying heat to the soil and collecting volatile and semi-volatile contaminants. Vapor and liquid extraction is common in all thermal techniques. The collected gas steam is then treated to satisfy environmental criteria prior to discharge. Thermal treatments can be used for a wide variety of contaminants, such as chlorinated volatile organic compounds, semi-volatile organic compounds, petroleum hydrocarbons, creosote and coal tar. Four common thermal treatment technologies include electrical resistance heating, steam injection and extraction, conductive heating and radio-frequency heating (US EPA 2004). In-situ thermal treatment can be applied in places where excavation is not practical because of the increased risk of contaminant dispersion (Davis 1977). The most important advantage of thermal remediation techniques is that no surfactants and co-solvents are injected into the ground, thus eliminating the contact between contaminants and injected chemicals. Heat effect on chemical and physical properties of contaminants has been studied by Davis (1977). This research demonstrates that an increase in temperature in turn increases vapor pressure, solubility and decreases viscosity and absorption of organic contaminants. The co-boiling temperature of NAPLs and water is less than the boiling point of water; therefore, NAPLs could be removed by increasing temperature to that point (Davis 1977).

Electrical resistance heating (ERH) generates heat in the ground by applying an electric current between triangular electrode arrays (Beyke & Fleming 2005). ERH can be used in any depth as long as there is enough moisture content to conduct an electrical current. In the case of semi-volatile NAPLs and high groundwater flow, liquids could be collected during the treatment (Beyke & Fleming 2002). Contaminants would then be removed by direct volatilization and steam stripping by a soil vapor extraction system (SVE).

Steam injection and extraction rely on the injection of steam and the collection of vaporized contaminants from recovery wells. When injected steam loses heat, it condenses into hot water, which replaces air and water in the porous soil. Eventually the temperature of the soil layer nearest the injection well reaches steam temperature. As a result, a steam front propagates forward from the injection well. Propagation of water due to vapor pressure displaces NAPLs while the high temperature reduces NAPL viscosity. Recovery wells contain the contaminant (US EPA 2004). The downward migration of contaminants could be controlled by injecting steam and air into the injection well (Schmidt et al., 2002; Kaslusky & Udell 2002). The success of the technique depends on the soil permeability, the degree of heterogeneity and contaminant type (Davis 1998). The existence of a low permeable zone, which prevents the movement of steam, could limit the application of the technique. The best design for the injection and extraction well is placing four to six injection wells all around the contaminated area and placing an extraction well in the middle of the zone (Davis 1998).

In a thermal conductive heating technique (TCH), a surface heater blanket or array of heater/vacuum wells is used. This is a suitable technique for unsaturated soils. The most common configuration places six heater wells in a hexagonal network with a heater vacuum well in the center. Volatilized contaminants are then collected in the vacuum well (Baker & Kuhlman 2002). The distance between the wells is determined based on soil type, water content, contamination type, depth of the contaminated zone, required temperature and timescale for remediation procedure (US EPA 2004). Temperature increases around the heating zone creating a cylinder column of dry zone. Steam is generated at the margin of this zone. The transfer of water into this dry zone leads to the vaporization of water. The method is effective for the remediation of a wide range of

volatile contaminants since oxidation and pyrolysis may occur near the heating elements (Stegemeier & Vinegar 2001).

Radio-frequency heating relies on the presence of dielectric minerals in the ground. Applying a high frequency alternating electric field results in the vibration of polar molecules which generate mechanical heat (US EPA 2004).

2.3 Smoldering Combustion for NAPL Remediation

Smoldering combustion is a self-sustaining, flameless exothermic reaction that occurs due to the oxidation of the fuel surface embedded in a porous medium (Ohlemiller 1985). The most important difference between smoldering combustion and flaming combustion is as follows: in flaming combustion, the oxidation reaction occurs in the gas phase unlike an oxidation reaction in the smoldering combustion which takes place on the solid surface. The smoldering combustion typically has a lower temperature, propagation rate and will release heat during oxidation (Rein 2009).

Effective energy recirculation is one of the most important features of smoldering. Heat produced from the oxidation site is transferred by combustion gases to the reactants and leads to the propagation of the smoldering front (Pironi et al., 2009). In thermal remediation techniques, energy is required for volatilizing. Thus, the thermal degradation of NAPL should be applied continuously as all processes are endothermic; significantly, NAPL combustion only needs a short duration of energy input (Switzer et al., 2009).

Smoldering can occur within a wide range of temperatures. The use of a solid matrix as fuel or a mixture of fuel and a solid porous medium could improve the reaction because of its large surface area, which decreases heat loss and facilitates the transport of oxygen to the reaction zone. A successful smoldering reaction relies on the availability of oxygen and the rate of heat loss during the reaction (Ohlemiller 1985; Torero & Fernandez-Pello 1996).

Smoldering propagation could occur in either a forward or opposed mode, defined based on the oxidizer flux direction in comparison to the smoldering direction (Ohlemiller 2002). The forward mode is more energy efficient because released oxidation energy is

used to preheat the remaining fuel embedded in the porous media (Pironi et al., 2011). Two reactions of pyrolysis and oxidation in the forward smoldering experiments conducted on cellulose samples (Ohlemiller & Lucca 1983) and polyurethane foam (Torero & Fernandez-Pello 1996) were observed. In the endothermic pyrolysis reaction, char is produced and then consumed, which causes energy to be released in followed exothermic oxidation reaction.

Smoldering combustion in solid fuels has been reviewed comprehensively in material synthesis studies (Merzhanov & Khaikin 1988) and in fire safety research (Ohlemiller 1985; Torero & Fernandez-Pello 1996; Bar-Ilan et al., 2005). However, there is limited data on the smoldering combustion of a liquid fuel. An example of combustion of a liquid fuel is in-situ combustion (ISC), which is a thermal approach to improve oil recovery in petroleum reservoirs (Greaves et al., 2000; Akkutlu & Yortsos 2003). Another example of liquid fuel combustion is lagging fires in fire safety engineering which initiates fire in porous mediums saturated with oils (Drysdale 2008).

Smoldering for NAPL remediation is a novel approach and only a few studies have, so far, been published on the subject (Pironi et al., 2009; Switzer et al., 2009; Pironi et al., 2011; MacPhee et al., 2012). The potential for combustion for liquid fuels embedded in a porous medium has been explored by Pironi et al. (2009) as a remediation technique. They conducted series of small-scaled proof-of-concept experiments using coal tar. The experimental apparatus for forward smoldering combustion at the beaker scale used by Pironi et al. (2009) is shown in Figure 2.1. The cylinder was 100 mm in diameter, 175 cm in height and contained 60 mm of sand/coal tar mixture. In the base case scenario, the saturation of the coal tar was 25%. The propagation of the smoldering front was monitored using sets of thermocouples and a digital camera. The effect of the oxidant injection rate and fuel content on the smoldering front propagation was explored.

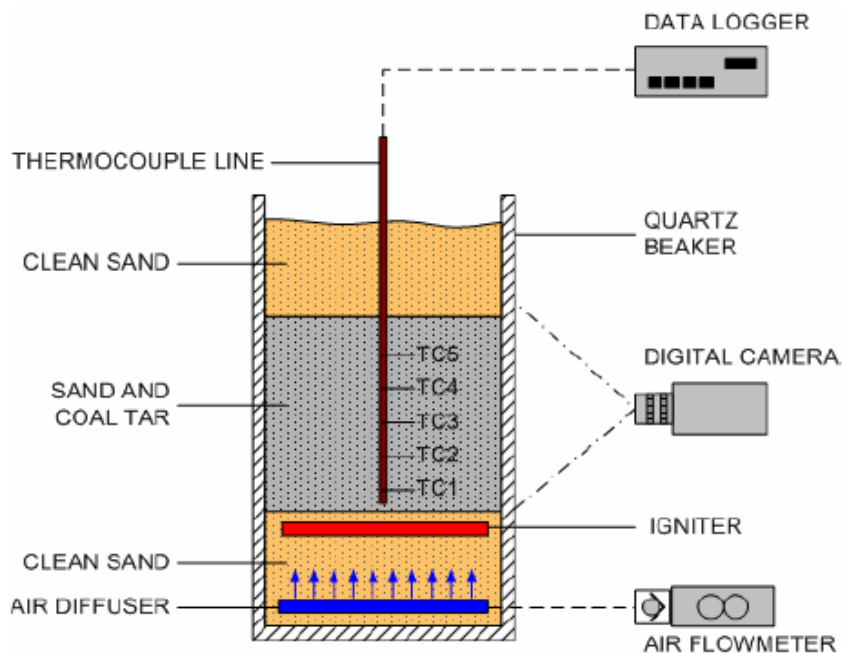


Figure 2.1. Cross section of experimental setup for small scale proof of concept experiment to assess potential of combustion as NAPL remediation technique (Pironi et al., 2009).

Average smoldering velocity as a function of air flux and observed peak temperature for various air fluxes are shown in Figure 2.2. Average smoldering velocity and air flux rate showed a linear relationship due to the oxygen-limited smoldering propagation characteristic. Experimental results showed that a faster propagation is observed in higher air flux velocity, but it is not necessarily accompanied with the highest observed peak temperature. The results indicate the balance between oxygen consumption and heat transfer in combustion processes (Pironi et al., 2009). Experiments conducted for studying the dependence of smoldering on fuel saturation showed that increases in fuel saturation decrease the average smoldering velocity and also observed peak temperature increases as a function of fuel saturation although the dependence is not linear (Pironi et al., 2009). At high inlet air flux, a cooling effect is observed due to excess air (Pironi et al., 2011).

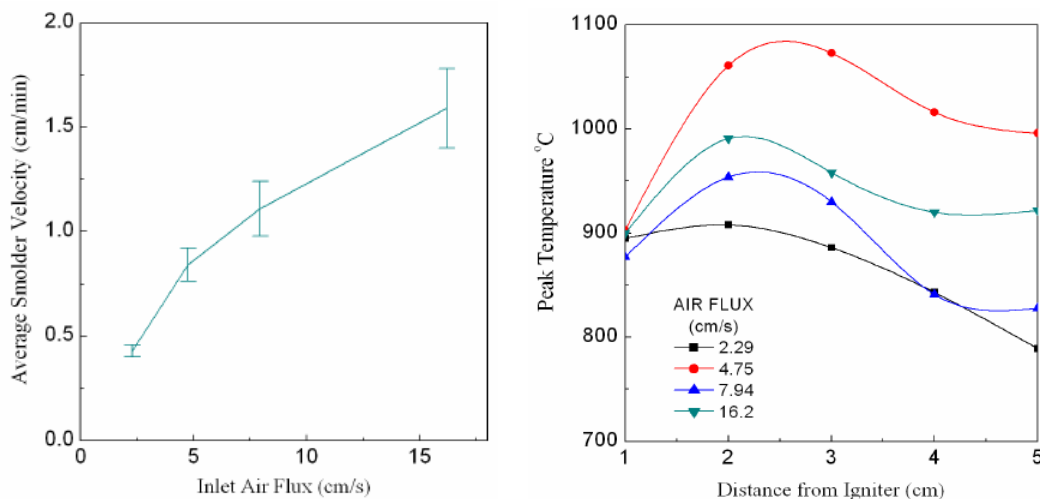


Figure 2.2. (a) Average smolder velocity as function of the inlet air flux (b) Observed peak temperature along the sample for different air flux (Pironi et al., 2009).

A series of bench-scale experiments were conducted to systematically assess the sensitivity of smoldering combustion to NAPL concentration (5%-50% NAPL-occupied porosity), soil type (various mean grain size), water saturation (0, 25, 50, and 75% water-occupied porosity) and air flow rate for crude oil and coal tar by Pironi et al. (2011). Forward smoldering combustion experiments were conducted in a column 138 mm in diameter and 275 mm in height (Pironi et al., 2011). Smoldering temperature depends on soil type, which determines heat capacity, and the thermal conductivity of the porous medium and NAPL concentration. Ignition in the presence of 0-75% water-occupied porosity water content was successful; however, the preheating period increased because of the required time for the evaporation of water. Observed peak temperature decreased as water content increased in the system, but as water content was more than the threshold, the self-sustaining smoldering velocity was not affected (Pironi et al., 2011). Maximum peak temperature and average velocity was observed in coarse and medium sand, and indicated a balance between the expected increases in the smoldering reaction rate due to decreased pore size (Pironi et al., 2011). Also, experimental results showed that smoldering velocity depends on soil grain size, NAPL type and concentration. Self-sustaining smoldering could be achieved even with a low air flow rate. The threshold for air delivery rate depends on soil and NAPL type and the scale of the experiment. Lower

bound for contaminant concentration depends on the energy content of the NAPL. Pironi et al. (2011) demonstrated that the required minimum NAPL content and air delivery rate decreases and operative maximum grain size increases when the scale of the experiment increases because of reduced heat loss effects.

A series of demonstration experiments conducted by Switzer et al. (2009) showed that NAPL smoldering is a successful remediation technique for a range of contaminants, such as mixtures of DCA/grease, TCE/oil, vegetable oil, crude oil and mineral oil. The experimental setting was a quartz glass column 138mm in diameter and 275 mm in height. In the base case experiment, coarse sand was mixed with a 25% concentration of coal tar. The column was packed in a standard sequence. Fifteen type K thermocouples were placed along the column central axis in 1 cm intervals in the coal tar/sand mixture. The sand just above the igniter was preheated to 400 °C and then air was initiated and kept at a certain flux until the end of the experiment. The igniter was terminated when the temperature of the first thermocouple just above the igniter began to decrease. Temperature history of the base case experiment (25% coal tar concentration) is presented in Figure 2.3. Temperature profiles represented a strong, self-sustaining smoldering combustion for the coal tar in the base case experiment conditions. Integrating temperature over time for each thermocouple represents the total energy accumulated in the position of the thermocouple (Switzer et al., 2009).

The potential for employing smoldering combustion as a NAPL remediation technique was demonstrated by Switzer et al. (2009) across a range of soil types, contaminant types and saturations. Salman (2012) explored the feasibility of smoldering combustion for seven different vegetable oil types (e.g., canola oil, peanut oil, olive oil) and 23 different TCE to oil mass ratios samples in terms of the peak temperature, the propagation velocity and the degree of the remediation. This work concluded that robust self-staining smoldering is exhibited in canola oil in various experimental conditions (Salman 2012).

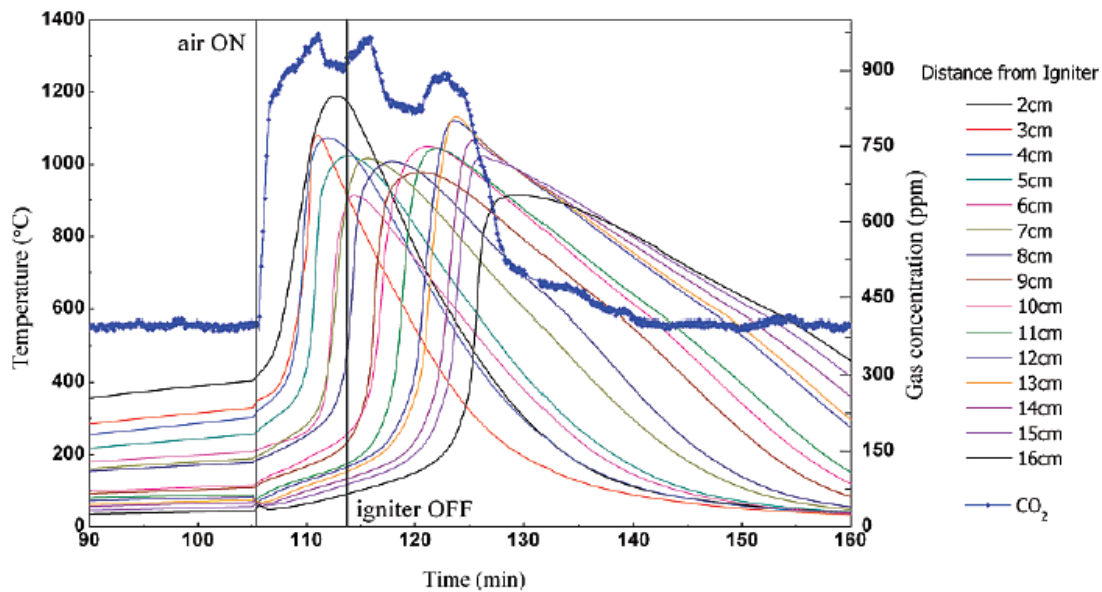


Figure 2.3. Temperature history data from the base case experiment conducted by Switzer et al. (2009).

The potential of smoldering combustion as a remedial action has been examined in the field scale recently by conducting several pilot-scale tests at a site contaminated by coal tar. The tests were conducted in two soil layers; shallow fill (3 m below ground surface) and deep alluvium (8 m below ground surface). Smoldering combustion propagation was monitored using temperature data obtained by a network of thermocouples. Thermocouples installed in different depth and locations via direct push drilling methods. In the deep test thermocouples were installed at radial distances of 0.3, 0.6, 1.5 and 3.7 m (Scholes 2013). In both trials, smoldering reaction was sustained for 10 days, while in the shallow test 99.3% and in deep test 97.3% of coal tar were destroyed (Scholes 2013).

2.4 Self-potential Technique

During the past several decades, interest in geophysical techniques in the environmental application of shallow depth targets has rapidly increased. Recently, self-potential (SP) techniques have been widely used in environmental and engineering applications.

The SP is a passive geophysical method which can be performed at the surface or in the boreholes and is associated with the existence of an in-situ generating source of electrical

currents (Revil et al., 2012). The first SP measurements were performed in 1830 by R.W. Fox, who used copper electrodes to discover underground copper sulphide vein mineralization in Cornwall, England (Reynolds 1997). The first commercial discovery of ore body by SP was done by Norway and Muenster in 1906. Field equipment for performing SP measurements consists of a pair of non-polarizable electrodes, electrical cables and a high sensitivity multichannel voltmeter. Non-polarizing electrodes were developed by M.V Matteucci in 1865, vastly improving the accuracy of geophysical measurements. A non-polarizing electrode consists of a metallic electrode that is in contact with a saturated solution of its salt (Ag-AgCl, Cu-CuSO₄ and Pb-PbCl₂). A schematic picture of a porous pot electrode is showed in Figure 2.4. Petiau (2000) performed a detailed study about concentration of salt, the internal pH condition, and salt diffusion rate from porous tip to the ground in terms of non-polarizing electrode stability. All electrodes have a temperature dependence potential due to chemical reactions in the electrolyte. As a result, ambient temperature should be recorded at the surface alongside of SP stations for proper temperature correction of measured self-potential data (Ansuini & Dimond 1994). Petiau & Dupis (1980) compared different type of non-polarizing electrodes in term of temperature correction coefficient, stability over time and noise spectrum. Temperature coefficient of different electrodes is showed in Table 2.1. Degradation and drift of electrodes in long term monitoring purposes have been studied by Perrier & Pant (2005), enabling them to develop a comprehensive set of guidelines.

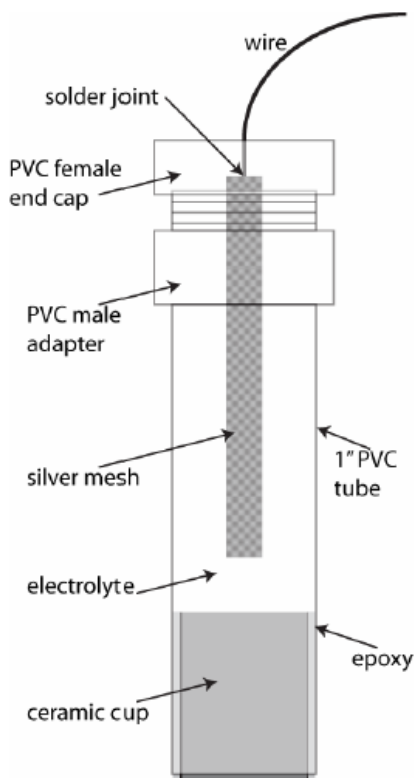


Figure 2.4. Sketch of non-polarizing Ag/ AgCl electrode (Minsley 2007).

Table 2.1. Temperature Coefficients of SP Electrodes (Petiau & Dupis 1980).

Electrode type	Temperature Coefficient ($\mu\text{V}/^\circ\text{C}$)
Ag-AgCl	-410
Hg-Hg ₂ Cl ₂	-660
Cu-CuSO ₄	-360
Pb-PbCl ₂	-40
Cd-CdCl ₂	+460

Two electrode configurations can be used for measurements: dipole and fixed-based configuration. In dipole configuration, two electrodes and a voltmeter are moved along measuring profiles. In the fixed-based configuration, a measuring electrode is moved along the measuring profile while a fixed electrode is used as a reference to reduce the

level of cumulative error in data (Sharma 1997). The reference electrode should be located further than the radius of influence of the causative source (Revil & Jardani 2013). For monitoring purposes, changes of SP is measured in a network of electrodes at the surface (Revil & Jardani 2013).

SP data obtained in an environmental investigation are sensitive to noise level because of their relatively small amplitude. Common geological noise sources for SP measurements are changes in resistivity, soil type and saturation condition. It is a common practice to measure resistivity in the survey area to detect resistivity lateral changes (Sharma 1997).

SP data are sets of profiles or equipotential contours that could be used to compare with known patterns for characterizing simple sources (Sharma 1997). In early works, SP data has been interpreted using semi-empirical models that analyze measured SP data in terms of thickness of vadose zone (Aubert & Atangana 1996) or piezometric level of aquifer (Fournier 1989). Self-potential source inversion identifies 3D distribution of SP generating source in the ground. In SP inversion, which is a linear problem, source distribution is defined as a discretized model that satisfies both measured SP data and known resistivity distribution of the ground (Patella 1997; Minsley 2007; Dmitriev 2012). SP source inversion is widely used in data analysis in geothermal studies (Fitterman & Corwin 1982; Jardani & Revil 2009), for mineral exploration (Mendonça 2008), contamination detection (Minsley et al., 2007), the interpretation of hydraulic condition (Sheffer 2007) and detecting burning front of a coal seam fire (Revil et al., 2013; Karaoulis et al., 2014).

Different generating mechanisms of the SP anomaly can be used in different applications such as exploring ore bodies, characterizing volcano and geothermal fields, geohazard applications (such as landslide and flank stability, sinkhole and karst detection, delineating leakages in dams and embankments) and water resource applications (such as the reconstruction of piezometric head surface, identifying the flow and thickness of vadose zone and delineating contaminated groundwater flow in a landfill).

2.4.1 Origin of the Self-potential

In the thermodynamics of irreversible process, when more than one flux (q) exist in the system, each flux could be expressed as linearly related combination of all forces (X). Linear system of coupled forces and fluxes (Onsager's reciprocal relations) would be (Nourbehecht 1959):

$$\begin{bmatrix} q_1 \\ q_2 \\ q_3 \\ q_4 \end{bmatrix} = \begin{bmatrix} L_{11} & L_{12} & L_{13} & L_{14} \\ L_{21} & L_{22} & L_{23} & L_{24} \\ L_{31} & L_{32} & L_{33} & L_{34} \\ L_{41} & L_{42} & L_{43} & L_{44} \end{bmatrix} \begin{bmatrix} X_1 \\ X_2 \\ X_3 \\ X_4 \end{bmatrix} \quad 2-1$$

Typical force and flux relations are governed by: Fourier Law (thermal gradient and heat flux), Darcy Law (hydraulic gradient and fluid flow), Fick's Law (chemical gradient and solute flow) and Ohm Law (electric potential gradient and current density). All possible phenomena are summarized in Table 2.2. When more than one flow exists in a system, each flow could be expressed as a combination of all other forces. As a result, current density could be expressed as:

$$j(X) = j_c + j_k + j_d + j_t \quad 2-2$$

In Equation 2-2, j_c , j_k , j_d and j_t represent conduction current, streaming current, diffusion current and current due to temperature gradient respectively (Nourbehecht 1959; Minsley 2007). The self-potential signal could be associated to one of following contributions: streaming current (Abaza et al., 1969; Revil et al., 1999; Revil et al., 2003; Rizzo et al., 2004), diffusion current (Ikard et al., 2012), gradient of the redox potential (Naude t et al., 2004; Risgaard-Petersen et al., 2012) or thermoelectric effect (Marshall & Madden 1959; Corwin & Hoover 1979; Fitterman & Corwin 1982; Revil 1999; Leinov et al., 2010; Revil et al., 2013).

Table 2.2. Coupled Forces and Fluxes (Minsley 2007)

		Forces			
		Electrical gradient	Hydraulic gradient	Chemical gradient	Temperature gradient
Fluxes	Electric	Ohm's Law	Electrokinetic effect	Electro-diffusion	Seebeck effect
	Fluid	Electro-osmosis	Darcy's Law	Chemico-osmosis	Thermo-osmosis
	Solute	Electrophoresis	Ultrafiltration	Fick's Law	Soret effect
	Heat	Peltier effect	Thermal filtration	Dufour effect	Fourier Law

Electrical Double Layer

Electrical double layer is a key concept in describing SP related phenomena. When minerals come into contact with water, they become charged due to chemical reactions occurring between the water and the mineral surface. Mineral surfaces can act as either an acid or a base and, by donating or gaining a proton, become either positively or negatively charged. As a result, a diffuse layer is generated in vicinity of the surface with high concentration of counter-ions and depletion of co-ions. The electrochemical system around the mineral surface is called the electrical double layer (Haartsen et al., 1998; Block & Harris 2006; Revil & Jardani 2013).

Zeta potential (ξ) represents the surface electrical charge when a mineral surface contacts with water. Most of the particles' surface charge in pH condition of 5-9 is negative. Four mechanisms that can generate surface charge are: absorption of ions to particle surface, dissociation or ionization at the surface, lattice imperfections at the solid surface and isomorphous replacements within the lattice (Kim & Lawler 2005). A sketch of Silica mineral in contact with water is shown in Figure 2.5. Revil et al. (1999) developed analytical equations for zeta potential and the specific surface conductance of silica grain. The equation was used to describe the relationship between zeta potential and effective parameters such as temperature, fluid salinity and pH. Developed model and experimental data showed that zeta potential increased when temperature and pH

increased and decreased with increasing salinity of pore water (Figure 2.6). Lorne et al. (1999) studied zeta potential sensitivity to electrolyte resistivity, size and valence of the ions in the solution and grain size and permeability of the sample. Zeta potential and surface conductivity in clay water interface for a range of clay type and thermodynamic conditions is predicted by an electrochemical model developed by Leroy & Revil (2004). Electrochemical charge and zeta potential for silica sand in contact with high-ionic-strength solutions (1 mM to 1 M) and the effect of electrical double layers' overlap in narrow channels have been studied by Wang & Revil (2010).

Electrical double layer have been studied comprehensively by Lorne et al. (1999) and Leroy & Revil (2004). Leroy & Revil (2004) developed an electrical triple-layer model for predicting the electrochemical properties of clay/water interface.

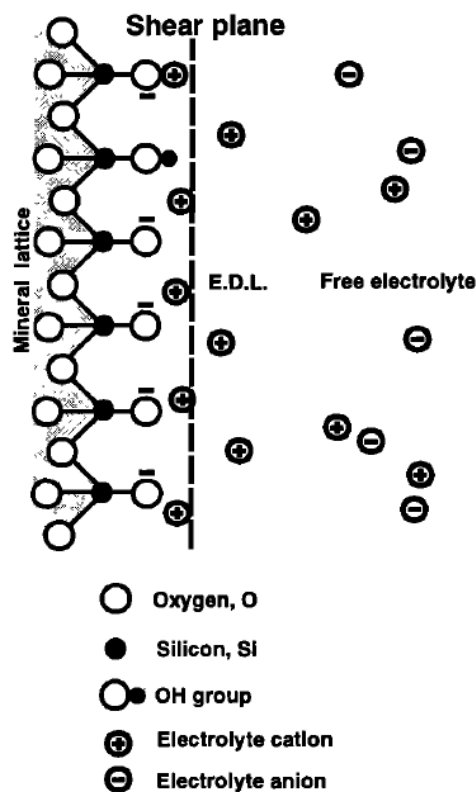


Figure 2.5. Sketch of silica surface in pH condition of 3-8, surface group is mostly consisting of siloxane, silanol and silicic acid group. E.D.L denotes the electrical diffuse layer (Kim & Lawler 2005).

Three conclusions can arise from the existence of the electrical double layer: pore water in contact with mineral is never uncharged; surface conductivity is due to excess of electrical conductivity in water/mineral interface and the polarization of porous material is due to the electrical double layer (Revil & Jardani 2013)

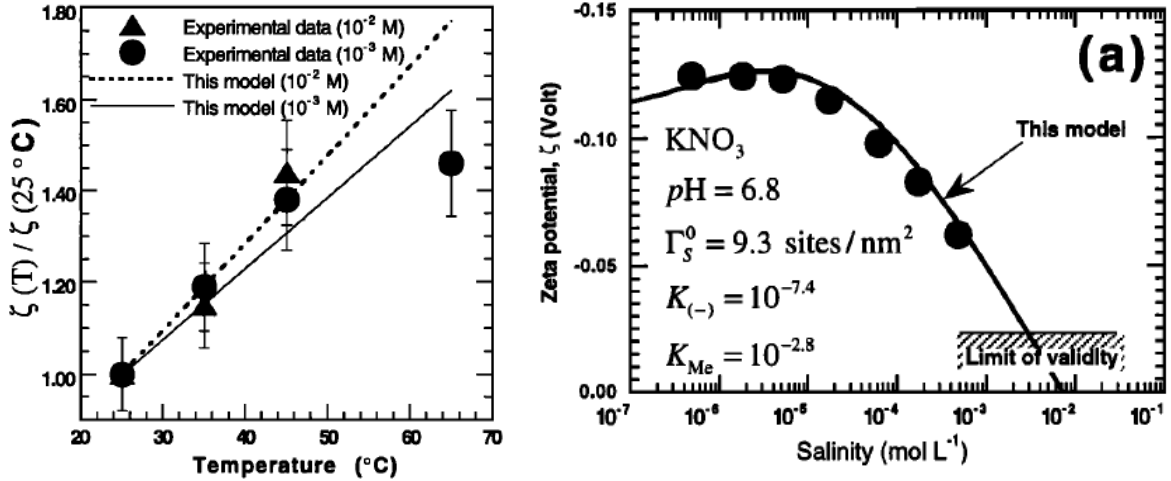


Figure 2.6. Zeta potential as function of temperature and salinity (Revil et al., 1999).

2.4.1.1 Streaming Potential (Electrofiltration Potential)

Streaming potential generates a macroscopic electrical field due to the movement of pore water through the capillary or porous medium (Barde-Cabusson et al., 2009; Sharma 1997). Nourbehecht (1959) demonstrated a linear relationship between generalized Darcy law and Ohm laws based on non-equilibrium thermodynamics equations. Theories about electrokinetic effects were developed by upscaling two equations of Nernst-Planck and Navier-Stokes by Pride (1994). The relation between fluid volume flux (J_E) and electric current density (I_E) due to the forces of electric potential gradient ($\nabla\phi$) and the pore pressure gradient (∇P) are:

$$J_E = -(\phi \varepsilon \zeta / \eta) \nabla\phi - (k/\eta) \nabla P \quad 2-3$$

$$I_E = -\phi \sigma \nabla\phi - (\kappa \varepsilon \zeta / \eta) \nabla P \quad 2-4$$

where ϕ denotes the porosity and ε is the dielectric constant. ζ , η , k and σ are the zeta potential, pore fluid viscosity, permeability and electric conductivity, respectively. In

Equation 2-4, the first term is flux due to electro-osmotic effect and the second one represents the Darcy law. In Equation 2-4 the first term is electric current density (Ohm's law) and the second term represents the electrokinetic potential. In an equilibrium state ($I_E = 0$), Equation 2-4 would be:

$$C_k = \nabla\phi/\nabla P = -\varepsilon\zeta/\sigma\eta \quad 2-5$$

The term $(\nabla\phi/\nabla P)$, is the electrokinetic coupling coefficient. The voltage across the Helmholtz double layer (zeta potential; ζ) has a crucial role in the electrokinetic coupling coefficient amplitude (Zlotnicki & Nishida 2003). Two effective parameters for electrical conductivity in porous media (σ) are porosity and the mobility of fluid for moving through the pore space. Fluid mobility depends on temperature, pressure, ionic mobilities, concentration and viscosity of solution (Reynolds 1997).

Streaming potential contribution in unsaturated conditions have been studied by (Revil et al., 2007; Linde et al., 2007). Revil et al. (2007) derived the equation for water saturation and streaming potential and electro-osmosis relations. Numerical modeling of drainage and imbibition experiments showed that the streaming potential coupling coefficient magnitude depends on the water saturation, sample's material properties and the saturation history. As illustrated in Figure 2.7, experimental data has showed that increasing water saturation leads to an increase in the self-potential coupling coefficient (Revil et al., 2007; Revil & Cerepi 2004). At irreducible water saturation, the streaming potential coupling coefficient would be null (Revil et al., 2007). There is no streaming potential associated with dry steam (Barde-Cabusson et al., 2009). SP anomalies associated with streaming potential have been observed over hydrothermal and volcanic areas and in wells that are in the vicinity of porous layers invaded by drilling fluids (Sharma 1997), near injection sites and pumping wells (Suski et al., 2004; Crespy et al., 2008) and where water leaks through faults and cracks in the reservoir rock (Ogilvy et al., 1969).

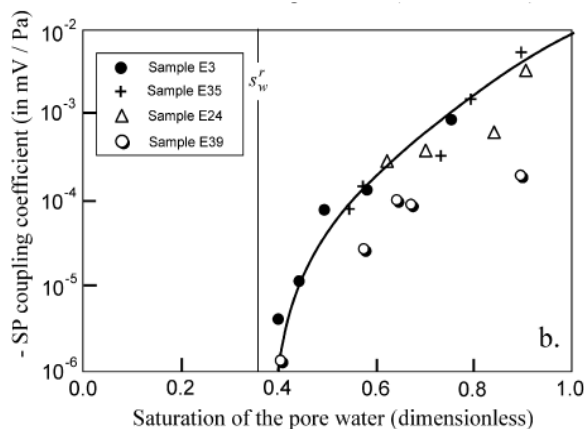


Figure 2.7. Streaming potential coupling coefficient vs. water saturation (Revil et al., 2007).

Transient SP anomalies due to hydro-mechanical disturbances have been examined in a controlled sandbox experiment (Crespy et al., 2008) and for field data (Legaz et al., 2009). Crespy et al. (2008) performed two sets of water injection and withdrawal tests in a sandbox to define the voltage associated with the sudden change in the fluid pressure. SP data showed a negative SP anomaly of $-12 \mu\text{V}$ above the injection point while a positive anomaly of $6 \mu\text{V}$ was detected above the withdrawal point.

2.4.1.2 Thermoelectric Potential

The generation of voltage associated with the presence of a macroscopic thermal gradient in the absence of water flux is called thermoelectric potential (Corwin & Hoover 1979; Revil 1999; Leinov et al., 2010). The conversion of temperature difference to electricity was explained by Thomas Seebeck in 1821 (Seebeck effect). The presence of temperature gradient at an electrified junction was discovered by Jean Peltier in 1834 (Peltier effect). Nevertheless, there is limited research focusing on this phenomenon in porous media. Thermoelectric potential in porous materials has been experimentally studied by Nourbehecht (1959), Marshall & Madden (1959) Corwin & Hoover (1979) and Fitterman & Corwin (1982). Although the origin of thermoelectric potential is not very clear, it is believed that the voltage is associated with the temperature dependence of chemical potential of charge carriers (Revil et al., 2013; Revil & Linde 2006). Thermoelectric coupling coefficient (C_{TE}) is defined as the voltage difference to the temperature

difference ($\Delta V/\Delta T$) and is measured experimentally. A sketch of the experimental setup is showed in Figure 2.8. Thermoelectric coupling coefficient measured in the laboratory changes within the range of -0.25 and 1.5 $\text{mV}/^\circ\text{C}$ for a variety of rocks (Nourbehecht 1959; Yamashita 1961; Dorfman et al., 1977). Corwin & Hoover (1979) believed that the thermoelectric coupling coefficient measured in-situ is larger than the one measured in the laboratory. Limited number of studies has been done on the thermoelectric effect in porous medium and there are several drawbacks about available measured C_{TE} . In most studies experimental conditions are not described in details. Also, it is not clear if the author corrected reported data for internal temperature dependence of electrodes. Furthermore Revil et al. (2013) believe that some reported positive C_{TE} value in geothermal regions could be affected by streaming potential.

Equations governing the potential distribution due to coupling of flows was derived from the thermodynamics of irreversible processes by Nourbehecht (1959). Solving these equations analytically for simple-source geometry leads to models that calculate maximum expected SP anomaly (Nourbehecht 1959; Corwin & Hoover 1979). Based on the model, a spherical heat source that is in contact with two layers with a coupling coefficient difference of $(C_1 - C_2)$ generates a maximum SP anomaly of $0.15(C_1 - C_2)\nabla T$ (mV) (Figure 2.9). In this model, the elevated temperature region should be in contact with two layers which have distinct coupling coefficients. The sign of the coupling coefficient difference determines the amplitude of the anomaly.

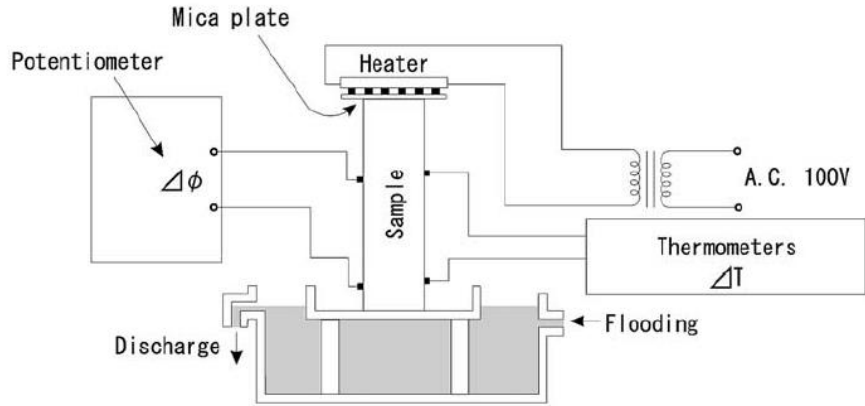


Figure 2.8. Experimental sketch for measuring thermoelectric coupling coefficient in a rock sample (Yamashita 1961).

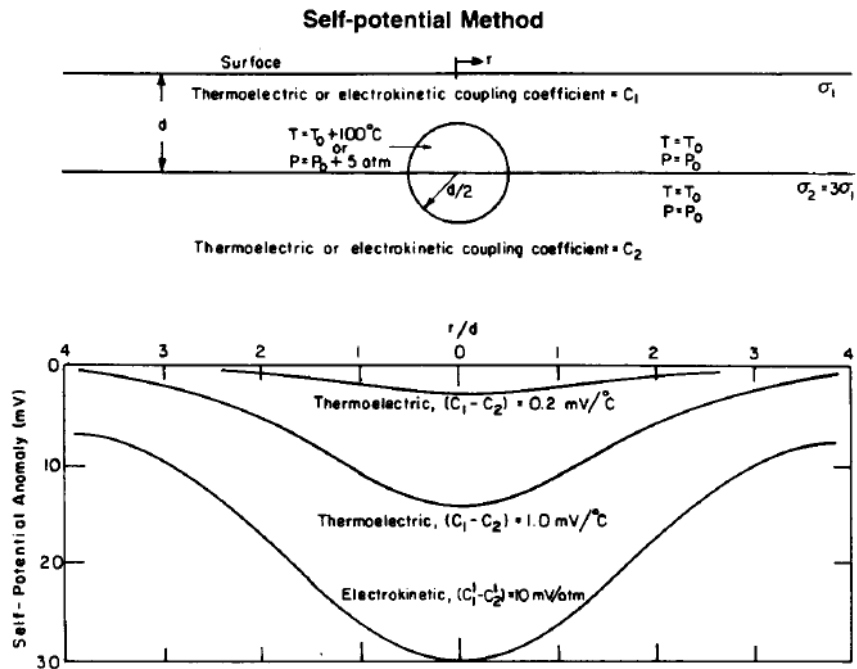


Figure 2.9. Thermoelectric self-potential generated by spherical body of elevated temperature (Nourbehecht 1959; Corwin & Hoover 1979).

The relationship between coupled flow of heat (J_T), electric current density (I_T) and temperature gradient ∇T and potential gradient is governed by equations:

$$J_T = -\sigma \nabla \psi - \kappa \nabla T$$

$$I_T = -\sigma \nabla \psi - \theta \nabla T \quad 2-7$$

In Equation 2-6 and 2-7, σ , κ , θ and π denotes the electric and thermal conductivities, thermoelectric and Peltier coefficients. The first term in Equation 2-7 represents the electric current density (Ohm's law) and the second terms represents the thermoelectric or Seebeck effect (Zlotnicki & Nishida 2003).

Thermoelectric potential governing equation has been developed by Revil et al. (2013) using a phenomenological approach. Thermoelectric potential would be:

$$\psi^0(R) = \frac{1}{4\pi} \left(\frac{C_{TE}}{\kappa} \right) \frac{1}{R} Q_H \quad 2-8$$

where C_{TE} (V/°C) is thermoelectric coupling coefficient and is derived experimentally. ψ^0 , Q_H and κ represent the monopole term of voltage, the heat source (Wm^{-3}) and thermal conductivity ($Wm^{-1}K^{-1}$). Thermoelectric potential would be monopolar in far field and the amplitude depends on C_{TE} sign (Revil et al., 2013). The theory is confirmed by field measurements in Marshal in which the SP associated with thermoelectric effect was negative monopolar anomaly.

Thermoelectric potentials, membrane, ionic diffusion and electrical conductivity are four closely related phenomena that play crucial roles in the transport of ions in pore scale. Solid particle surfaces are not neutral due to the chemical reaction between the pore fluid and the solid surface. The resulting excess of charge is counterbalanced by ions with opposite sign (counterions) that are located in electrical double layer. Surface electrical conductivity is also due to the existence of counter-ions in the electrical double layer. Distribution of ions in pore space in the presence of chemical potential gradient is described by ionic diffusivity terms. Produced microscopic electrical field due to the separation of ions when a salt diffuses into a porous material is called "membrane potential". When a macroscopic electrical field exists, the ion's transport is described by electrical conductivity (Revil 1999).

Revil (1999) modeled thermoelectric potentials in terms of macroscopic phenomenological coefficients in granular porous materials. Representative elementary volume (REV) is defined as an isotropic granular porous material that consists of a solid particle, an electrical double layer and an electrolyte. The REV is in mechanical equilibrium while the heat and the ionic transport are the only processes in the system. The thermal agitation of ions increases in the presence of a thermal gradient. In the presence of a temperature gradient, a separation of charge occurs due to differences in the ionic mobility.

The governing equation for the relation between thermodynamic forces and the resulted fluxes are:

$$\begin{pmatrix} J_{(+)} \\ J_{(-)} \\ J_s \end{pmatrix} = - \begin{pmatrix} \sigma_{(+)} / e^2 & 0 & l_{13} \\ 0 & \sigma_{(-)} / e^2 & l_{23} \\ l_{13} & l_{23} & l_{33} \end{pmatrix} \begin{pmatrix} \nabla \tilde{\mu}_{(+)}^f \\ \nabla \tilde{\mu}_{(-)}^f \\ \nabla T \end{pmatrix} \quad 2-9$$

where macroscopic electrical current density (J) is defined as: $J = e (J_{(+)} + J_{(-)})$. The terms l_{ij} are phenomenological coefficients which are positive value and independent of fluxes and forces. σ represents the macroscopic electrical conductivity ($\sigma = \sigma_{(+)} + \sigma_{(-)}$) and $\sigma_{(+)}$; $\sigma_{(-)}$ denotes the ionic contributions to σ and e represents the elementary charge (C, which is always positive). $\nabla \tilde{\mu}_{(\pm)}^f$ denotes the ionic electrochemical potential gradient in the electrolyte and ∇T is the temperature gradient (K).

The thermoelectric coupling coefficient governing equation is:

$$C_{TE} \equiv \left(\frac{d\Psi}{dT} \right)_J = \frac{T_{(+)}}{e} \left(S_{(+)} - \frac{Q_{(\pm)}}{T} \right) - \frac{T_{(-)}}{e} \left(S_{(-)} - \frac{Q_{(-)}}{T} \right) \quad 2-10$$

where $T_{(+)}$ and $T_{(-)}$ are the macroscopic Hittorf transport numbers ($T_{(\pm)} \equiv \sigma_{(\pm)} / \sigma$) and $T_{(-)} = 1 - T_{(+)}$. In the case of negotiable surface charge:

$$\lim_{\xi \rightarrow 0} T_{(\pm)} = t_{(\pm)}^f \quad 2-11$$

In a perfect membrane, electrical conductivity of the electrolyte is dominated by electrical surface conductivity ($T_{(+)} = 1$). In the case of diffusion of a salt, the ions cannot

diffuse independently in spite of their differing mobilities. The separation of ions is due to the fact that ions with higher mobilities move faster, resulting in the generation of a microscopic electrical field called the “liquid junction potential”. The member potential changes within the range of the liquid junction potential value and the perfect membrane potential value (the grains–water interface is negatively charged) ($t_{(+)}^f \leq T_+ \leq 1$). Change in the member potential depends on the salinity condition of porous media. $S_{(\pm)}$ denotes the ions’ molar partial entropies and the Q_{\pm} is the heat transported with a unit diffusion flux of ions.

The thermoelectric coupling coefficient upper and lower bound is:

$$C_T \rightarrow C_T^M = \frac{1}{e} \left(S_{(+)} - \frac{Q_{(\pm)}}{T} \right); T_{(+)} = 1 \quad 2-12$$

(Perfect membrane)

$$C_T \rightarrow C_T^j = \frac{1}{e} \left[t_{(+)}^f \left(S_{(+)} - \frac{Q_{(+)}}{T} \right) - t_{(-)}^f \left(S_{(-)} - \frac{Q_{(-)}}{T} \right) \right]; T_{(\pm)} = t_{(\pm)}^f \quad 2-13$$

(Uncharged membrane)

Upper bound occurs when one type of ionic contribution is dominant whereas the lower case corresponds to an uncharged solid particle surface. Salinity dependence of C_{TE} in sandstone samples that were saturated with NaCl brine were studied by Leinov et al. (2010) The concentrations ranged within 1×10^{-4} and 1 M and the measured coupling coefficient ranged from 0.370 mVK^{-1} at low salinity and 0.055 mVK^{-1} at high salinity. The developed model by Revil (1999) was used for modeling by Leinov et al. (2010) and accounts for the salinity dependence of coupling coefficient in the model.

Measured thermoelectric coupling coefficient for two measuring setups (plug and column) as a function of sample salinity is shown in Figure 2.10. Brine salinity controls the electrical double layer (mineral surface-brine interface) thickness in a sample. In the condition of low salinity, the electrical double layer is thick and fills the narrow throats of the sample. As a result of excluding negative ions, the sample acts as a perfect membrane. In high salinity conditions, the electrical double layer is thin and neural brine fills the sample pore-throat’s space. In this case, the sample acts as an uncharged porous

medium. Brine salinity, radius of the pore-throats and sand texture controls the thickness of the electrical double layer and C_{TE} salinity dependence is due to electrical double layer thickness in a sample (Leinov et al., 2010).

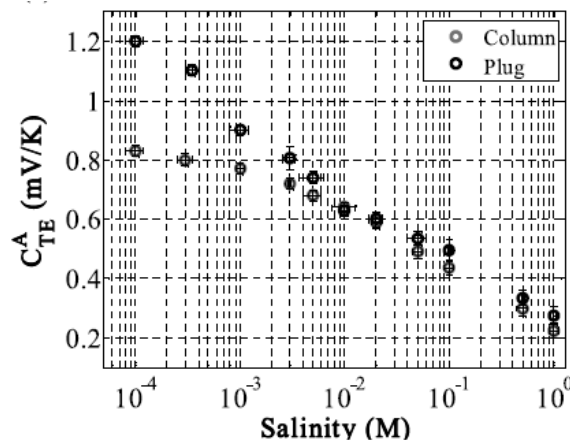


Figure 2.10. Measured thermoelectric coefficients vs salinity (Leinov et al., 2010).

In geothermal systems, coal mine fire and in the vicinity of steam and fire flood wells (a technique for the recovery of petroleum), the thermoelectric effect could be studied (Corwin & Hoover 1979a). SP anomalies generated by a thermoelectric mechanism are of smaller amplitudes than usually seen in the geothermal areas. However, the boundaries of SP anomalies measured in several geothermal areas appear to correlate with zones of high heat flow. This allows for the possibility that at least a portion of these anomalies is generated by a thermoelectric mechanism (Sharma 1997). In situ burning coal, which is called a coal-seam fire, is an exothermic reaction that can increase the temperature up to 540°C (DeKok 1986). Thermoelectric self-potential is the dominant component of the observed SP anomaly associated with coal-seam fires (Revil et al., 2013). The burning front position of a coal-seam fire can be tracked by SP technique (Corwin & Hoover 1979; Revil et al., 2013; Karaoulis et al., 2014). Revil et al. (2013) and Karaoulis et al. (2014) used joint inversion (using a cross-gradient approach) of self-potential and resistivity data to localize the position of burning front in coal-seam fire in underground mines at 9 m depth. They showed that the normalized results determined from the joint inversion of self-potential and resistivity data is slightly more accurate than the independent inversion of two sets of data in localizing positions of burning front.

Dorfman et al. (1977) showed that SP could be used to identify heat distribution and to track the heat front during thermal oil recovery flood techniques.

2.4.1.3 Electrochemical Potential

Electrochemical or diffusion potential is the result of coupling between the chemical gradient (force) and the electric current density (flux). The potential is generated because of the difference in the ion's mobilities in different solutions' concentrations (Sharma 1997; Minsley 2007).

Electric potential gradient is governed by the Planck-Henderson equation:

$$\Delta\psi = \frac{-RT(u_+ - u_-)}{|z|F(u_+ + u_-)} \ln \frac{c_1}{c_0} \quad 2-14$$

where C ($\text{mol}\cdot\text{m}^{-3}$) is the concentration, u ($\text{m}^2\cdot\text{V}^{-1}\cdot\text{s}^{-1}$) is the ionic mobility, T denotes the temperature (K), F is Faraday's constant ($96,500 \text{ C}\cdot\text{mol}^{-1}$), R is gas constant ($8.314 \text{ J}\cdot\text{mol}^{-1}\cdot\text{K}^{-1}$), $\Delta\psi$ is electrical potential drop and z is ionic charge (C). The relation between concentration gradient and generated potential is not linear because of fluid conductivity dependence on concentration (Minsley et al., 2007). In the case of one ionic species, the Planck-Henderson equation reduces to the Nernst equation.

The electrochemical potential amplitude for NaCl solution for two concentrations of C_1 and C_2 in the temperature of T ($^{\circ}\text{C}$) is given by (Telford & Sheriff 1990):

$$E_c = - \frac{70.7(T+273)}{273 \ln \frac{C_1}{C_2}} \quad 2-15$$

Electrochemical potential associated with the oxidation-reduction process could be used in ore body exploration and to detect contamination. A stable negative self-potential (several hundreds of mV) can occur over conductive deposits such as pyrite, chalcopyrite, pyrrhotite, magnetite, and graphite (Sharma 1997). Most of the works that are done in this field are based on the model that Sato & Mooney (1960) developed, which described the ore body and surrounding soil as an electrochemical cell. The "geobattery" model was developed by correlating all measured self-potential anomalies associated with the existence of the ore bodies performed up to that date. In the model, the ore body acts as

an electronic conductor (Figure 2.11). The top part of the ore acts as a cathode (reduction process) and the bottom part acts as an anode (oxidation process). Measured negative SP anomaly at the surface is due to the movement of ions in the ground and the movement of electrons in the conductive ore body. A model similar to the geobattery model was proposed by Arora et al. (2007) and Linde & Revil (2007) to describe measured self-potential anomalies over an area of organic contaminants.

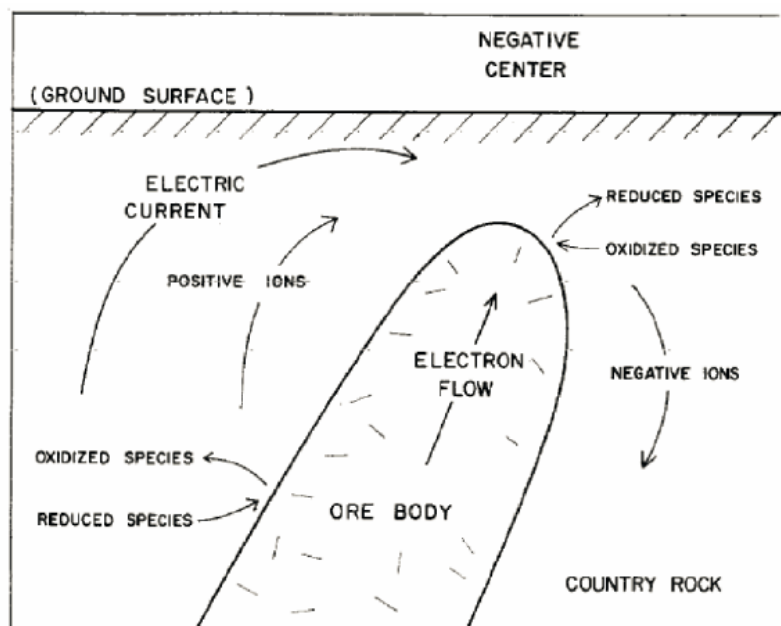


Figure 2.11. Self-potential generating mechanism over an ore body (Sato & Mooney 1960).

Degradation of contaminants is extensively discussed in the literature (Vogel et al., 1987; Christensen et al., 2000; Kao et al., 2003). Degradation is believed to be due to the presence of microorganisms in the earth (Lovley et al., 1994; Magnuson et al., 1998; Naudet et al., 2004; Naudet & Revil 2005; Williams et al., 2005).

The reduction of oxygen, iron, nitrate, carbon dioxide and sulphate in the earth leads to the oxidation of organic contaminants. The charge transfer in the redox process between the oxidized and reduced species generates a measurable self-potential signal. For other contaminant such as tetrachloroethylene (PCE), an oxidized contaminant, reduction can occur when organic materials are oxidized. Degradation of contaminants depends on the

spatial distribution of the contaminant and the microorganism in the aquifer (Minsley et al., 2007). Spatial distribution of contamination was determined by the inversion of 3D self-potential measurements at the Savannah River site, which is heavily contaminated by DNAPLs (Minsley et al., 2007). A case study result for the contamination detection is shown in Figure 2.12.

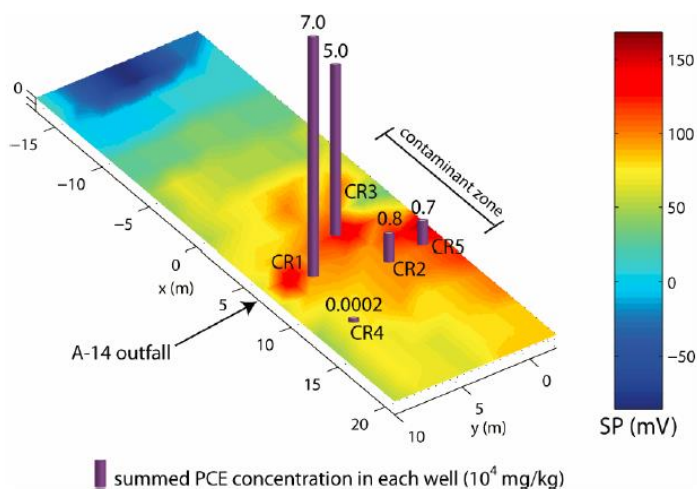


Figure 2.12. Comparison between self-potential measurements at the surface and PCE concentration in the wells in Savannah River site (Minsley et al., 2007).

2.4.2 Self-Potential Anomalies on Volcanoes and Geothermal Regions

SP anomaly amplitude can range from a few mV to 1-2 V in volcano regions. The SP anomaly source size controls spatial distribution of the observed SP anomaly. Self-potential anomalies on volcanoes could be due to electrochemical, electrokinetic (including topographic effect and hydrothermal circulation) and thermoelectric effects. The origin of the SP anomaly on volcanoes have been comprehensively studied by Zlotnicki & Nishida (2003). Electrochemical effect could be due to concentration difference among gas, water discharges, fumarolic areas and also due to the chemical reactions. Chemical reactions can generate HCO_3^- , CO_3^- and SO_4^- and as a result relatively small negative SP anomaly is generated. Considering the average thermoelectric coupling coefficient and the measured SP anomaly in the volcanic area,

thermoelectric effect could be important in the area with superheated gas fluxes (Zlotnicki & Nishida 2003).

Observed anomalies in volcanic areas are categorized into the following 5 types: positive, negative, co-existing positive and negative, structure dependent and no anomaly type. A strong positive anomalies (more than 1V) have been reported in some volcanic and geothermal regions (Zohdy et al., 1973; Zablocki 1975; Anderson & Johnson 1976; Nishida & Tomiya 1987; Matsushima et al., 1990; Hashimoto & Tanaka 1995; Lewicki et al., 2003; Finizola et al., 2003; Aizawa 2004; Finizola et al., 2006;). Corwin & Hoover (1979) believed that the only possible source of large SP anomalies (in order of 1-2 V) over volcanic areas could be electrokinetic effects. Streaming potential is the causative source of positive self-potential anomaly in geothermal and volcanic region (Goldstein et al., 1989; Finizola et al., 2003; Barde-Cabusson et al., 2009). The mechanism of generating positive self-potential over a volcanic area is illustrated in Figure 2.13. In volcanic rock, the zeta potential at pH=7 is negative and resulting streaming potential would be positive in the direction of flow (Barde-Cabusson et al., 2009). The self-potential anomaly magnitude depends on ground electrical resistivity (Ishido 2004). On the other hand, resistivity is dependent on the temperature (Revil 2002) and rock water content (Legaz et al., 2009). On Mt. Pelée volcano in Martinique Island, a negative SP anomaly was observed (Zlotnicki et al., 1998). The maximum amplitude of the anomaly was located on the summit at approximately -1700 mV. Zlotnicki et al. (1998) believed that the negative anomaly is due to topographic effect. Zlotnicki & Nishida (2003) suggested that observed negative anomaly (-400 mV) in the belt surrounding the mountainsides of Esan volcano (Japan) on highly resistive permeable lava is due to downward fluxes of rainfall water. Co-existing positive and negative anomaly was found by Anderson & Johnson (1976) in Long Valley caldera and also observed on Miyakejima Volcano in Japan by Nishida et al. (1996) and Sasai, Y. et al. (1997). In this type of anomaly, the negative anomaly is observed in a permeable recharge area and the positive part of the anomaly is linked with upward flow of heated recharge water through the summit area.

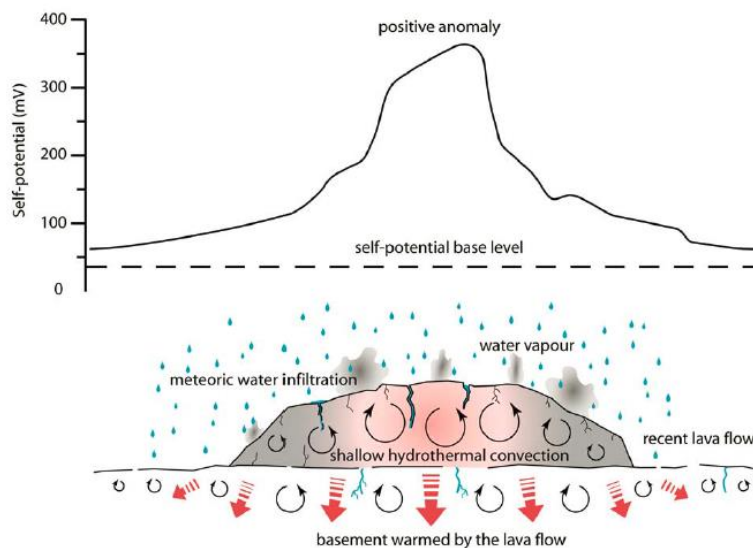


Figure 2.13. Positive self-potential generating mechanism above the lava flows (Barde-Cabusson et al., 2009).

In some volcanic regions, despite intense fumarolic activity (temperature $>500\text{ }^{\circ}\text{C}$), the associated self-potential anomaly is less than tens of mV (Nishida & Tomiya 1987; Matsushima et al., 1990). Existence of super-heated gas that is not capable of transporting the electric charge and low pH conditions are the main reasons for negligible SP anomaly. In low pH condition, the small amplitude of the zeta potential generates small electrokinetic coupling coefficient and, as a result, negligible SP anomalies are observed (Zlotnicki & Nishida 2003). Wavelength of the SP anomaly could be used for the monitoring purposes. Changing in the depth, location and the extent of the hydrothermal system would change the wavelength of the anomaly (Aizawa 2004). Signal processing of the SP anomaly could delineate the position of water flow in a hydrothermal system (Mauri et al., 2010).

2.5 Summary and Gaps

In this chapter, scientific literature for available NAPLs remediation techniques including thermal treatment technologies and STAR has been summarized. In addition, self-potential method and its generating source mechanisms and applications have been reviewed. From this review, the following observations can be made:

- NAPLs are one of the most common soils and groundwater contaminants while available remediation techniques are either expensive or time-consuming in treating NAPL contaminations.
- Self-sustaining treatment for active remediation (STAR), which is based on smoldering combustion, shows significant potential for remediating sites contaminated by NAPLs.
- Spatial propagation of the combustion front in the field is monitored through temperature data collected in thermocouple monitoring network, the density of which is limited.
- The self-potential technique is an inexpensive method applied at the surface and sensitive to signals from numerous different naturally occurring voltage sources in the subsurface.
- Thermoelectric potential is a dominant contribution in measured SP data over high temperature regions in the ground (e.g., coal-seam fire in an underground mine).

Based on available literature, there are still many unknown concepts in relation to thermoelectric self-potential origin and its potential applications in environmental studies:

- Little work has been done on the thermoelectric effect in porous media. A range of values has been reported for the thermoelectric coupling coefficient for similar scenarios, indicating the sensitivity of the measurements to the experimental conditions and sample properties. Therefore, it is important to investigate the polarity and magnitude of the thermoelectric coupling coefficient for a particular scenario.
- SP technique as a potential non-intrusive monitoring tool has not been investigated in monitoring STAR at any scale.

2.6 References

Abaza, M. M. I and Clyde, C. G. (1969). Evaluation of the Rate of Flow through Porous Media Using Electrokinetic Phenomena. *Water Resource Research*, 5(2), 470–483.

- Aizawa, K. (2004). A large self-potential anomaly and its changes on the quiet Mt. Fuji, Japan. *Geophysical Research Letters*, 31(5), 1–4.
- Akkutlu, I. Y., & Yortsos, Y. C. (2003). The dynamics of in-situ combustion fronts in porous media. *Combustion and Flame*, 134(3), 229–247.
- Anderson, L. a., & Johnson, G. R. (1976). Application of the self-potential method to geothermal exploration in Long Valley, California. *Journal of Geophysical Research*, 81(8), 1527–1532.
- Ansuini, F. J., & Dimond, J. R. (1994). Factors Affecting the Accuracy of Reference Electrodes. *Materials Performance*, 33(11), 14–17.
- Arora, T., Linde, N., Revil, A., & Castermant, J. (2007). Non-intrusive determination of the redox potential of contaminant plums by using the self potential method. *Contaminant Hydrology*, 92, 274–292.
- Aubert, M., & Atangana, Q. (1996). Self-potential method in hydrogeological exploration of volcanic area. *Ground Water*, 34(6), 1010–1016.
- Baker, R., & Kuhlman, M. (2002). A description of the mechanisms of in-situ thermal destruction (ISTD) reactions. In *2nd International Conf. on Oxidation and Reduction Technologies for Soil and Groundwater, ORTs-2, Toronto, Ontario, Canada, Nov. 17-21* (pp. 1–10). Retrieved from 2nd International Conf. on Oxidation and Reduction Technologies for Soil and Groundwater, ORTs-2, Toronto, Ontario, Canada, Nov. 17-21.
- Barde-Cabusson, S., Levieux, G., Lénat, J.-F., Finizola, A., Revil, A., Chaput, M., ... Vieille, M. (2009). Transient self-potential anomalies associated with recent lava flows at Piton de la Fournaise volcano (Réunion Island, Indian Ocean). *Journal of Volcanology and Geothermal Research*, 187(3-4), 158–166.
- Bar-Ilan, a., Putzeys, O. M., Rein, G., Fernandez-Pello, a. C., & Urban, D. L. (2005). Transition from forward smoldering to flaming in small polyurethane foam samples. *Proceedings of the Combustion Institute*, 30(2), 2295–2302.
- Beyke, G., & Fleming, D. (2002). Enhanced removal of separate phase viscous fuel by electrical resistance heating and multi-phase extraction. In *9th Annual International Petroleum Environmental Conference, October 22-25, Albuquerque, NM*.
- Beyke, G., & Fleming, D. (2005). In situ thermal remediation of DNAPL and LNAPL using electrical resistance heating. *Remediation Journal*, 15(3), 5–22.
- Block, G. I., & Harris, J. G. (2006). Conductivity dependence of seismoelectric wave phenomena in fluid-saturated sediments. *Journal of Geophysical Research*, 111(B1), 1–12.

- Christensen, T.H., Bjerg, P. L., Banwart, S. A., Yvetot, P., & Alberchtsen, H. J. (2000). Characterization of redox conditions in groundwater contaminant plumes. *Contaminant Hydrology*, 45(3-4), 165–241.
- Corwin, R. F., & Hoover, D. B. (1979a). The self-potential method in geothermal exploration. *Geophysics*, 44(2), 226–245.
- Crespy, A., Revil, A., Linde, N., Byrdina, S., Jardani, A., Bolève, A., & Henry, P. (2008a). Detection and localization of hydromechanical disturbances in a sandbox using the self-potential method. *Journal of Geophysical Research*, 113(B1), B01205- B01228.
- Davis, E. (1977). Ground Water Issue: How Heat Can Enhance In-situ Soil and Aquifer Remediation: Important Chemical Properties and Guidance on Choosing the Appropriate Technique. EPA 540/S-97/502. U.S. EPA., *Office of Research and Development*, 1–18.
- Davis, E. (1998). *Steam Injection for Soil and Aquifer Remediation*, EPA 540/S-97/505. U.S. EPA, *Office of Research and Development* (pp. 1–16).
- DeKok, D. (1986). Unseen danger: A tragedy of people, government, and the Centralia mine fire. *University of Pennsylvania Press*. Retrieved from <http://daviddekok.com>
- Dmitriev, a. N. (2012). Forward and inverse self-potential modeling: a new approach. *Russian Geology and Geophysics*, 53(6), 611–622.
- Dorfman, N. H., Oskay, M. M., & Gaddis, M. P. (1977). Self-Potential Profiling: A New Technique for Determination of Heat Movement in a Thermal Oil Recovery Flood. In *Presented at the SPE Annual Fall Technical Conference and Exhibition: American Institute of Mining, Metallurgical, and Petroleum Engineers*. Denver.
- Drysdale, D. D. (2008). *Ignition of Liquids (Chapter 18), The SFPE Handbook of Fire Protection Engineering (4th edition)*. Quincy, MA.
- Finizola, A., Revil, A., Rizzo, E., Piscitelli, S., Ricci, T., Morin, J., ... Sortino, F. (2006). Hydrogeological insights at Stromboli volcano (Italy) from geoelectrical, temperature, and CO₂ soil degassing investigations. *Geophysical Research Letters*, 33(17), 1–4.
- Finizola, A., Sortino, F., Lenat, J.-F., Aubert, M., Ripepe, M., & Valenza, M. (2003). The summit hydrothermal system of Stromboli. New insights from self-potential, temperature, CO₂ and fumarolic fluid measurements, with structural and monitoring implications. *Bulletin of Volcanology*, 65(7), 486–504.
- Fitterman, D. V., & Corwin, R. F. (1982a). Inversion of self potential data from the Cerro Prieto geothermal field, Mexico. *Geophysics*, 47(6), 938–945.

- Fitterman, D. V., & Corwin, R. F. (1982b). Inversion of self-potential from the Cerro Prieto geothermal field, Mexico. *Geophysics*, 47(6), 938–945.
- Fournier, C. (1989). Spontaneous potentials and resistivity surveys applied to hydrogeology in a volcanic area: case history of the chaîne des puys (PUY-DE-DOME, FRANCE). *Geophys. Prosp.*, 37(July 1987), 647–668.
- Goldstein, N. E., Halfman, S., Corwin, R. F., & Martinez, J. (1989). Self-potential anomaly changes at the East Mesa and Cerro Prieto geothermal fields. In *14th Workshop on Geothermal Reservoir Engineering*. Stanford University, Stanford, California.
- Greaves, M., Young, T. J., El-usta, S., Rathbone, R. R., Ren, S. R., & Xia, T. X. (2000). Air Injection Into Light And Medium Heavy Oil Reservoirs : Combustion Tube Studies On West Of Shetlands Clair Oil And Light Australian Oil. *Chemical Engineering Research and Design*, 78(July), 1–9.
- Haartsen, M. W., Dong, W., & Toksîz, M. N. (1998). Dynamic streaming currents from seismic point sources in homogeneous poroelastic media. *Geophys. J. Int.*, 132, 256–274.
- Hashimoto, T., & Tanaka, Y. (1995). A large self-potential anomaly on Unzen volcano , Shimabara peninsula , Kyushu island , Japan 1990- Eruption of Unzen Volcano, 22(3), 191–194.
- Ikard, S. J., Revil, A., Jardani, A., Woodruff, W. F., Parekh, M., & Mooney, M. (2012). Saline pulse test monitoring with the self-potential method to nonintrusively determine the velocity of the pore water in leaking areas of earth dams and embankments. *Water Resources Research*, 48(4), 1–17.
- Ishido, T. (2004). Electrokinetic mechanism for the “W”-shaped self-potential profile on volcanoes. *Geophysical Research Letters*, 31(15), L15616– L15621.
- Jardani, a., & Revil, a. (2009). Stochastic joint inversion of temperature and self-potential data. *Geophysical Journal International*, 179(1), 640–654.
- Kao, C. M., Chen, S. C., Wang, J. K., Chen, Y. L., & Lee, S. Z. (2003). Remediation of PCE-contaminated aquifer by an in situ two-layer biobarrier: laboratory batch and column studies. *Water Resource*, 37(1), 27–38.
- Karaoulis, M., Revil, a., & Mao, D. (2014). Localization of a coal seam fire using combined self-potential and resistivity data. *International Journal of Coal Geology*, 128-129, 109–118.
- Kaslusky, S. F., & Udell, K. S. (2002). A theoretical model of air and steam co-injection to prevent the downward migration of DNAPLs during steam-enhanced extraction. *Journal of Contaminant Hydrology*, 55(3-4), 213–232.

- Kim, J., & Lawler, D. F. (2005). Characteristics of Zeta Potential Distribution in Silica Particles. *Korean Chemistry Society*, 26(7), 1083–1089.
- Legaz, A., Vandemeulebrouck, J., Revil, A., Kemna, A., Hurst, a. W., Reeves, R., & Papasin, R. (2009). A case study of resistivity and self-potential signatures of hydrothermal instabilities, Inferno Crater Lake, Waimangu, New Zealand. *Geophysical Research Letters*, 36(12), L12306– L12311.
- Leinov, E., Vinogradov, J., & Jackson, M. D. (2010). Salinity dependence of the thermoelectric coupling coefficient in brine-saturated sandstones. *Geophysical Research Letters*, 37(23), L23308– L23314.
- Leroy, P., & Revil, A. (2004). A triple-layer model of the surface electrochemical properties of clay minerals. *Journal of Colloid and Interface Science*, 270(2), 371–380.
- Lewicki, J.-L., Connor, C., St-Amand, K., Stix, J., & Spinner, W. (2003). Self-potential, soil CO₂ flux, and temperature on Masaya volcano, Nicaragua. *Geophys. Res. Lett*, 30(15), 1–4.
- Linde, N., Jougnot, D., Revil, a., Matthäi, S. K., Arora, T., Renard, D., & Doussan, C. (2007). Streaming current generation in two-phase flow conditions. *Geophysical Research Letters*, 34(3), L03306- L03311.
- Linde, N., & Revil, A. (2007). Inverting residual self-potential data for redox potentials of contaminant plumes. *Geophys. Res. Lett*, 34, L14302.
- Lorne, B., Avouac, J., & Perrier, F. (1999). Streaming potential measurements 1. Properties of the electrical double layer from crushed rock sample. *Geophysical Research*, 104, 17857–17877.
- Lovley, D. R., Chapelle, F. H., & Woodward, J. C. (1994). Use of dissolved H₂ concentrations to determine distribution of microbially catalyzed redox reactions in Anoxic groundwater. *Environ. Sci. Tech*, 28(7), 1205–1210.
- MacPhee, S. L., Gerhard, J. I., & Rein, G. (2012). A novel method for simulating smoldering propagation and its application to STAR (Self-sustaining Treatment for Active Remediation). *Environmental Modelling & Software*, 31, 84–98.
- Magnuson, J. K., Stern, R. V., Gosset, J. M., Zinder, S. H., & Burris, D. R. (1998). Reductive dechlorination of tetrachloroethene to ethene by two-component enzyme pathway. *Appl. Environ. Microbil.*, 64(4), 1270–1275.
- Marshall, D. J., & Madden, T. R. (1959). Induced Polarization, A study of its cause. *Geophysics*, XXIV(4), 790–816.

- Matsushima, N., Michiwaki, M., Okazaki, N., Ichikawa, R., Takagi, A., & Nishida, Y. (1990). Self-Potential Studies in Volcanic Areas (2) -Usu , Hokkaido Komagatake and Me-akan-. *Geophysics*, 8(5), 465–477.
- Mauri, G., Williams-Jones, G., & Saracco, G. (2010). Depth determinations of shallow hydrothermal systems by self-potential and multi-scale wavelet tomography. *Journal of Volcanology and Geothermal Research*, 191(3-4), 233–244.
- Mendonça, C. A. (2008). Forward and inverse self-potential modeling in mineral exploration. *Geophysics*, 73(1), F33–F43.
- Merzhanov, A. G., & Khaikin, B. I. (1988). Theory of combustion waves in homogeneous media. *Progress in Energy and Combustion Science*, 14(1), 1–98.
- Minsley, B. J. (2007). *Modeling and Inversion of Self-Potential Data by*. Massachusetts Institute of Technology.
- Minsley, B. J., Sogade, J., & Morgan, F. D. (2007). Three-dimensional self-potential inversion for subsurface DNAPL contaminant detection at the Savannah River Site, South Carolina. *Water Resources Research*, 43(4), W04429– W04442.
- Naudet, V., Revil, a., Rizzo, E., Bottero, J.-Y., & Bégassat, P. (2004). Groundwater redox conditions and conductivity in a contaminant plume from geoelectrical investigations. *Hydrology and Earth System Sciences*, 8(1), 8–22.
- Naudet, V., & Revil, A. (2005). A sandbox experiment to investigate bacteria-mediated redox processes on self-potential signals. *Geophysical Research Letter*, 32, L11401- L11404.
- Naudet, V., Revil, A., Rizzo, E., Bottero, J. Y., & Begassat, P. (2004). Groundwater redox conditions and conductivity in a contaminant plum from geoelectrical investigations. *Hydrol. Earth. Syst. Sci*, 8(1), 8–22.
- Nishida, Y., Matsushima, N., & Goto, A. (1996). Self-Potential Studies in Volcanic Areas (3) -Miyake-jima, Esan and Usu-. *Geophysics*, 10, 63–77.
- Nishida, Y., & Tomiya, H. (1987). Self- Potential Studies in Volcanic Areas (1)-Usu Volcano-. *Geophysics*, 8(2), 173–190.
- Nourbehecht, B. (1959). *Irreversible thermodynamic effects in inhomogeneous media and their applications in certain geoelectric problems*. Massachusetts Institute of Technology.
- Ogilvy, A. A., Ayed, M. A., & Bogoslovsky, V. A. (1969). Geophysical studies of water leakages from reservoirs. *Geophys.Prosp*, 17, 36–62.
- Ohlemiller, T. J. (1985). Modeling of smouldering propagation. *Progress in Energy and Combustion Science*, 11(4), 277–310.

- Ohlemiller, T. J. (2002). CHAPTER 9 Smoldering Combustion. In *SFPE Handbook of Fire Protection Engineering* (pp. 200–210).
- Ohlemiller, T. J., & Lucca, D. A. (1983). An experimental comparison of forward and reverse smolder propagation in permeable fuel beds. *Combustion and Flame*, *54*(1-3), 131–147.
- Pankow, J. F., & Cherry, J. A. (1996). *Dense chlorinated solvents and other DNAPLs ground water*. Portland (Oregon): Waterloo Press.
- Patella, D. (1997). Introduction to ground surface self-potential tomography. *Geophysical Prospecting*, *45*, 653–681.
- Perrier, F., & Pant, S. R. (2005). Noise Reduction in Long-term Self-potential Monitoring with Travelling Electrode Referencing. *Pure and Applied Geophysics*, *162*(1), 165-179.
- Petiau, G. (2000). Second Generation of Lead-lead Chloride Electrodes for Geophysical Applications. *Pure and Applied Geophysics*, *157*(3), 357–382.
- Petiau, G., & Dupis, A. (1980). Noise, temperature coefficient, and long time stability of electrodes for telluric observations. *Geophysical Prospecting*, *28*(1980), 792–804.
- Pironi, P., Switzer, C., Gerhard, J. I., Rein, G., & Torero, J. L. (2011). Self-sustaining smoldering combustion for NAPL remediation: laboratory evaluation of process sensitivity to key parameters. *Environmental Science & Technology*, *45*(7), 2980–2986.
- Pironi, P., Switzer, C., Rein, G., Fuentes, A., Gerhard, J. I., & Torero, J. L. (2009). Small-scale forward smoldering experiments for remediation of coal tar in inert media. *Proceedings of the Combustion Institute*, *32*(2), 1957–1964.
- Pride, S. (1994). Governing equations for the coupled electromagnetics and acoustics of a porous media. *Phys. Rev. B*, *50*(21), 15678–15696.
- Rein, G. (2009). Smoldering Combustion Phenomena in Science and Technology. *International Review of Chemical Engineering*, *1*, 3–18.
- Revil, A. (2002). Comment on “Rapid fluid disruption: A source for self-potential anomalies on volcanoes” by M. J. S. Johnston, J. D. Byerlee, and D. Lockner. *Journal of Geophysical Research*, *107*(B8), 2155.
- Revil, A. (1999). Ionic Diffusivity , Electrical Conductivity , Membrane and Thermoelectric Potentials in Colloids and Granular Porous Media: A Unified Model. *Journal of Colloid and Interface Science*, *522*(212), 503–522.
- Revil, A., & Cerepi, A. (2004). Streaming potentials in two-phase flow conditions. *Geophysical Research Letters*, *31*(11), L11605- L11609.

- Revil, A., & Jardani, A. (2013). *The self potential method, theory and applications in environmental Geosciences* (p. 369). Cambridge University press.
- Revil, A., Karaoulis, M., Johnson, T., & Kemna, A. (2012). Review: Some low-frequency electrical methods for subsurface characterization and monitoring in hydrogeology. *Hydrogeology Journal*, 20(4), 617–658.
- Revil, A., Karaoulis, M., Srivastava, S., & Byrdina, S. (2013). Case History Thermoelectric self-potential and resistivity data localize the burning front of underground coal fires. *Geophysics*, 78(5), 259–273.
- Revil, A., & Linde, N. (2006). Chemico-electromechanical coupling in microporous media. *Journal of Colloid and Interface Science*, 302(2), 682–94.
- Revil, A., Linde, N., Cerepi, A., Jougnot, D., Matthäi, S., & Finsterle, S. (2007). Electrokinetic coupling in unsaturated porous media. *Journal of Colloid and Interface Science*, 313(1), 315–27.
- Revil, A., Naudet, V., Nouzaret, J., & Pessel, M. (2003). Principles of electrography applied to self-potential electrokinetic sources and hydrogeological applications. *Water Resources Research*, 39(5), SBH1–SBH15.
- Revil, A., Pezard, P. A., & Glover, P. W. J. (1999). Streaming potential in porous media: 1. Theory of the zeta potential. *Journal of Geophysical Research*, 104(B9), 20021–20031.
- Reynolds, J. M. (1997). *An introduction to Applied and Environmental Geophysics* (pp. 191–521). John Wiley & Sons Ltd.
- Risgaard-Petersen, N., Revil, A., Meister, P., & Nielsen, L. P. (2012). Sulfur, iron-, and calcium cycling associated with natural electric currents running through marine sediment. *Geochimica et Cosmochimica Acta*, 92, 1–13.
- Rizzo, E., Suski, B. and Revil, A. (2004). Self-potential signals associated with pumping tests experiments. *Journal of Geophysical Research*, 109(B10), B10203- B10217.
- Salman, M. (2012). *Smoldering of vegetable oil for remediation of trichloroethylene contaminated soil*. University of Western Ontario.
- Sasai, Y., J., Zlotnicki, Y., Nishida, P., Yvetot, P., Morat, H., Murakami, H., ... Sekiguchi, W. (1997). Electromagnetic Monitoring of Miyake-jima Volcano, Izu-Bonn Arc, Japan: Preliminary Report. *Geomagn. Geoelectr.*, 49, 1293–1316.
- Sato, M., & Mooney, H. M. (1960). The electrochemical mechanism of sulfide self potentials. *Geophysics*, 25, 226–249.
- Schmidt, R., Gudbjerg, J., Sonnenborg, T. O., & Jensen, K. H. (2002). Removal of NAPLs from the unsaturated zone using steam: prevention of downward

- migration by injecting mixtures of steam and air. *Journal of Contaminant Hydrology*, 55(3-4), 233–260.
- Scholes, G. C. (2013). *Ignition method development and first field demonstration of In Situ smouldering remediation*. University of Western Ontario.
- Sharma, P. V. (1997). *Environmental and Engineering geophysics*. Cambridge University press.
- Sheffer, M. R. (2007). *Forward modelling and inversion of streaming potential for the interpretation of hydraulic conditions from self-potential data*. The University of British Columbia.
- Sousa, C. D. (2001). Contaminated sites: The Canadian situation in an international context. *Journal of Environmental Management*, 62(2), 131–154.
- Stegemeier, G. L., & Vinegar, H. J. (2001). Thermal conduction heating for in situ thermal desorption of soils. In *Hazardous & Radioactive Waste Treatment Technologies Handbook* (pp. 1–37).
- Suski, B., Rizzo, E., & Revil, a. (2004). A Sandbox Experiment of Self-Potential Signals Associated with a Pumping Test. *Vadose Zone Journal*, 3(4), 1193–1199.
- Switzer, C., Pironi, P., Gerhard, J. I., Rein, G., & Torero, J. L. (2009). Self-Sustaining Smoldering Combustion: A Novel Remediation Process for Non-Aqueous-Phase Liquids in Porous Media. *Environmental Science & Technology*, 43(15), 5871–5877.
- Telford, W. M., & Sheriff, R. E. (1990). *Applied Geophysics* (p. 770). Cambridge University press.
- Torero, J. L., & Fernandez-Pello, A. C. (1996). Forward Smolder of Polyurethane Foam in a Forced Air Flow. *Combustion and Flame*, 106(1-2), 89–109.
- US EPA. (2004). *In Situ Thermal Treatment of Chlorinated Solvents: Fundamentals and Field Applications*, EPA 542/R-04/010. Office of Solid Waste and Emergency Response (p. 145).
- Vogel, T. M., Criddle, C. S., & Mccarty, P. L. (1987). Transformation of halogenated aliphatic-compounds. *Environ. Sci. Tech*, 21(8), 722–736.
- Wang, M., & Revil, A. (2010). Electrochemical charge of silica surfaces at high ionic strength in narrow channels. *Journal of Colloid and Interface Science*, 343(1), 381–386.
- Williams, K. H., Ntarlagiannis, D., Slater, L. D., Dohnalkova, A., Hubbard, S. S., & Banfield, J. F. (2005). Geophysical imaging of simulated microbial biomineralization. *Environ. Sci. Tech*, 39(19), 7592–7600.

- Yamashita, S. (1961). The Electromotive Force Generated within the Ore body by the Temperature Difference. *Min. Coll., Akita Univ., 1*, 69–78.
- Zablocki, C. J. (1975). Mapping thermal anomalies on an active volcano by the self potential method. In *2nd U.N. Symposium on the Development and Use of Geothermal Resources* (pp. 1299–1309). San Francisco, California.
- Zlotnicki, J., Boudon, G., & Viode, J. P. (1998). Hydrothermal circulation beneath Mount Pelee inferred by self potential surveying . Structural and tectonic implications. *Volcanology and Geothermal Research, 84*, 73–91.
- Zlotnicki, J., & Nishida, Y. (2003). Review on morphological insights of self-potential anomalies on volcanoes. *Surveys in Geophysics, 24*, 291–338.
- Zohdy, A. A. R., Anderson, L. A., & Muffler, L. J. . (1973). self-potential and induced polarization surveys of a vapour-dominated geothermal system. *Geophysics, 38*(6), 1130–1144.

Chapter 3

3 Self-Potential Technique for Monitoring Self-sustaining Treatment for Active Remediation (STAR)

3.1 Introduction

Non-Aqueous Phase Liquids (NAPLs) are a class of industrial chemicals that represent one of the most problematic sources of soil and groundwater contaminants worldwide. The NAPLs most common at contaminated sites include chlorinated solvents and hydrocarbons such as creosote, coal tar and crude oil (Pankow & Cherry 1996). NAPLs are often found in the soil above and below the water table as a separate (oil) phase. This 'source zone' can generate a hazardous, long term vapour plume in the unsaturated zone and groundwater plume in the saturated zone (Kavanaugh et al., 2003). Remediation of sites contaminated with NAPLs is challenging due to their physical and chemical properties and the difficulties in locating and accessing them in the subsurface (Kueper et al., 1993). Available remediation techniques are often not ideal because they are typically either fast but expensive and energy intensive (e.g., excavation and disposal to a hazardous waste landfill, thermal treatment) or slow and incomplete (e.g., biodegradation) (Kavanaugh et al., 2003; US EPA 2004)

Self-sustaining Treatment for Active Remediation (STAR) (Switzer et al., 2009; Pironi et al., 2009; Pironi et al., 2011) is an emerging remediation technique that destroys NAPLs where they reside in the subsurface (i.e., in situ). The process is based on smoldering combustion. Smoldering is an exothermic, flameless, oxidation reaction that occurs where oxygen diffuses into the surface of the burning fuel (e.g., charcoal in a barbeque). Released heat from the reaction heats adjacent fuel, resulting in a self-propagating smoldering front (Ohlemiller 1985). The smoldering combustion of NAPLs as a remedial process was illustrated by Switzer et al. (2009) for a range of contamination types, saturations and soil types. Pironi et al. (2011) studied the effect of air flux and fuel saturation on the propagation velocity for crude oil and coal tar embedded in a porous medium. Chlorinated solvent-contaminated soil was treated successfully by using vegetable oil as supplementary fuel for smoldering (Salman, 2012).

The potential of STAR in the field has been studied recently (Scholes 2013). Several in situ pilot tests have been conducted at a former industrial site contaminated by coal tar. Hot air injection led to ignition within a few hours in the immediate vicinity (30 cm) of the pilot well, and the reaction propagated outwards in a self-sustaining manner for the next 10 days with the injection of unheated air. In the shallow test (3 m below ground surface) 3,728 kg of coal tar were destroyed, while in the deep test (8 m below ground surface) 864 kg of coal tar were destroyed. Successful smoldering led to 99.3% and 97.3% coal tar mass reductions in the treated area, respectively (Scholes 2013). Self-sustained smoldering was demonstrated as a successful remedial action and currently, this technique is preceded to full scale application at this site. However, tracking the smoldering front position in the field was limited due to number of inserted thermocouples.

Successful performance of a remedial action depends on accurate source zone and site characterization and also temporal and post-remediation monitoring (Kavanaugh et al., 2003). Monitoring well and soil sampling are standard monitoring tools; however, their application is limited because of low sampling density and low spatial resolution. Non-invasive geophysical techniques, widely applied in other contexts such as hydrogeology and resource development, could play a valuable role in monitoring remediation approaches (Wilson et al., 2009). The self-potential (SP) technique is here suggested as a promising tool for monitoring the smoldering process in STAR since it is associated with elevated temperature in the subsurface.

SP is a passive geophysical technique that measures naturally occurring voltage differences in the ground. The sources of the observed currents could be varied, including streaming potential, thermoelectric potential or diffusion potential (Revil & Jardani 2013). Thermoelectric potential is generated electrical potential due to the presence of a heat source in the ground (Revil 1999). SP is extensively used for mapping high temperature zones in geothermal and volcanic areas (Corwin & Hoover 1979; Zlotnicki & Nishida 2003). Also, the heat front in a thermal oil recovery flood occurring 150 m underground was tracked at the surface by SP profiling (Dorfman et al., 1977). Revil et al. (2013) and Karaoulis et al. (2014) illustrated the potential of SP for tracking the

burning front position in coal-seam fires. Those studies demonstrated the joint inversion of resistivity and SP data for locating the position of the burning front in a 2 to 4 m thick coal formation at a depth of about 10 m. The burning position was corroborated by a measured thermal anomaly (Karaoulis et al., 2014). In all of these studies, the thermoelectric effect was considered the dominant source of voltage variation from background.

STAR, in generating a moving burning front at temperatures between 500 °C and 1000 °C, could be expected to generate a substantial thermoelectric potential. However, the total electric current density could also be affected by streaming potential due to water movement. Complications in analyzing SP signals could arise, particularly at the scale of laboratory experiments, due to overlap of voltage generating sources in a conductive media (Revil & Linde, 2006).

Revil et al. (2013) described the multi-pole decomposition of a thermoelectric source at location P with respect to the origin of the heat source (O), OP=R, in three-dimensional (3D) space, for which the leading term was:

$$\psi^0(R) = \frac{1}{4\pi} \left(\frac{C_{TE}}{\kappa} \right) \frac{1}{R} Q_H \quad 3-1$$

where ψ is the electrical potential (V) (ψ^0 denotes the first term of decomposition called zeroth or monopole), κ is the thermal conductivity of the medium ($\text{W}\cdot\text{m}^{-1}\text{K}^{-1}$), Q_H denotes the heat source (Wm^{-3}), and C_{TE} represents thermoelectric coupling coefficient (VK^{-1}):

$$C_{TE} = \frac{\partial\psi}{\partial T} \quad 3-2$$

where T is the temperature (K). C_{TE} is a constant that depends on the properties of the medium and pore water (both saturation and ionic strength) and is usually measured experimentally. Equations 3-1 and 3-2 suggest that a monopolar anomaly is expected in the far field from a thermoelectric source and the sign of the signal depend on the sign of the C_{TE} .

Table 3-1 illustrates that there are many contradictions between reported C_{TE} in the literature, including opposite signs for coefficients measured in similar materials (e.g., Nourbehecht (1959) and Dorfman et al. (1977) versus Leinov et al. (2010)). There may be several reasons for this. First, it is not clear if the author corrected the SP measurements for the internal temperature dependence of the electrodes (Revil et al., 2013). Secondly, some positive C_{TE} value reported in geothermal regions could be incorrect due to influences of streaming potential (Revil et al., 1999). Correctly isolating and quantifying C_{TE} is clearly important for discerning the thermoelectric influence on SP.

Table 3.1. Reported C_{TE} in The Literature.

Sample	Salinity (M)	C_{TE} (mVC ⁻¹)
Sandstone, sandstone with clay, shale, limestone	Not Reported	0.23-0.48 ^a
Sedimentary rocks Altered volcanic Latite Porphyry Dakota sandstone	Not Reported	0.02-0.475 ^b 0.07-1.36 0.18-0.44 -0.09-1.12
Variety of sandstones	Not Reported	0.49-1.35 ^c
Sandstone, shale	0.372	0.01-0.18 ^d
Not Reported	Not Reported	-0.25-1.5 ^e
Sandstone	Range of salinity	0.04-0.06 ^f
Silica sand, saturated by demineralized water	Not Reported	-0.5 ^g

a: Marshall & Madden, 1959

b: Nourbehecht, 1959

c: Dorfman et al., 1977

d: Fitterman & Corwin, 1982

e: Zlotnicki & Nishida, 2003

f: Leinov et al., 2010

g: Revil et al., 2013

The main objective of this study was to evaluate the potential of the SP technique as a non-intrusive monitoring tool for identifying the subsurface combustion front during STAR. First, the polarity and magnitude of thermoelectric self-potential was investigated over a range of experimental conditions such as heat source types, water contents and sand sizes. The results were compared to published results for thermoelectric coupling

coefficient. Then SP measurements were conducted during a set of laboratory scale STAR experiments. The generated voltage as a function of time - before, during, and after the smoldering combustion reaction - was measured at the surface of a sandbox in a number of locations. In addition, the dependence of the magnitude of the observed SP anomaly on the distance between the smoldering front position and the SP measuring stations was quantified.

3.2 Materials and Methodology

Two uniform sands were used for the experiments: coarse (#12ST, Bell & Mackenzie, mean diameter = 0.88 mm) and fine (#550, Bell & Mackenzie, mean diameter = 0.212 mm). Both sands are mainly silicon dioxide (>99.6%). The compacted porosity for coarse and fine sands were 0.40 and 0.35, respectively. Canola oil was used as a non-toxic NAPL in the experiments. In the second series of experiments, canola oil occupied 25% of the coarse sand pore volume (64 g canola oil /kg sand) in the contaminated region. The physical properties of canola oil are summarized in Table 3-2.

Table 3.2. Physical Properties of Canola Oil.

Parameter	Value
Density (Kg/m ³ ; at 20°C)	920.2 ^a
Viscosity (Kinematic at 20°C, mm ² /sec)	93.99 ^a
Smoke Point (°C)	225 ^b
Specific Heat (J/kg. °C)	1.834 ^a
Thermal Conductivity (W/m°K)	0.166 ^a

a: Rojas et al., 2013

b: Gunstone, 2011

Two series of experiments were performed. In the first series (Heating1 to Heating4), the polarity and amplitude of the SP anomaly in the presence of a temperature gradient was investigated for different (non-smoldering) heat sources, sand types and water contents. In the second series (Smoldering1 to Smoldering5), SP measurements were performed during the application of STAR. The goal of the first series of experiments, detailed in Table 3-3, was to (i) validate the experimental setup against the published results of Revil et al. (2013), and (ii) quantify thermoelectric potential coupling coefficient (C_{TE}) for

various scenarios. The experimental apparatus and electrode stations are shown in Figure 3.1. The first series of experiments were conducted in a box that was 60 cm long x 30 cm wide x 40 cm deep made of high-density polyethylene, which ensured no interference with electrical field.

Table 3.3. Experiments for Measuring Thermoelectric Coupling Coefficient.

Experiment	Sand type	Heat source	Water content (%)
Heating1	Coarse sand	FRH	DI water, 100 %
Heating2	Fine sand	FRH	DI water, 100 %
Heating3	Fine sand	Heater	DI water, 100 %
Heating4	Fine sand (Repeated two times)	Heater	DI water, 30%

A flameless ration heater (FRH) was the heat source in Heating1 and Heating2. FRH is a water-activated oxidation of magnesium-iron-salt powder; the powder mixed with water can release approximately 350 kJ of heat per kilogram (Tocci & Viehland 1996). This represents the most straightforward system because this type of heater does not change the electrical conductivity of water around the reaction region (Revil et al., 2013). In Heating1, the box was filled with coarse sand saturated by deionized water, achieved by slowly pumping in water at the box's base to displace air upwards and minimize trapped air. In all experiments, deionized water was used in order to fix the water-related electrical conductivity. Once saturated, the background voltage was measured before introducing the heat source to the sand. Then, in Heating1, 9 gr of dried FRH powder was quickly inserted at a depth of 20 cm (Figure 3.1). Upon contact with the water, the exothermic chemical reaction began generating heat.

Non-polarizing Cu/CuSO₄ electrodes (6B pointed tip portable copper-copper sulfate reference electrode, TINKER and RASOR, CA, USA) were used for the voltage measurements in all experiments. In Heating1, one of the electrodes was fixed in the corner of the box as reference electrode and the other one was moved so as to measure SP at the sand surface along a single profile (E1-E9, see Figure 3.1). Voltage measurements involved recording the difference between the measurement electrode and the reference per second using a datalogger (CR300 Micrologger, Campbell Scientific). The electrode

was kept at each station for 30 s; the first 10 s of data were eliminated and the mean of the final 20 s was reported for each station (see Appendix A for detailed data and tests showing the reliability of this method). The temperature distribution at the electrode stations and at 20 cm depth along the profile (T1-T9, Figure 3.1) were determined using K-type thermocouples (Omega Ltd, Canada) connected to a datalogger (Multifunction Switch/Measure Unit 34980A, Agilent Technologies). Temperatures were recorded continuously and the SP profile was measured 15 minutes after initiating the heat source. The temperature measurements at the surface revealed that the sand temperature adjacent to the reference and moving electrodes temperature were constant (21 °C), avoiding any voltage associated with internal electrode temperature changes. C_{TE} was then determined by dividing the voltage difference (measured at the surface in the station located exactly above the heat source) by observed temperature difference (at heater depth) (Revil et al., 2013). Heating2 used fine sand instead of coarse sand to investigate the effect on measured C_{TE} . In this experiment 12 gr of FRH was introduced at the same location as in Heating1 (Figure 3.1).

To examine the effect of heat sources, an electrical heater – identical to that used in published STAR column studies (Switzer et al., 2009; Pironi et al., 2009) - was used in Heating3 and Heating4. The electric heater (120 V, 450 W, 3.25mm square cross section, 762 mm long, Zesta Engineering Ltd, Canada) was shaped into a flat spiral 8 cm in diameter. The heater was connected to an AC variable power supply (Model 3PN1010B, Staco Energy Products Co, US) and an energy meter (EM100, Blue Planet Ltd, China). In Heating3, the heat source position, measuring stations positions and water content was identical to Heating2. To examine the influence of water saturation, Heating4 was identical to Heating3 but the water saturation was 30%. This was achieved by pre-mixing the sand with a water volume equal to 30% of the sand pore volume in batches using a kitchen mixer. 30% saturation was determined through numerous trials to be practical at the experimental scale (see Appendix B); while smoldering can propagate below the water table in the field (Scholes 2013), fully saturated conditions extinguish the reaction at this small scale.

The second series of experiments, Smoldering1 to Smoldering5, were conducted to evaluate the SP technique potential in detecting STAR (see Table 3-4). The experimental setup, shown in Figure 3.2, is similar to that of the first series but has a few differences. The second series of experiments were conducted in polyethylene box which was 80 cm long x 50 cm wide x 40 cm deep. In particular, an air diffuser was placed at the bottom of the box just below the electric heater. The air diffuser was connected to laboratory compressed air by a mass flow meter (FMA5544, 0-500 L/min, Omega Ltd, Canada). A 1 cm layer of clean coarse sand was added to cover the air diffuser and the heater. Just above, coarse sand with 25% oil saturation was packed in an 8 cm diameter cylindrical shape to a height of 10 cm (see Appendix C for packing procedure).

The experimental conditions were otherwise similar to Heating4: the rest of the apparatus was filled with clean, fine sand saturated to 30% with deionized water, including 20 cm between the top of the smoldering zone and the surface. A multipoint thermocouple was inserted along the central vertical axis of the oil/sand region, measuring temperature at 1 cm intervals starting 1 cm above the heater (TC1); the first 10 readings (TC1-TC10) were in the oil/sand region and next five (TC11-TC15) were in the sand above the smoldering region. The air Darcy velocity (volumetric flow rate of air divided by cross-sectional area of oil/coarse sand cylinder) was 15 cm/s in all cases.

Voltage measurements were performed at the surface of the sand. A reference electrode was located at the corner of the sandbox furthest from the oil/sand region. Generally two measuring electrodes E1 and E2 were used and their deployment was specific to each experiment as illustrated in Figure 3.3. At the start of each experiment, background voltages for each station were collected for 30 minutes to evaluate the stability of the background voltage over time. Background voltage was measured until a stable signal was observed (see Appendix A).

Standard STAR procedure was employed to start and continue a self-sustaining smoldering reaction in each case (Switzer et al., 2009; Pironi et al., 2011). Briefly, the power to the electric heater was progressively increased for about 70 minutes after which air flow was initiated to ignite the reaction. The power to the heater was terminated 5

minutes later, but the air flow was kept constant until the end of the experiment. The smoldering reaction typically required approximately 20 min to propagate the 10 cm height of the oil/sand region and heat dissipation and cooling typically required a further 150 min.

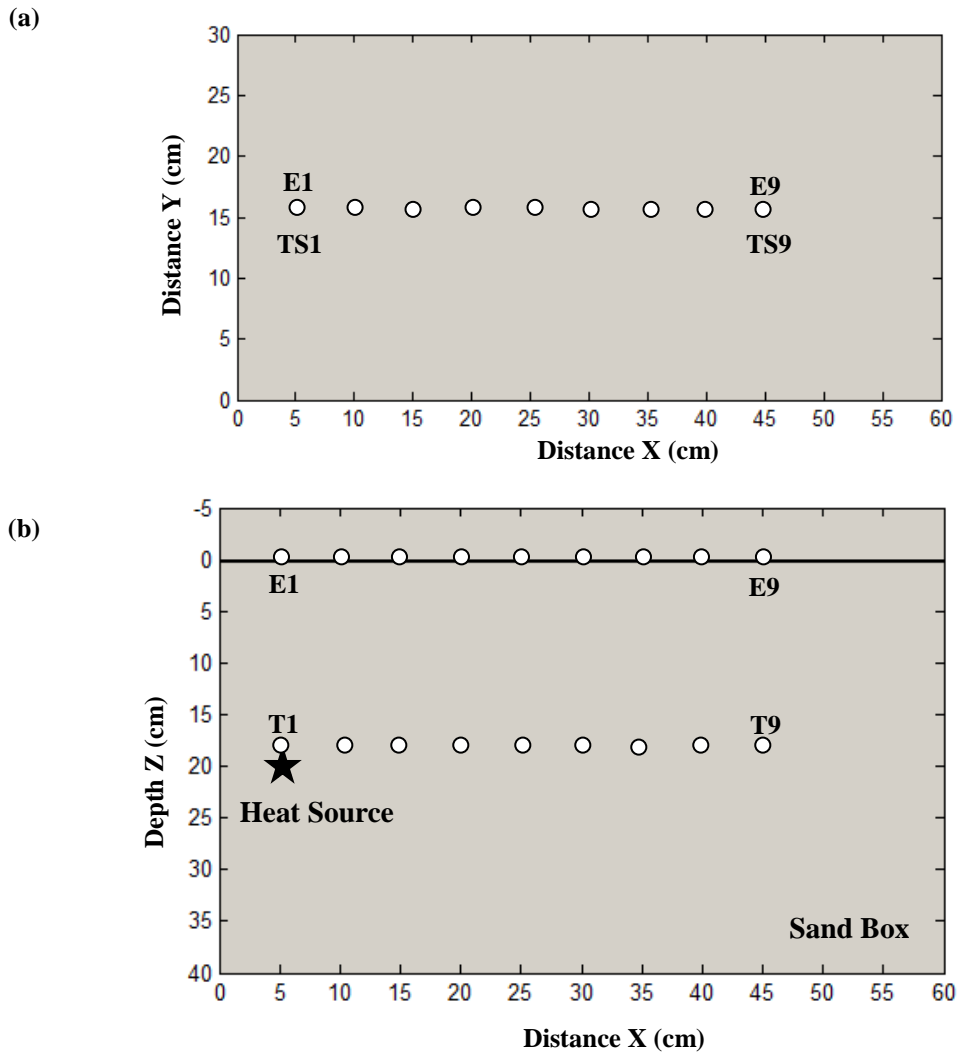


Figure 3.1. Experimental setup for measuring thermoelectric coupling coefficient in Heating1 – Heating4. (a) Apparatus plan view showing the position of reference electrode and SP measuring stations (E1-E9) and sand surface temperature measuring stations (TS1-TS9). (b) Apparatus cross-section showing the position of the heat source and depth temperature measuring stations (T1-T9).

In Smoldering1, SP distribution in space during smoldering was investigated by moving two electrodes through 28 measuring stations on a surface grid (see Figure 3.3). The electrode was kept at each station for 1 minute, and therefore a single snapshot of SP in space required 14 min to complete. The smoldering lasted for 18 min, which means only one snapshot could be completed; since it is demonstrated that SP changes over time during the smoldering period, this experiment only provides an approximation of a snapshot and primarily indicates the distribution of positive and negative anomalies at the surface. In Smoldering2 – Smoldering5, E1 and E2 were fixed, as illustrated in Figure 3.3, to get SP as a function of time during smoldering.

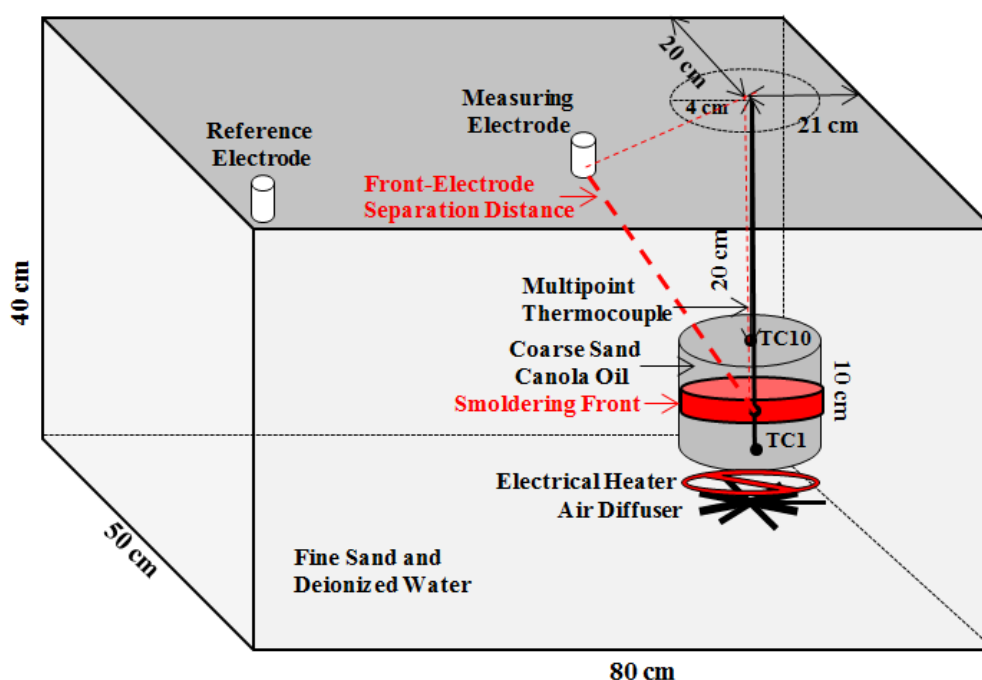


Figure 3.2. Geometry of the sandbox. Sand box is filled with fine silica sand and deionized water (30% water content). Non-polarizing Cu/CuSO₄ electrodes are located at the surface of the sand for voltage measurements. A cylinder of contaminated sand (coarse sand- canola oil) is located in the middle of the fine sand.

**Table 3.4. Performed Experiments for Monitoring STAR by Self-Potential
Technique.**

Experiment number	Distance of measuring electrode from the centre line of oil/sand region in plan view		Experiment goal
Smoldering1	Surface grid of 28 measuring stations		Investigating SP distribution during smoldering period at the surface
Smoldering2	9 cm		Base case Evaluate data repeatability
Smoldering3	9 cm		
Smoldering4	E1	12 cm	Investigating relationship between SP and distance from the smoldering position
	E2	16 cm	
Smoldering5	E1	23 cm	
	E2	25 cm	

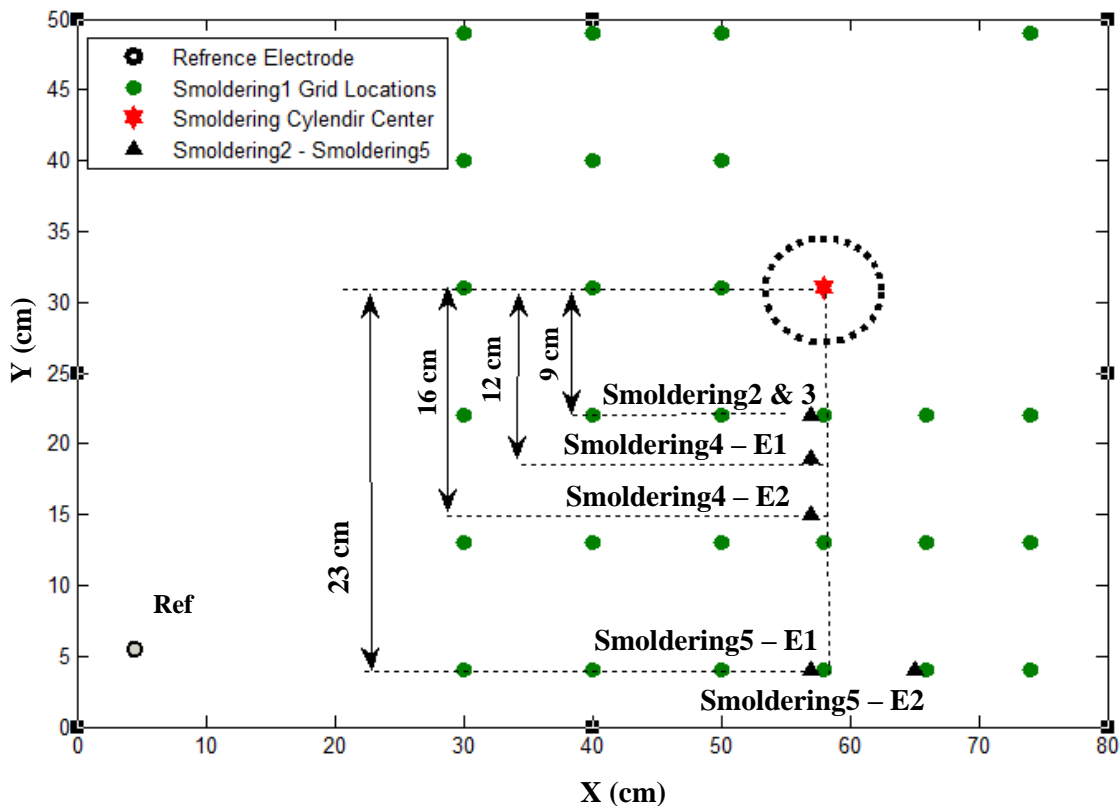


Figure 3.3. Plan view of experimental setup for Smoldering1 – Smoldering5.

SP data processing

SP measurements are typically on the order of a few millivolts in laboratory experiments, so signal to noise ratio requires significant attention. The most common sources of noise in SP measurements are poor contact between the electrodes and sand and electrode drift during the measurements (Reynolds 1997). Metal in the apparatus and poorly performing electrodes are further potential source of noises. The effect of the presence of metal equipment was evaluated by adding experimental equipment step by step and monitoring background voltage changes. A change in background voltage was observed by adding metal equipment; however, the background voltage remained stable over time. This experimental system was designed to minimize noise. SP data recording frequency was 1 s and the average of every 2 recordings was stored. Typical, stable background voltage data from this system is shown in Figure 3.4. The background noise level was checked before starting each test to ensure it was fluctuating within a range of ± 1 mV. No drift was observed in the measured SP data despite at least 30 minutes of background measuring (see Appendix A). The mean background value was recorded and used to shift all subsequent SP data for each test so that results are shown relative to a zero background potential. The measured SP data was smoothed over time. Smoothing was performed using a 100-point (3 min) moving average in MATLAB. The smoothing was discontinued when any boundary condition changed, such as initiating the air, so ensure detection of any potential change in the data's trend. An example of raw and smoothed data is presented in Appendix D.

Significant temperatures at the sand surface, and in particular within the electrode, could affect SP measurement (approximately 0.9 mV per °C, Tinker and Rasor, 2014). In STAR field applications, the scale is such that temperature increases at the surface are unlikely (Scholes 2013); however, in the relatively small experimental apparatus, the proximity of the reaction to the surface could have led to excessive temperature effects on the electrodes. Therefore, a pathway of coarse, dry sand was built leading from the top of the oil/sand (i.e., smoldering) region horizontally to the edge of the box and then vertically up the wall to the surface. This provided a chimney that directed the smoldering hot gas emissions away from the immediate vicinity of the SP measuring stations (not shown in

Figure 3.3 to improve clarity of the other key features). This feature was successful in ensuring that background temperatures at the SP measuring locations never increased more than 50 °C during any experiment which is less than the temperature threshold for Cu/CuSO₄ electrodes. Data is provided for both uncorrected and corrected for the temperature effect, as each provides different information about the subsurface processes. The SP signal was corrected for the temperature effect using temperature correction coefficient for Cu/CuSO₄ electrode.

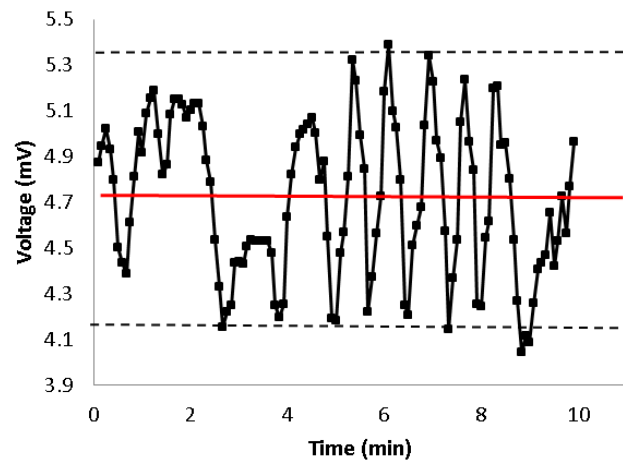


Figure 3.4. SP data sample which shows the fluctuating around an average value for background voltage.

3.3 Results and Discussion

3.3.1 Thermoelectric Coupling Coefficient Measurements

From Heating1 (FRH heat source, 100% saturated coarse sand), the temperature difference at 20 cm depth after 15 min of heating was approximately 15 °C (Figure 3.5a). The voltage anomaly on the surface at the same time was about -7 mV (Figure 3.5b). Recall that this experiment is a close replica of that presented in Revil et al (2013). Figure 3.5, comparing Heating1 to the results of Revil et al. (2013), illustrates that the temperature distribution at depth is similar after 15 min and the SP anomaly above the heat source is similar. The distribution of the voltage difference with distance from the heater has a different shape between the two experiments (Figure 3.5b); this may be due to the different types of electrodes used, different measurement protocol (e.g. shorter

measurement period for each station) or differences in the electrical properties (e.g., ion diffusivity) of the porous media.

The distribution of voltage difference at the surface at two times, 15 and 22 minutes after introducing FRH is illustrated in Figure 3.6a. The thermoelectric coupling coefficient calculation, using the peak voltage differences highlighted in Figure 3.6a, is shown in Figure 3.6b. The C_{TE} was determined to be approximately $-0.47 \text{ mV}^\circ\text{C}^{-1}$. Y intercept in Figure 3.6b is (0,0) which indicates when the temperature gradient is zero, no voltage difference is observed at the surface. This compares well with Revil et al. (2013) calculated C_{TE} which was $-0.5 \text{ mV}^\circ\text{C}^{-1}$. Measured C_{TE} for silica sand saturated with deionized water was negative, therefore in presence of a heat source a negative voltage anomaly is expected at the surface.

In Heating2 (FRH heat source, 100% saturated fine sand) a voltage difference of -3.2 mV was observed at the surface above the heat source corresponding to a 22°C increase at 20 cm depth. By considering 4 times for this electrode position, a best-fit (linear regression) C_{TE} for saturated fine sand was determined to be $-0.15 \text{ mV}^\circ\text{C}^{-1}$ (see Figure 3.7). This is approximately three times less than C_{TE} for coarse sand, which is likely due to the slightly reduced porosity and significantly lower permeability of the fine sand. Ionic diffusion in a porous material is related to the microgeometry (Guo 2012) and ion diffusivity (Revil 1999). Ion diffusivity and membrane potential are known to be reduced with a decrease in porosity and permeability (Revil 1999). In less permeable porous media increases in the tortuosity of the interconnected pore space results in lower ion diffusivity

In Heating3 (Electric heat source, 100% saturated fine sand) the determined C_{TE} of $-0.19 \text{ mV}^\circ\text{C}^{-1}$ (Figure 3.7) was similar to that determined for the FRH heat source, which suggests that the source of the heat (electrical or not) has little influence. In Heating4 (electric heat source, 30% saturated fine sand) a further four-fold reduction in C_{TE} to $-0.05 \text{ mV}^\circ\text{C}^{-1}$ (Figure 3.7) was observed. This can be explained by the increase in the tortuosity for diffusion pathway for ions with increasing air saturation (Revil 1999). Note

that a duplicate experiment of Heating4 was conducted, finding that the measured C_{TE} was repeatable. (See Figure 3.7).

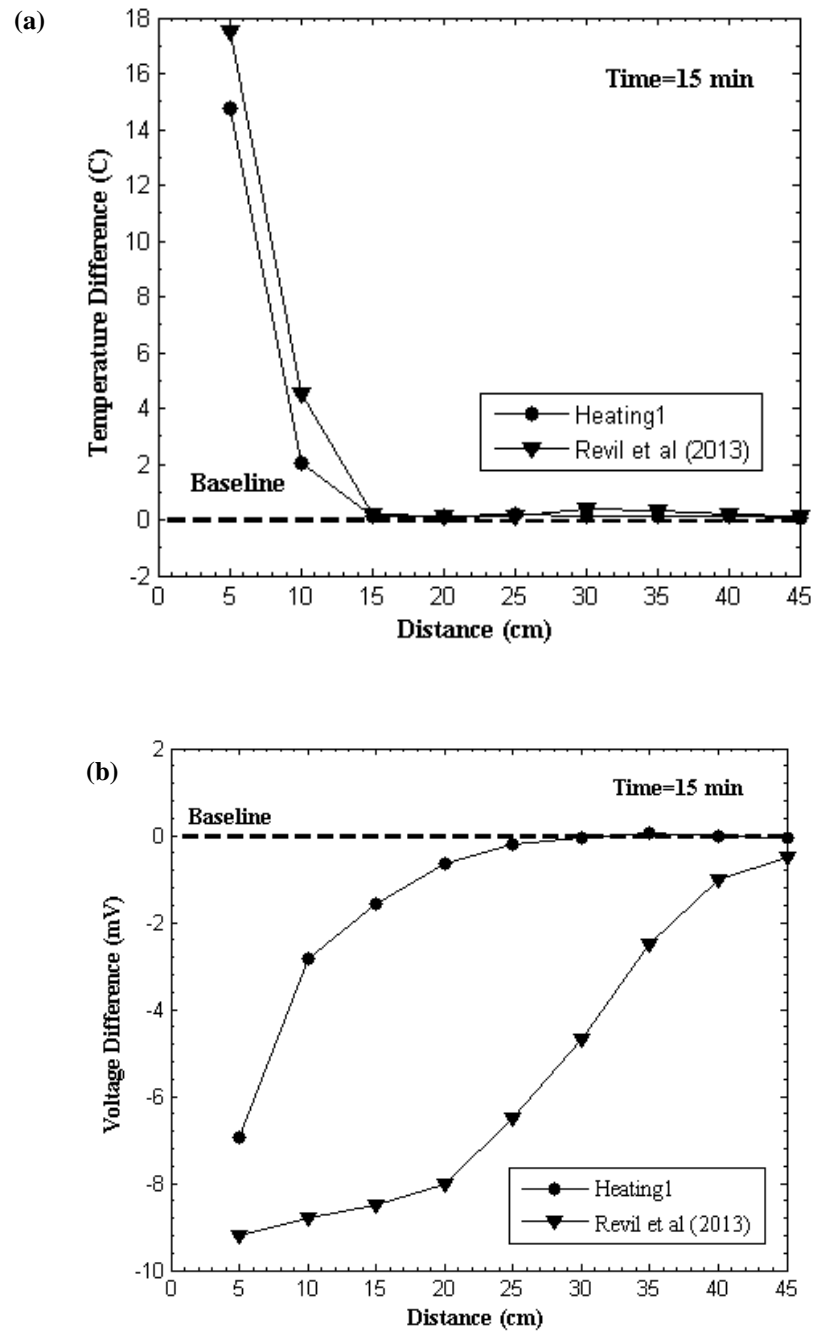


Figure 3.5. (a) Distribution of temperature at depth of 20 cm (b) SP at top of the tank after introducing the heat source ($t=15$ min).

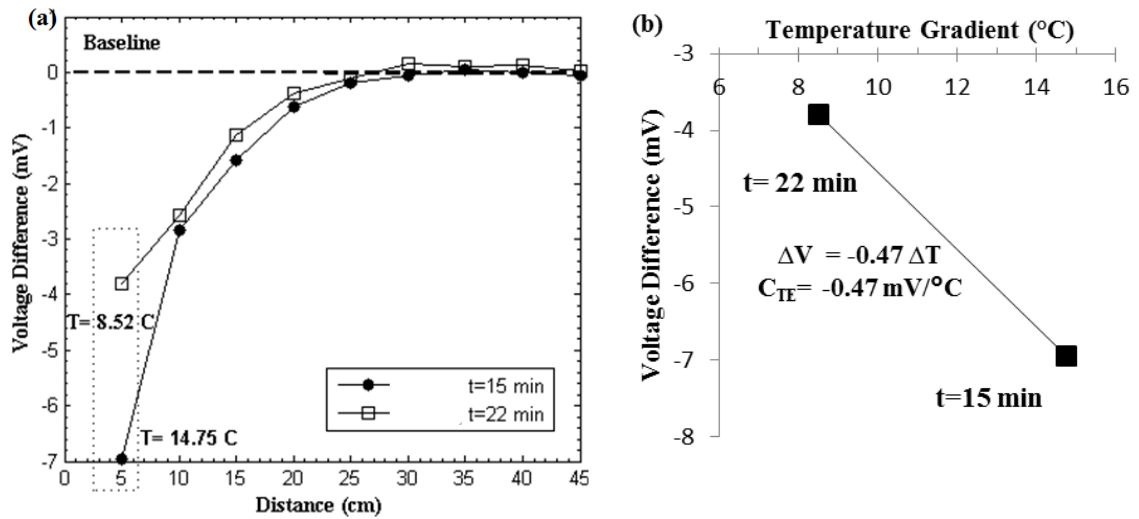


Figure 3.6. (a) SP distribution at top of the tank after introducing the heat source at time 15 and 22 minutes in Heating1. (b) Thermoelectric coupling coefficient calculation using SP measurements exactly above the heat source.

For operational reasons at this scale, the STAR experiments require the use of scenario Heating4 (see Appendix B). This means that the C_{TE} for the STAR experiments is expected to be quite small, perhaps on the order of 10 times less, than observed for conditions of more permeable soil and higher groundwater saturations. As a result, the experimental design is quite conservative, meaning that the magnitude of the SP anomaly observed in these experiments may only be a fraction of that observed in larger, field scenarios.

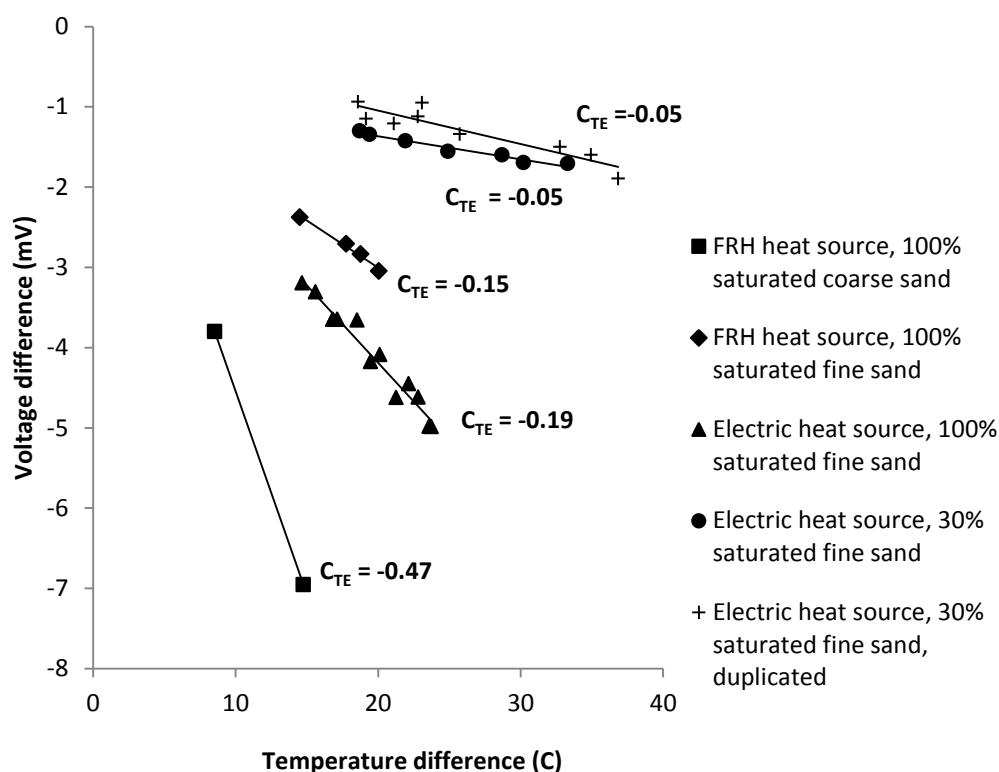


Figure 3.7. Measured C_{TE} for different sand sizes, water contents and heat sources.

3.3.2 Self-potential Anomaly Associated with Smoldering

Smoldering1 was the first of the series of experiments examining SP during smoldering. Temperature-time histories of the 15 thermocouples vertically aligned along the center of the oil/sand region are shown in Figure 3.8; this pattern is very similar for all smoldering experiments in this work and closely matches other NAPL smoldering studies (Switzer et al., 2009; Pironi et al., 2011). The heater was turned on at $t=3$ minutes and the preheating period was approximately 70 minutes. Upon initiating the airflow at $t=73$ minutes, temperature profiles spiked indicating the onset of smoldering. The heater was terminated five minutes after initiating the airflow. As indicated by Figure 3.8, the smoldering period lasted for 18 minutes. A self-sustaining reaction is suggested by the succession of crossing temp-time curves as energy is transferred forwards. The observed peak temperatures are observed to decrease during smoldering in this case, likely because the reaction slightly weakened due to close proximity of water in the experimental system.

Self-sustaining conditions for smoldering are known to be most challenging in small scale experiments and the reaction is generally more robust, even in the presence of significant amounts of water, at larger scales (Switzer et al., 2014). The rate of smoldering propagation was 0.48 cm/s for an air Darcy flux of 15 cm/s, and observed peak temperatures in the smoldering period were in a range of 360-200 °C. Regardless if the reaction was technically self-sustaining or not, it is clear that the smoldering created sustained high temperatures and propagated vertically in space in a manner consistent with smoldering in field systems (Scholes 2013). After all the oil was consumed, the system required 100 minutes for thermocouples to cool back to ambient temperature.

In Smoldering1, SP was mapped at the surface during the smoldering. As illustrated in Figure 3.9a, there is a zone around the cylinder at the surface exhibiting a positive anomaly during the smoldering period. This is likely associated with increased temperature at the surface above the smoldering reaction and also the contribution of streaming potential associated with moving water and/or air; see Appendix E for details of experiments demonstrating the influence of air flow in the absence of heat/smoldering. A positive SP is expected from streaming potential because surface electrical charge (zeta potential) of silica sand in contact with water is negative. This excess of charge is counterbalanced by cations in the electrical double layer. Therefore, upward movement of water due to initiating air can carry positive charge to the surface. Recall, the experimental design aimed to limit the streaming potential in the monitoring zone by providing an alternate air exit pathway. Nevertheless, some water/air migration above the reaction zone was inevitable at this scale.

Figure 3.9b illustrates the distribution of the temperature recorded alongside the SP stations at the surface. The possible temperature effect on voltage readings was removed from data by applying the published temperature correction (Figure 3.9c). Corrected data showed a maximum negative SP anomaly around the smoldering region which diminished with increasing distance from smoldering region. The maximum observed SP anomaly after temperature correction (Figure 3.9c) showed a shift in position compared with the smoldering region center, which is the expected position of the maximum observed SP anomaly. This is due to lack of data at the surface in the immediate vicinity

of the contaminated column (see Fig. 3.9). This is because, in this region, the temperature increase during smoldering exceeded the electrode temperature tolerance. It is noted that, since the surface scan required 14 min to obtain with two moving electrodes during which the reaction was travelling, this is not a true ‘snapshot’; Smoldering1 results are provided mainly to provide a qualitative distribution of SP and temperature at the surface during STAR.

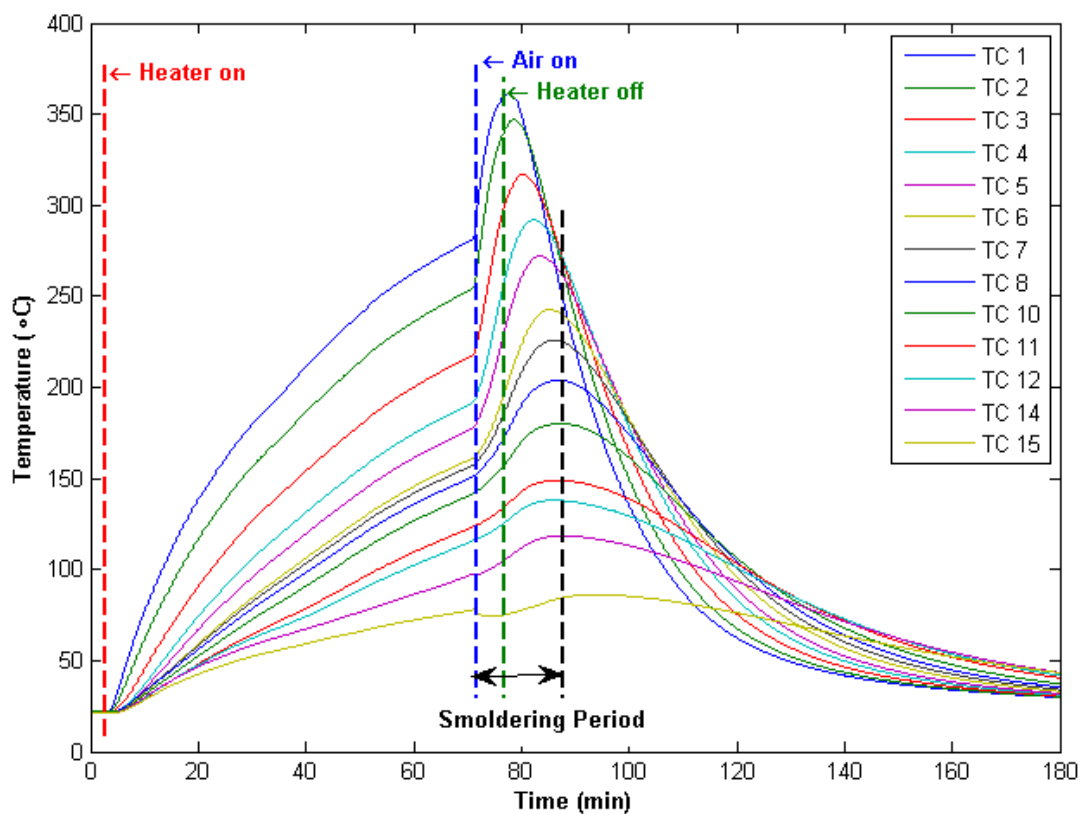
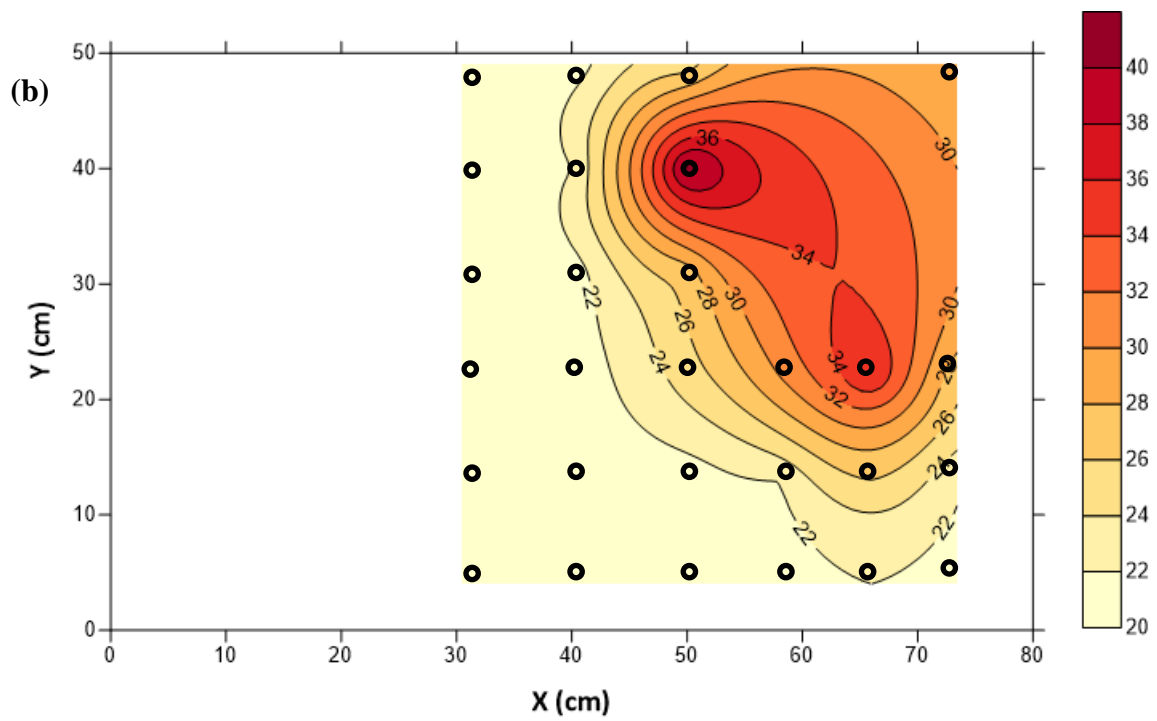
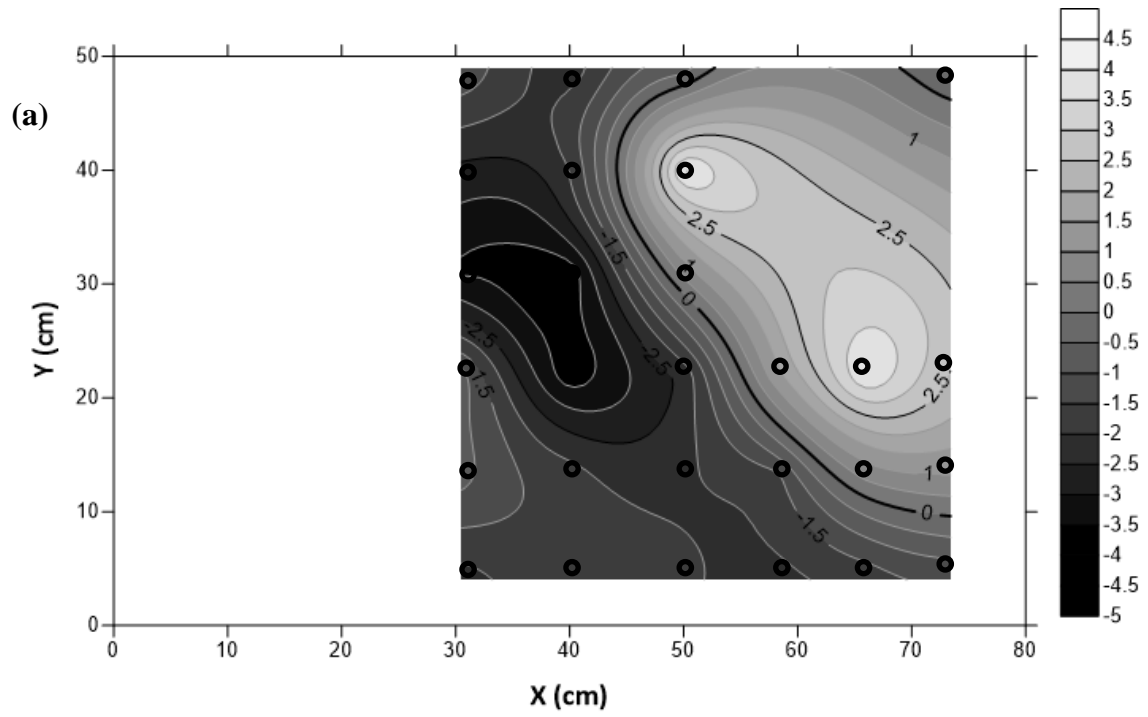


Figure 3.8. Temperature time histories for thermocouples in center of oil/sand cylinder for Smoldering1.



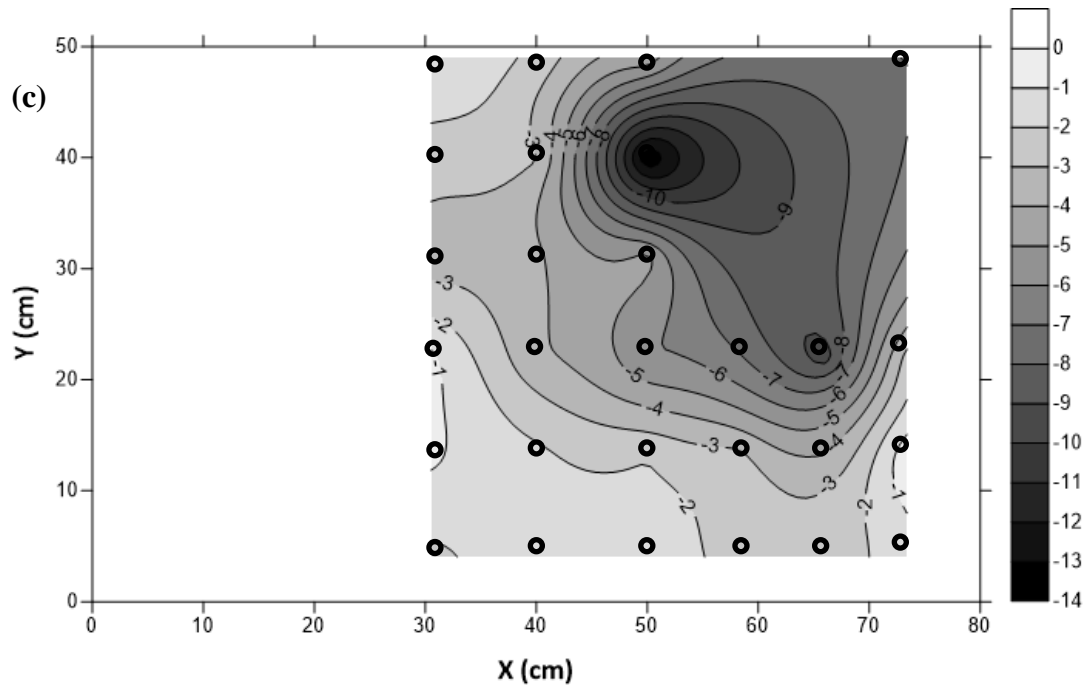


Figure 3.9. (a) A snapshot of the measured voltage difference in the smoldering period at the surface in Smoldering1. Two moving electrodes moved along profiles and collect data during the smoldering period. (b) Temperature distribution at the surface during the smoldering period. (c) A snapshot of the voltage difference in the smoldering period at the surface corrected for the temperature effect. SP measuring stations are shown by dots in the figure.

In Smoldering2, SP was measured as a function of time 9 cm from the center of the oil/sand region (in plan view). The SP anomaly is illustrated in Figure 3.10; The SP data is not corrected for the temperature effect. The SP data can be generally categorized into four phases. In phase one background voltage was stable. Phase two corresponds to the preheating period, during which a steadily increasing negative SP anomaly was observed. This is expected due to the negative C_{TE} observed for this experimental setup, as shown in Heating4. Phase three corresponds to the smoldering period, exhibiting a relatively stable anomaly of -4 mV. A small positive increase in SP, approximately 0.5 mV, is observed immediately upon initiating air flow; this positive displacement is much larger within the footprint of the smoldering region and results in the positive overall SP anomaly noted above. The negative SP anomaly suggests that, like in the heating only

cases, the prominent phenomenon is the thermoelectric effect. In phase four, the SP anomaly recovered to the background value. In this case, the recovery phase started when the last thermocouple in the contaminated sand reached its peak temperature.

The repeatability of SP data in an identical STAR test is examined in Smoldering3. As Figure 3.10 illustrates, the SP anomaly shape and value over the first 3 phases were similar in both experiments. The only difference was during the recovery phase where Smoldering2 exhibited a faster increase in SP and achieved a positive anomaly after the reaction terminated. This was due to higher temperatures at the electrode on the surface, reaching 40 °C whereas in Smoldering3 they reached maximum of 35 °C. Temperature time histories for Smoldering2 and Smoldering3 demonstrate that the former produced higher and more consistent peak temperatures and thus the more significant heating of the surface after the reaction terminated (Appendix F, see Figure F.5). The sensitivity to subtle differences in the reaction are likely due to the close proximity of the electrode to the reaction in these two experiments.

In Smoldering4 SP data were collected in two measuring stations; E1 and E2. E1 and E2 distances from centerline of the oil/sand cylinder in the plan view were 12 and 16 cm, respectively. Temperature histories for 15 thermocouples and SP data of E1 and E2 are presented in Appendix F. The SP measurements over time (not corrected for temperature effect) exhibited a negative anomaly with a maximum of -1 mV during the preheating. The SP appeared to increase in strength (i.e., more negative) corresponding to the upward movement of smoldering front towards the surface in smoldering period. Two different trends were observed in the SP data after smoldering period. For E1, the recovery phase started just after TC10 (the last/highest thermocouple in contaminated zone) reached its peak temperature. For E2, located in distance of 16 cm from the centerline of the contaminated region, the recovery phase did not start immediately after the time that TC10 reached its peak temperature. A stable negative voltage is observed between the recovery phase and smoldering phase which could be associated with lateral and upward propagation of the heat in the sandbox. In Smoldrring5, SP anomalies were measured at the surface at distances of 23 cm (E1) and 25 cm (E2) from the oil/sand region. SP

measurement showed a negatively increasing voltage over time for smoldering period. The same trend as E2 in Smoldering4 was observed after smoldering period.

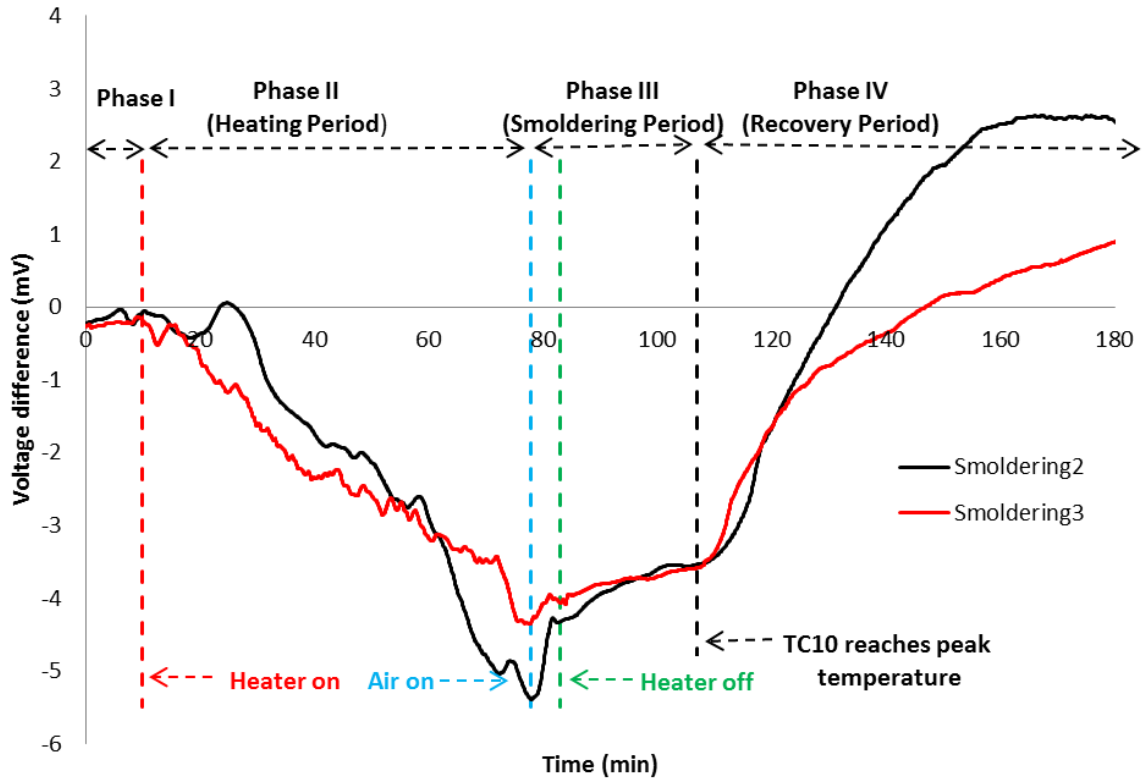


Figure 3.10. Measured SP anomaly over time during STAR test for Smoldering2 and Smoldering3 (not corrected for the temperature effect). Measuring electrode distance from the center of the smoldering region was 9 cm in the plan view. Phase II, III and IV are corresponded to the heating, smoldering and recovery periods respectively.

Smoldering4 and Smoldering5 provided more data on variation of SP anomalies with distance from the smoldering region as a function of time. Figure 3.11 plots these results along with Smoldering2 to get SP versus time at five distances (9, 12, 16, 23, and 25 cm) for otherwise identical experiments. First, it was observed that the maximum negative SP anomaly decreased with increasing distance from the contaminated region. Second, the SP response was observed to shift towards later times with increased distance from the front. Both of these are clearly associated with the distance from the electrode to the heat

front and its peak temperature: during smoldering this front is very hot, relatively narrow and moving primarily upwards, while after smoldering is complete the peak temperature diminishes but lateral heat conduction creates a growing warm zone. Figure 3.12 illustrates the temperature over time for Smoldering1 – Smoldering5 in the same position as SP measuring stations. Corrected measured SP over time for the temperature effect is shown in Figure 3.13. It was observed that measured SP at the surface would be larger in magnitude if the temperature effect eliminated. The effect is related to inner potential of non-polarizing electrodes, which is temperature-dependent, that generates positive SP by increasing temperature of the electrodes.

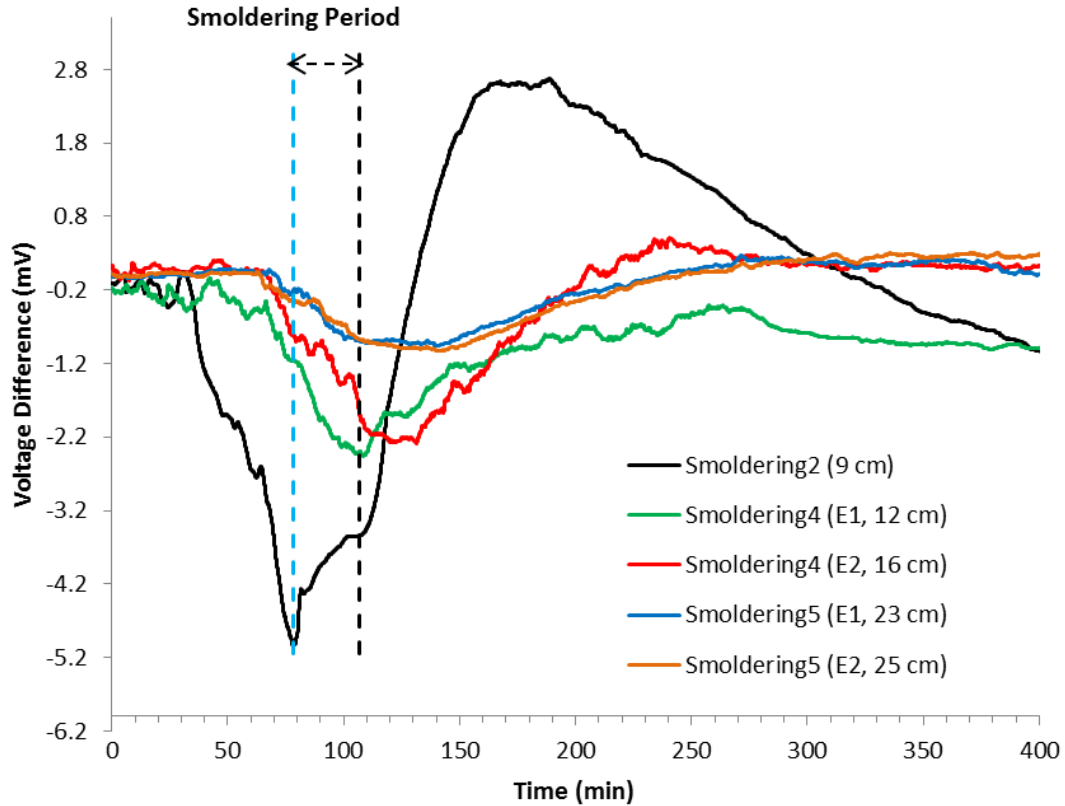


Figure 3.11. Measured SP over time for 5 different distances from the contaminated region being smoldered, compiled from 3 different experiments with otherwise similar conditions (not corrected for the temperature effect).

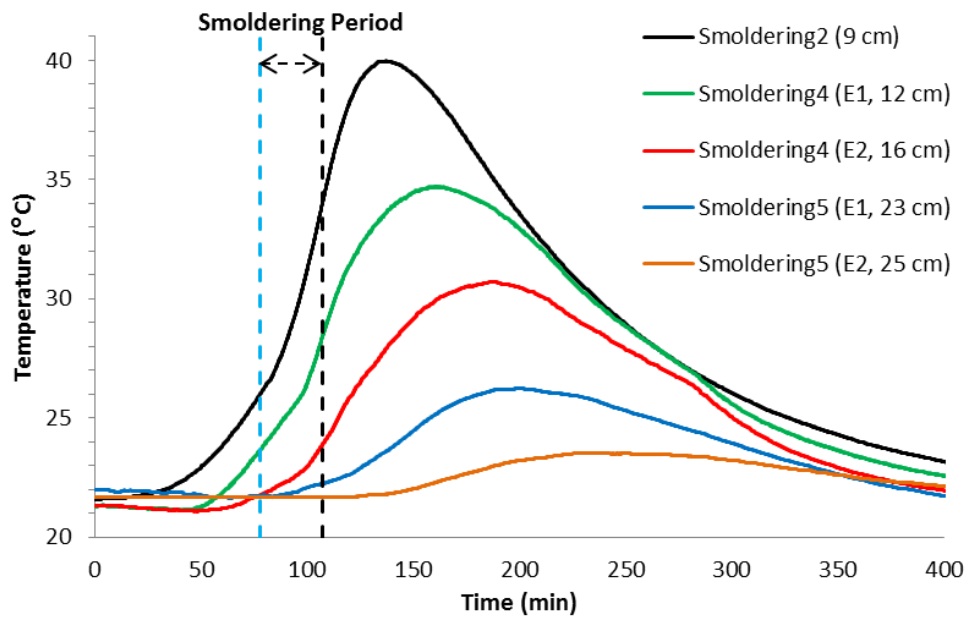


Figure 3.12. Measured temperature over time for 5 measuring SP stations in Smoldering2 – Smoldering5.

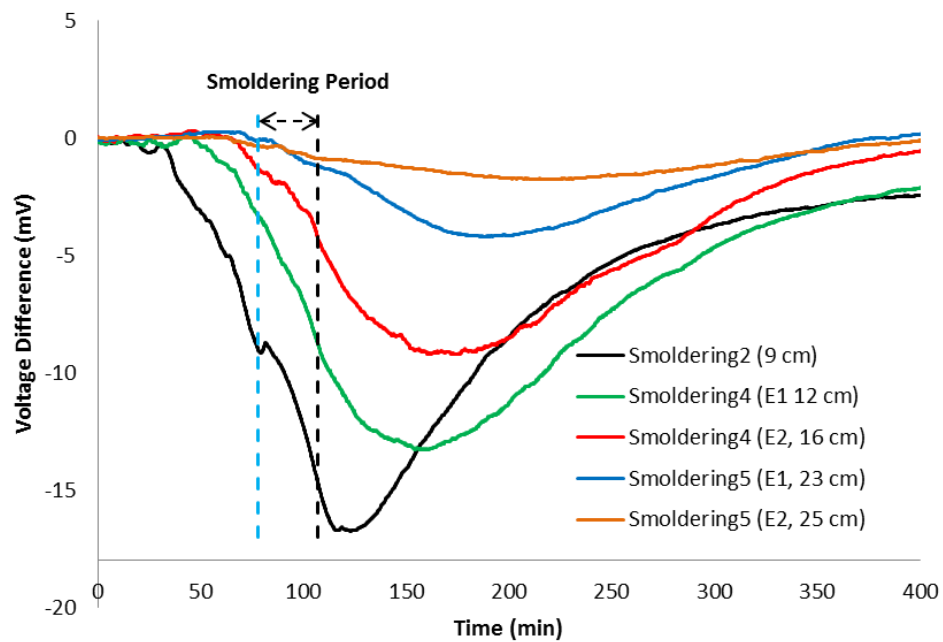


Figure 3.13. Measured SP over time corrected for temperature effect for 5 different distances from the contaminated region being smoldered, compiled from 3 different experiments with otherwise similar conditions.

Both raw and temperature-corrected SP data are provided as both data sets revealed valuable information. The uncorrected signals reveal a change in behavior at the end of smoldering period. However, this is not apparent in the corrected signals because the surface heats up at the same time, causing the voltage anomaly from electrode heating to swamp the thermoelectric influence predominantly in the period after the smoldering is complete. This problem would not be expected, or not be as severe, in the field as (a) the surface is not expected to experience as high temperatures, and (b) the SP anomaly is expected to be of higher magnitude in the field.

A quantified relationship between the location of the electrode and the SP anomaly during the smoldering period was sought. The ‘front-electrode separation distance’ was defined as the straight-line distance between the location of the smoldering front, which varies with time as the front propagates, and an electrode location on the surface; this is defined graphically in Figure 3.2. The smoldering front location was defined as the location of the peak smoldering temperature at a given time. Figures 3.14 and 3.15 plot the ‘front-electrode separation distance’ for all of the electrodes in smoldering period presented in Figure 3.11 except one: Smoldering2 was excluded because, as illustrated in Figure 3.10, some influence of streaming potential was apparent at this distance (9 cm). Therefore, Figure 3.14 focuses on the influence of distance on SP dominated by thermoelectric potential. The quantified relationship was investigated for both raw SP data and SP data corrected for temperature as shown in Figures 3.14 and 3.15, respectively.

Figure 3.14 reveals a strong linear relationship between ‘front-electrode separation distance’ and observed SP anomaly. R-squared for a linear regression of all the data was 0.83, indicating that the majority of the differences in voltage observed could be explained by the distance of the electrode to the smoldering front. A similar analysis, as well as a multivariable analysis, was conducted for the influence of smoldering temperature on the SP anomaly over time; both showed no improvement in the correlation. Adding front temperature to the linear regression caused a minor improvement in R-squared (R-squared=0.84). A similar analysis was conducted for SP data after temperature correction (Figure 3.15). R-squared for linear regression in this

case was 0.75 and it slightly improved to 0.76 by including front temperature in the regression results. The anomaly was relatively insensitive to the smoldering temperature, since the value of C_{TE} in the experiments was found to be quite small due to experimental scale and experimental design. It is expected in the case where C_{TE} be higher; smoldering temperature in the subsurface may play more significant role on the magnitude of the SP anomaly.

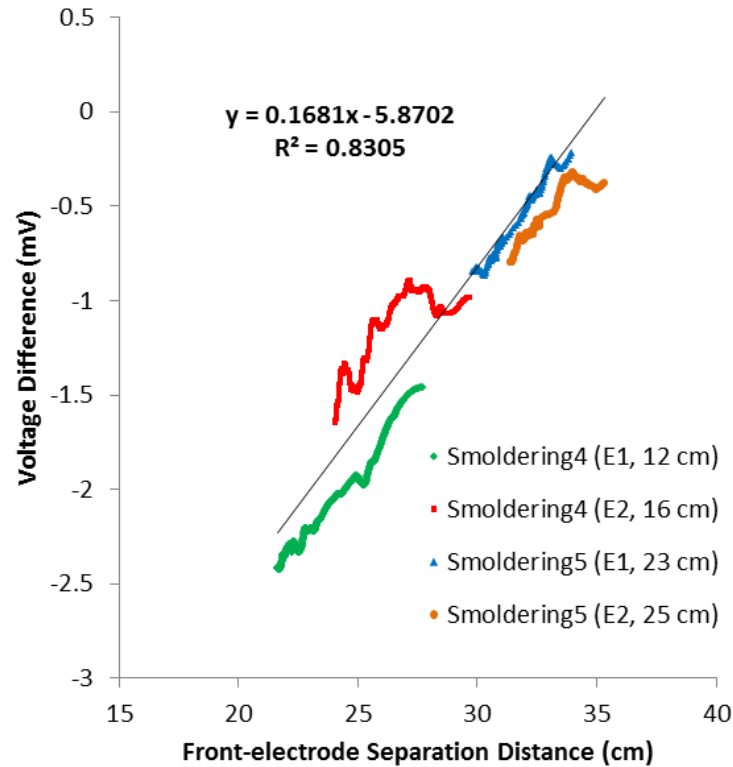


Figure 3.14. Voltage difference over front-electrode separation distance (cm) for Smoldering4 (E1 and E2) and Smoldering5 (E1 and E2).

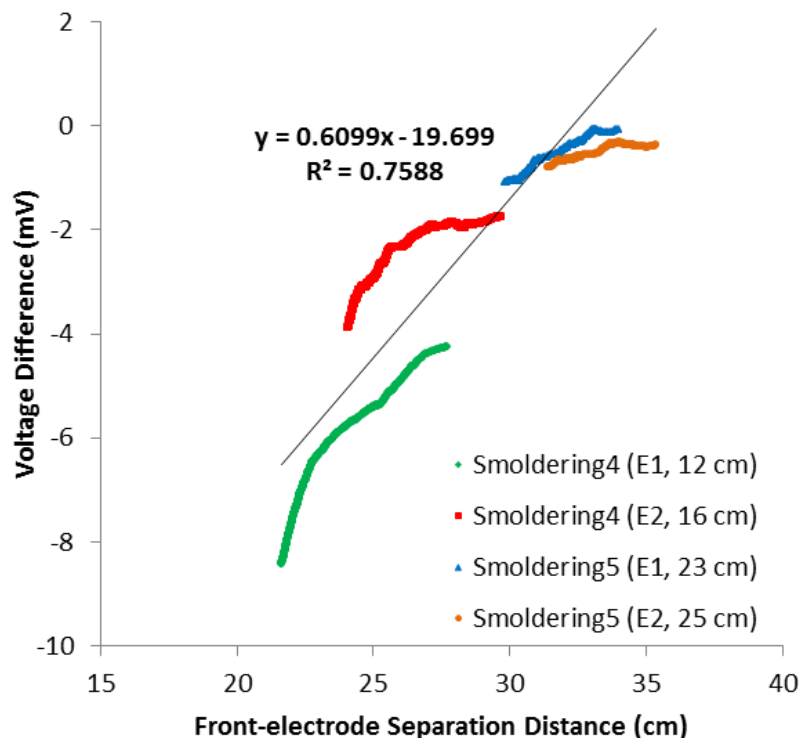


Figure 3.15. Voltage difference corrected for temperature effect over front-electrode separation distance (cm) for Smoldering4 (E1 and E2) and Smoldering5 (E1 and E2).

3.4 Summary and Conclusions

The thermoelectric coupling coefficient measurements showed that the source of the heat, chemical versus electrical resistance, had no effect on measured C_{TE} . The C_{TE} value was $-0.19 \text{ mV}/^\circ\text{C}$ for fine sand saturated with water and it changed to $-0.05 \text{ mV}/^\circ\text{C}$ when water saturation diminished to 30%. A repeatable, significant SP signal was observed during STAR applications. The maximum anomaly was observed in SP stations nearest to the smoldering region and decreased in magnitude and shifted in time for stations further from the smoldering region. The SP anomaly was highly correlated to the distance between the smoldering front and the electrode location. This suggests that inversion of SP data is highly promising and could provide the position of the front over time.

This study was challenging due to small scale of experiments. The maximum size of the experimental apparatus was dictated by the size of the fume hood in which the

experiments were conducted. This had several effects. First, it limited the distance between the reference electrode and reaction zone. Thus, the reference electrode may not have been outside the radius of influence of the reaction. This may have reduced the observable SP anomaly from the reaction. Second, the limited height of the apparatus resulted in a limited smoldering period (e.g., 20 minutes); this meant that only one set of surface measurements could be conducted. Third, the proximity of the reaction to the surface resulted in an increase in surface temperature; while this could be corrected in the data away from the reaction, it resulted in limited data collection immediately above the reaction. Fourth, it meant that water-saturated sand could not be employed since, at this scale, it would extinguish the reaction.

All of these factors reduced the ability of the reaction to be observed by SP, either by limiting the amount of data, reducing the difference from the reference, or reducing the C_{TE} . In this way, the system can be said to be conservative; in other words, observing a clear and repeatable SP signal in this case suggests that in more realistic and robust conditions, the signal may be even stronger. Indeed, the field scale studies discussed in the introduction (e.g. coal seam fires at tens of meters depth) provide SP anomalies on the order of 10 times that observed here on the benchtop. It is noted that STAR field studies would easily allow a reference electrode far from the treatment zone, would have a reaction at depth that is not expected to heat the surface, and is routinely conducted in water-saturated soil. Therefore, SP anomalies for STAR at the field scale may be expected to be even stronger than observed in this conservative, proof-of-concept study.

As C_{TE} is site specific, it should be measured in the field to acquire an accurate temperature coupling coefficient for further analysis and for the inversion process. It would be ideal to have a fixed network of electrodes over the site, particularly if inversion of the data is pursued. However, if ground conditions or infrastructure make this difficult, or if air flow or temperature rise is substantial at the surface in some cases, this work suggests that a viable option may be monitoring in the perimeter of the treatment zone and/or periodic surveys with portable electrodes. The results of this work need to be confirmed at the field scale during a STAR pilot test.

3.5 References

- Corwin, R. F., & Hoover, D. B. (1979). The self-potential method in geothermal exploration. *Geophysics*, 44(2), 226–245.
- Dorfman, N. H., Oskay, M. M., & Gaddis, M. P. (1977). Self-Potential Profiling: A New Technique for Determination of Heat Movement in a Thermal Oil Recovery Flood. In *Presented at the SPE Annual Fall Technical Conference and Exhibition: American Institute of Mining, Metallurgical, and Petroleum Engineers*. Denver.
- Fitterman, D. V., & Corwin, R. F. (1982). Inversion of self-potential from the Cerro Prieto geothermal field, Mexico. *Geophysics*, 47(6), 938–945.
- Gunstone, F. D. (2011). *Vegetable oils in food technology; composition, properties and uses, 2d ed* (p. 353). John Wiley & Sons Ltd.
- Guo, P. (2012). Dependency of Tortuosity and Permeability of Porous Media on Directional Distribution of Pore Voids. *Transport in Porous Media*, 95(2), 285–303.
- Karaoulis, M., Revil, a., & Mao, D. (2014). Localization of a coal seam fire using combined self-potential and resistivity data. *International Journal of Coal Geology*, 128-129, 109–118.
- Kavanaugh, M. C., Rao, P. S. C., Abriola, L., Newell, C., Cherry, J., Sale, T., ... Udell, K. (2003). Challenge : Is There a Case for Source Depletion? The DNAPL Remediation Challenge : Is There a Case for Source Depletion? *US Environmental Protection Agency, Washington DC*.
- Kueper, B. H., Redman, D., Starr, R. C., Reitsma, S., & M., M. (1993). A field experiment to study the behavior of tetrachloroethylene below the water table: spatial distribution of residual and pooled DNAPL. *Ground Water*, 31, 756–766.
- Leinov, E., Vinogradov, J., & Jackson, M. D. (2010). Salinity dependence of the thermoelectric coupling coefficient in brine-saturated sandstones. *Geophysical Research Letters*, 37(23), L23308–L23314.
- Marshall, D. J., & Madden, T. R. (1959). Induced Polarization, A study of its cause. *Geophysics*, XXIV(4), 790–816.
- Nourbehecht, B. (1959). *Irreversible thermodynamic effects in inhomogeneous media and their applications in certain geoelectric problems*. Massachusetts Institute of Technology.
- Ohlemiller, T. J. (1985). Modeling of smouldering propagation. *Progress in Energy and Combustion Science*, 11(4), 277–310.

- Pankow, J. F., & Cherry, J. A. (1996). *Dense chlorinated solvents and other DNAPLs ground water*. Portland (Oregon): Waterloo Press.
- Pironi, P. (2009). *Smouldering Combustion of Organic Liquids in Porous Media for Remediating NAPL-contaminated Soils*. The University of Edinburgh.
- Pironi, P., Switzer, C., Gerhard, J. I., Rein, G., & Torero, J. L. (2011). Self-sustaining smoldering combustion for NAPL remediation: laboratory evaluation of process sensitivity to key parameters. *Environmental Science & Technology*, 45(7), 2980–2986.
- Pironi, P., Switzer, C., Rein, G., Fuentes, A., Gerhard, J. I., & Torero, J. L. (2009). Small-scale forward smoldering experiments for remediation of coal tar in inert media. *Proceedings of the Combustion Institute*, 32(2), 1957–1964.
- Power, C., Gerhard, J. I., Karaoulis, M., Tsourlos, P., & Giannopoulos, A. (2014). Evaluating four-dimensional time-lapse electrical resistivity tomography for monitoring DNAPL source zone remediation. *Journal of Contaminant Hydrology*, 162-163, 27–46.
- Power, C., Gerhard, J. I., Tsourlos, P., & Giannopoulos, A. (2013). A new coupled model for simulating the mapping of dense nonaqueous phase liquids (DNAPLs) using electrical resistivity tomography (ERT). *Geophysics*, 78(4), EN1–EN15.
- Power, C., Gerhard, J. I., Tsourlos, P., Soupios, P., Simyrdanis, K., & Karaoulis, M. (2015). Improved time-lapse electrical resistivity tomography monitoring of dense non-aqueous phase liquids with surface-to-horizontal borehole arrays. *Journal of Applied Geophysics*, 112, 1–13.
- Revil, A. (1999). Ionic Diffusivity , Electrical Conductivity , Membrane and Thermoelectric Potentials in Colloids and Granular Porous Media : A Unified Model. *Journal of Colloid and Interface Science*, 522(212), 503–522.
- Revil, A., & Jardani, A. (2013). *The self potential method, theory and applications in environmental Geosciences* (p. 369). Cambridge University press.
- Revil, A., Karaoulis, M., Srivastava, S., & Byrdina, S. (2013). Case History Thermoelectric self-potential and resistivity data localize the burning front of underground coal fires. *Geophysics*, 78(5), 259–273.
- Revil, A., & Linde, N. (2006). Chemico-electromechanical coupling in microporous media. *Journal of Colloid and Interface Science*, 302(2), 682–94.
- Revil, A., Pezard, P. A., & Glover, P. W. J. (1999). Streaming potential in porous media: 1. Theory of the zeta potential. *Journal of Geophysical Research*, 104(B9), 20021–20031.

- Reynolds, J. M. (1997). *An introduction to Applied and Environmental Geophysics* (pp. 191–521). John Wiley & Sons Ltd.
- Rojas, E. E. G., Coimbra, J. S. R., & Telis-Romero, J. (2013). Thermophysical Properties of Cotton, Canola, Sunflower and Soybean Oils as a Function of Temperature. *International Journal of Food Properties*, 16(7), 1620–1629.
- Salman, M. (2012). *Smoldering of vegetable oil for remediation of trichloroethylene contaminated soil*. University of Western Ontario.
- Scholes, G. C. (2013). *Ignition method development and first field demonstration of In Situ smouldering remediation*. University of Western Ontario.
- Switzer, C., Pironi, P., Gerhard, J. I., Rein, G., & Torero, J. L. (2009). Self-Sustaining Smoldering Combustion: A Novel Remediation Process for Non-Aqueous-Phase Liquids in Porous Media. *Environmental Science & Technology*, 43(15), 5871–5877.
- Tocci, S., & Viehland, C. (1996). *Holt Chemistry: Visualizing Matter* (p. 848 pages). Holt, Rinehart and Winston.
- US EPA. (2004). *In Situ Thermal Treatment of Chlorinated Solvents: Fundamentals and Field Applications*, EPA 542/R-04/010. Office of Solid Waste and Emergency Response (p. 145).
- Wilson, V., Power, C., Giannopoulos, A., Gerhard, J., & Grant, G. (2009). DNAPL mapping by ground penetrating radar examined via numerical simulation. *Journal of Applied Geophysics*, 69(3-4), 140–149.
- Zlotnicki, J., & Nishida, Y. (2003). Review on morphological insights of self-potential anomalies on volcanoes. *Surveys in Geophysics*, 24, 291–338.

Chapter 4

4 Summary and Recommendations

4.1 Summary and Conclusions

In this thesis, Self-Potential (SP) technique was used for the first time as a non-invasive tool for monitoring STAR at bench-scale experiments. Two sets of experiments were performed. In the first series of experiments, thermoelectric coupling coefficient was investigated at the surface of a sandbox in the presence of a heat source at depth. The sensitivity of the coefficient was examined over several experimental conditions. In the second series of experiments, SP was measured at the surface of a sand box at different distances from smoldering region. The quantitative relationship between the measured SP during smoldering period and distance from smoldering front was investigated by linear regression.

Results suggest that:

- Thermoelectric coupling coefficient measurements showed that in the presence of a heat source at the depth, a negative SP is expected at the surface of a sandbox. The results showed that the coefficient is a function of water saturation and sand grain size. Measured C_{TE} for coarse saturated sand was $-0.47 \text{ mV}/^{\circ}\text{C}$ which changed to $-0.15 \text{ mV}/^{\circ}\text{C}$ in the saturated fine sand. The coefficient changed to $-0.05 \text{ mV}/^{\circ}\text{C}$ by decreasing water saturation to 30%.
- SP measurements at the surface showed a zone around the smoldering region with positive SP anomaly. Observed positive anomaly was due to the streaming potential effect and more importantly increase in surface temperature due to the heat propagation. Since non-polarizing electrodes have temperature-dependence internal voltage, both raw SP data and SP data corrected for temperature effect were studied. By eliminating temperature effect, a region with maximum negative SP anomaly was observed near smoldering region. The anomaly magnitude was decreased by moving away from smoldering region.

- Results of SP measurements with distance from the contaminated region as a function of time revealed that the maximum observed negative SP anomaly decreased with increasing distance from the contaminated region. Furthermore, there was a shift in time when the maximum anomaly observed by increasing the distance. The observed results could be due to lateral and upward propagation of heat source during the smoldering period.
- SP anomalies during smoldering period showed a strong linear relationship with front-electrode separation distance. R-squared for linear regression was 0.83 which showed that the dominant factor in SP anomaly magnitude is distance from the burning front in the smoldering period in each time.

Overall, a repeatable, significant SP signal was observed during STAR applications. The SP anomaly was highly correlated to the distance between the smoldering front and the electrode location which confirm high potential of SP technique in monitoring smoldering front in STAR.

4.2 Recommendations for Future Work

This work presents the successful monitoring of STAR technique in the smoldering period in laboratory scale.

The followings are recommended:

- Most of the challenges associated with experiments were due to small experimental scale which affects robustness of smoldering in the presence of water. Increasing the experimental scale could improve self-potential data by eliminating the streaming potential effect and keeping the temperature at the surface constant. Consequently, artifacts associated with the inner temperature dependence potential could be eliminated.
- In larger experimental scale, different configurations for the contaminated region rather than vertical cylinder could be used to evaluate associated SP response.

- Using time-lapsed inversion algorithm for localizing the SP source could provide valuable information about smoldering front characteristics in each time lapse. Therefore, SP data could act as a valuable tool in tracking the smoldering front in field trials for determining spatial distribution of the heat underground and localizing the position of the burning front.

Appendices

Appendix A. Background Self-potential Measurement Methodology

In all experiments background voltage was measured at least 30 minutes before heating procedure. In Figure A.1, experiment result for finding appropriate waiting time for reading voltage using a moving electrode is illustrated. The red dashed line represents the time when the electrode was removed and inserted at the surface in a same position. The experiment showed that reliable voltage which represents voltage associated with a certain position could be read after a few seconds. A slight shift in measured voltage was observed; however, average measured voltage change is in order of 0.05 mV. Unsmoothed background voltage measurements for three different experiments are shown in Figure A.2. The SP data fluctuated in a range of 1mV in all experiments. Even there was a slight change in voltage in two first experiments; they became stable after 10 minutes.

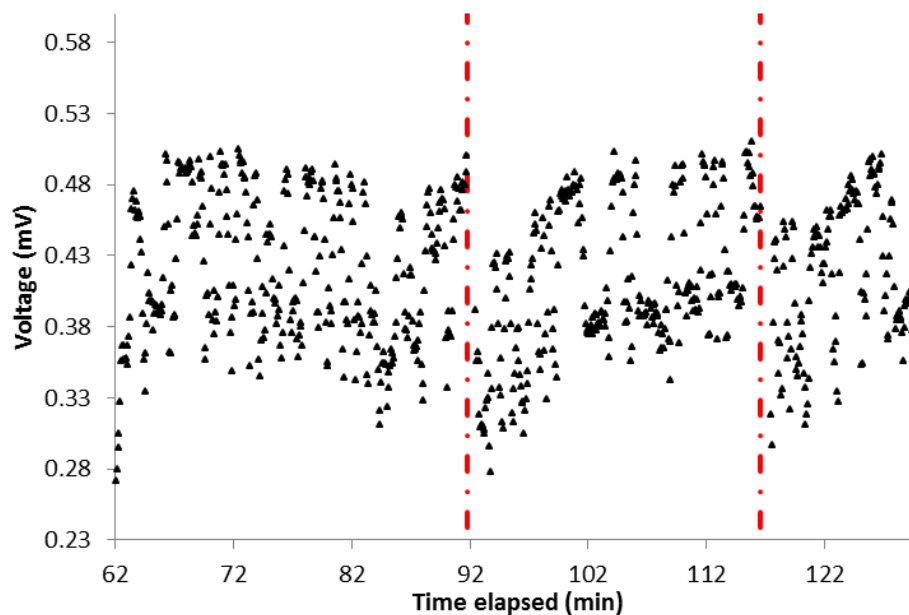


Figure A.1. Voltage measurement using moving electrode.

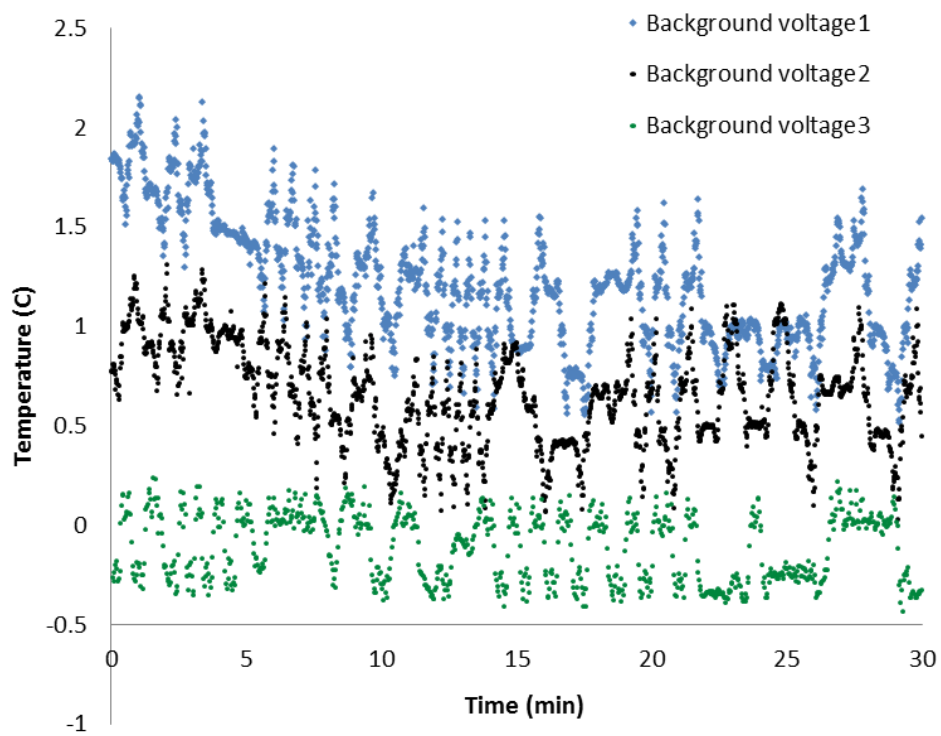


Figure A.2. Background voltage measurements for three experiments.

Appendix B. Experimental Setup: Parameter Selection

A series of experiments were conducted to find optimum parameters so that both the smoldering process and SP measurements are executable. More than 20 experiments were conducted to figure out the water saturation, temperature distribution in the experimental sandbox and experiment scale. Temperature distribution data were used for electrode position selection as the non-polarizing electrode could tolerate a maximum of 50 °C and voltage measurements are highly effected when the temperature of the measuring position is more than 35 °C.

Two factors should be controlled during the experiments: migration of water to the oil/sand mixture and forcing air to go through the contaminated sand for propagating heat and smoldering reaction. To satisfy both needs, two different kinds of sand were used: coarse sand for the oil/sand region and fine sand for filling the box.

For this set of experiments, the radius of the contaminated cylinder was 4 cm which is small enough to keep the surface temperature of the sand within a reasonable range for measuring voltage and do not affect the reference electrode temperature. On the other hand, it is large enough to sustain smoldering in low water content condition.

One of the limiting factors in smoldering propagation is heat loss from the reaction zone (Pironi, 2009). As Salman (2012) showed adding water to the oil/sand mixture would affect propagation of heat and smoldering front because of high heat capacity of water. Thermoelectric coupling coefficient, C_{TE} , measurements showed that water content is a prominent controlling parameter in measured voltage value. Decreasing in water content would lead to a decrease in voltage magnitude. Smoldering was not applicable in a saturated condition at a small scale, such as our experiment, because the water was penetrating into the coarse sand. In zero water content no SP anomaly was observed. An optimized value for fine sand water content was needed to satisfy the trade-off between porous media conductivity and smoldering.

Exploratory experiments were conducted to find the optimum value for sand water content. The ignition was not achieved in neither of 100% nor 60% water content

conditions. In successful case of smoldering, each thermocouple reached a temperature equal to or higher than prior measurements (Figure B.1). In Figure B.2 an unsuccessful case of smoldering is presented. The reaction weakened as front propagated upward and thermocouples failed to exceed the previous thermocouple maximum temperature. The decay that observed in thermocouple peak temperature is due to existence of water in the system.

Based on electrokinetic theory, streaming potential coupling coefficient decreases when the water saturation decreases. Therefore, low water content helps achieving sustainable smoldering and reduces the streaming potential factor in observed SP anomaly.

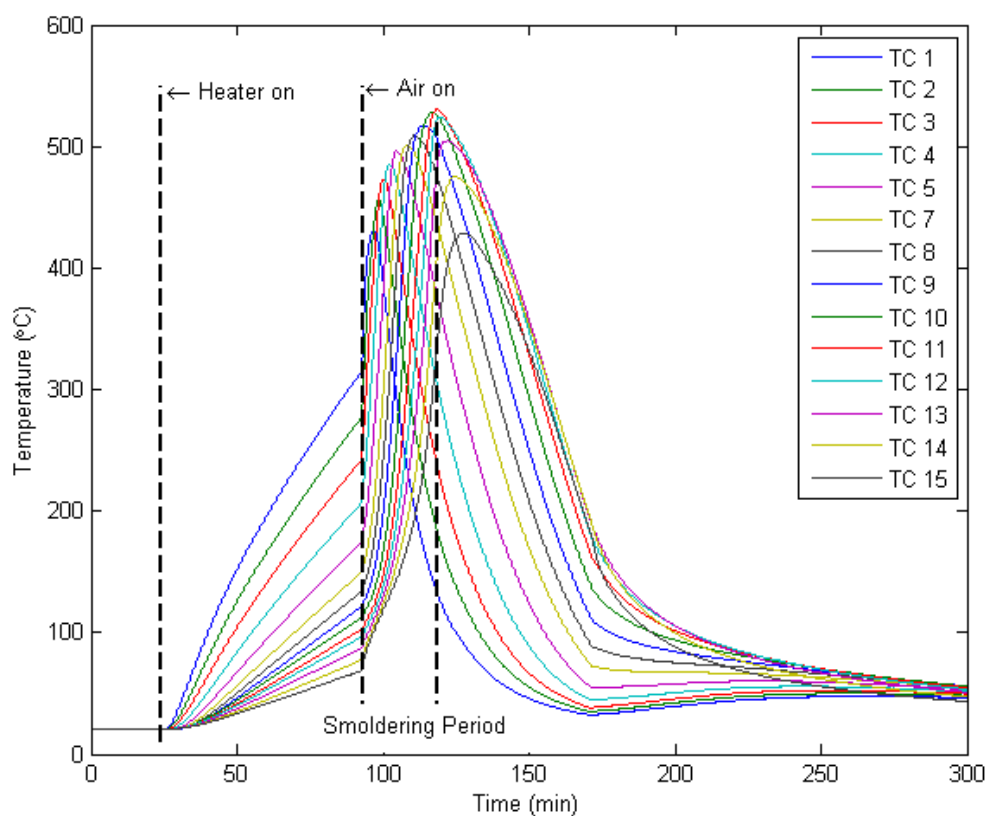


Figure B.1. Effect of water content in smoldering propagation, 15% water content.

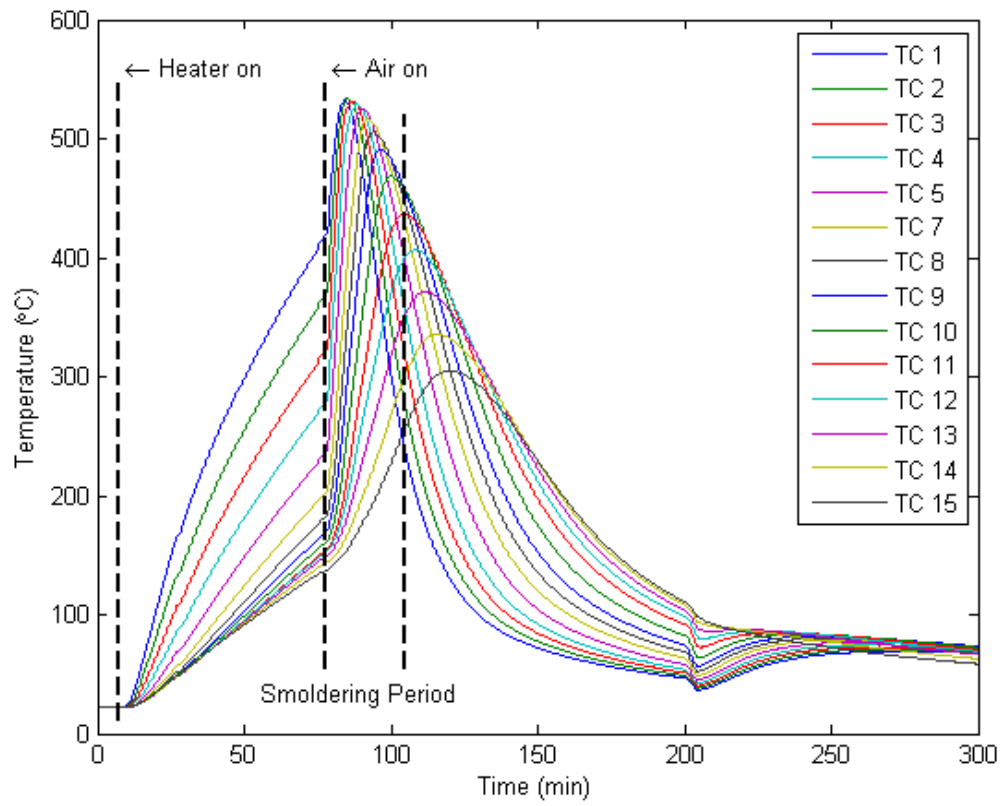


Figure B.2. Effect of water content in smoldering propagation, 30% water content.

Appendix C. Experimental Setup: Packing Procedure

Packing procedure for Smoldering1-Smoldering5 is presented in Figure C.1.

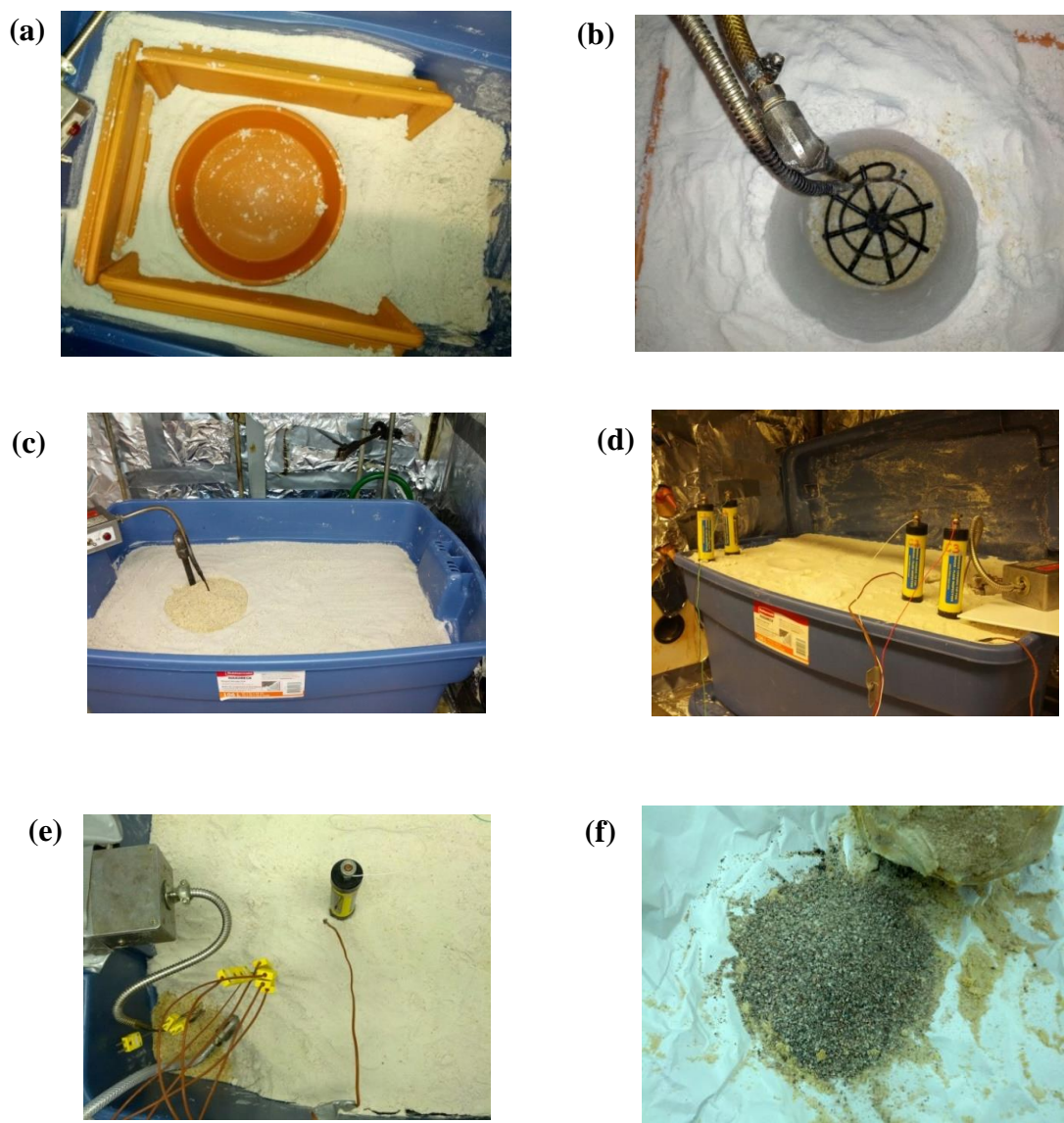


Figure C.1. (a) Clay trays for protecting the sand box from high smoldering temperature. (b) Position of the heater and air diffuser in the fine sand. (c) Coarse sand/canola oil cylinder emplaced in fine sand. (d) Non-polarizing electrode placed at the surface of the sand. (e) The pathway of coarse sand along the wall of the box (f) Cleaned coarse sand after smoldering.

Appendix D. Smoothing of Self-potential Data

An example of raw measured SP data and smoothed SP data over time is illustrated in Figure D.1.

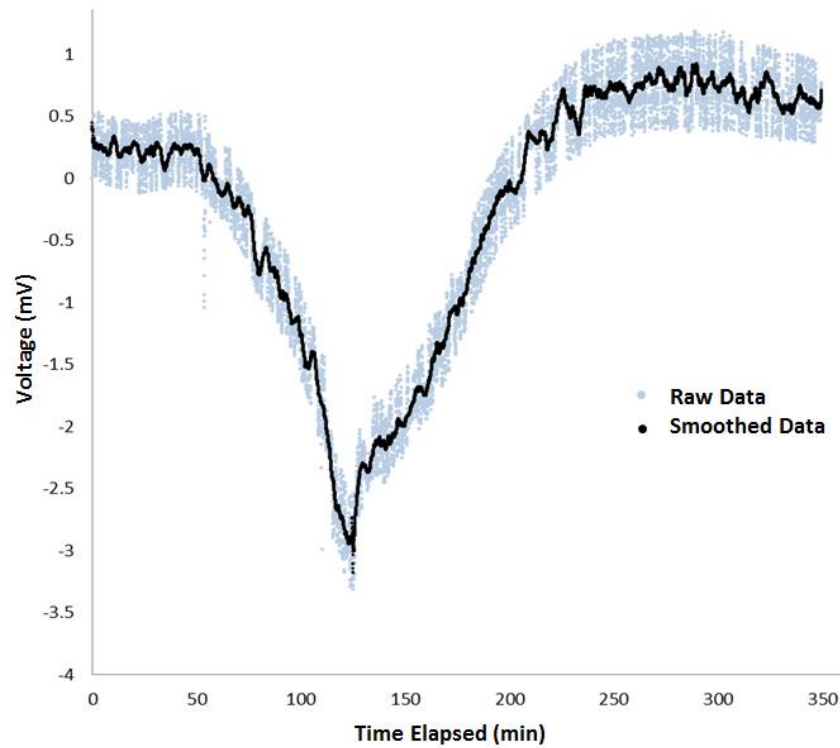


Figure D.1. Raw and smoothed SP data over time.

Appendix E. Streaming Potential Associated with Blowing Air in STAR

For examining the effect of blowing air on SP data, air flow of 15 cm/s was initiated for 9 minutes and its single effect on SP was analyzed. The experimental setup was identical to the smoldering experiments except the fact that the coarse sand cylinder was continued to the surface. The experiment was repeated two times. Three measuring electrodes were placed at the surface in 4 cm (E1), 7 cm (E2) and 9 cm (E3) distance from the centerline of the coarse sand cylinder. Electrode position is shown in Figure E.1a. SP measurements over time for E1, E2 and E3 are shown in Figure E.1b. As illustrated in Figure E.1b, the SP data could be affected significantly by streaming potential in distance less than 7 cm from the center of the smoldering region in experimental scale. In E1, SP data showed a positive SP anomaly of 5 mV after initiating air. The streaming potential was negligible in distance more than 9 cm as E3 showed 0.5 mV anomaly after initiating airflow. Experimental results determined that to avoid the streaming potential effect, the electrodes should be placed at least 7-9 cm from the diffuser (in plan view).

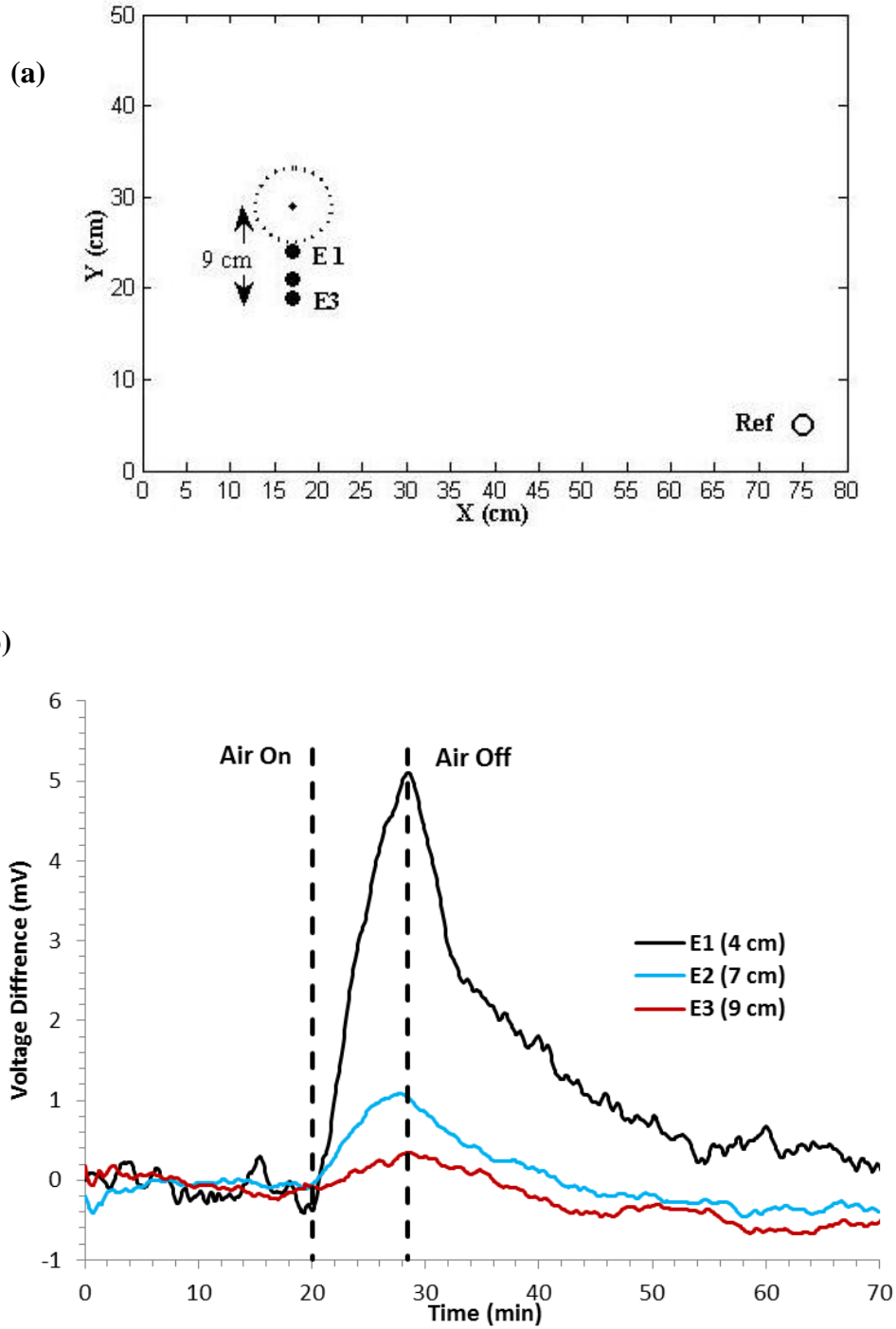


Figure E.1. (a) Electrode position in plan view. (b) Voltage differences against time associated with blowing air; experimental setup is exactly identical to STAR test.

Appendix F. Temperature Profiles

Characteristic temperature time histories and self-potential anomaly against time for the Smoldering1 to Smoldering5 are presented in Figure F.1 to Figure F.4, respectively. In Figure F.1 to Figure F.4 the SP data is not corrected for the temperature effect. In Figure F.5 surface temperature and corrected SP data for temperature effect over time for smoldering3 is illustrated.

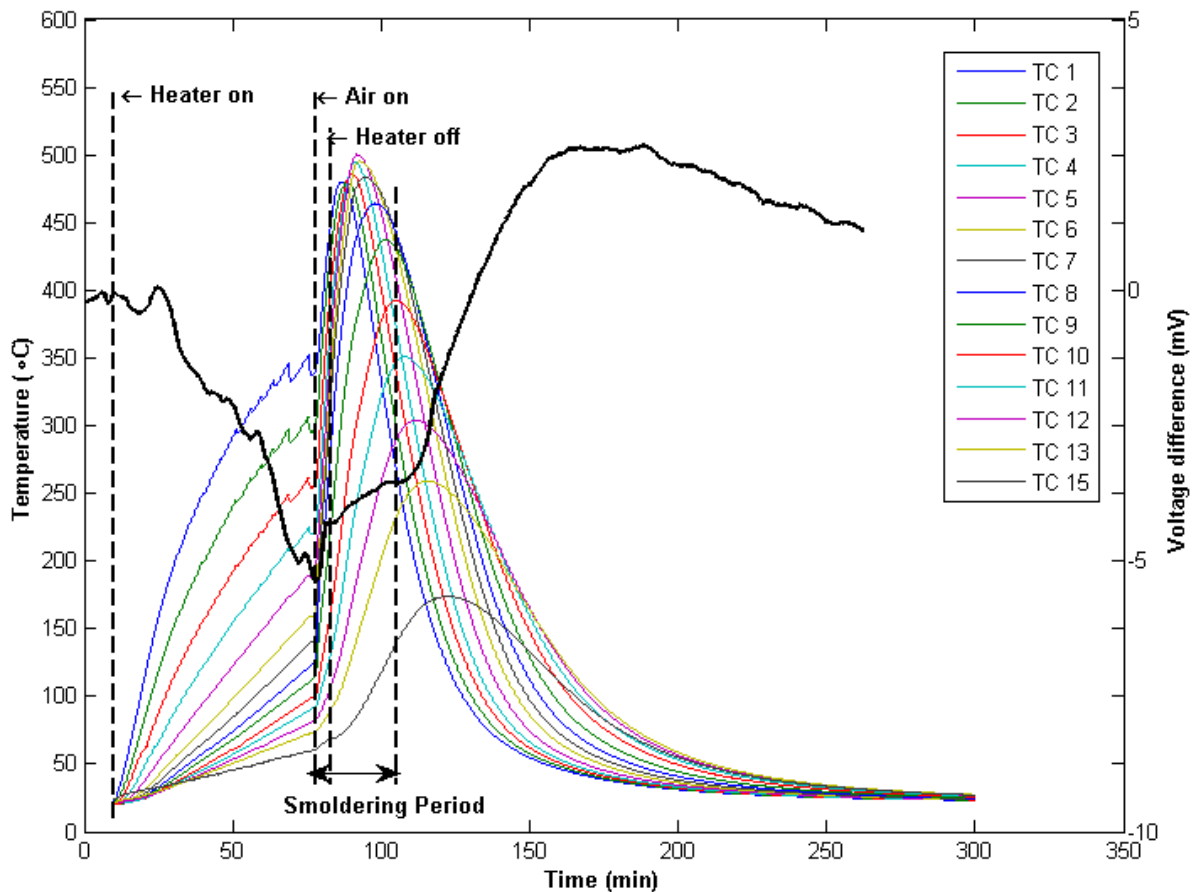


Figure F.1. SP data (not corrected for the temperature effect) over time vs temperature histories for TC1-TC15 in Smoldering2; Electrode position is corresponded to 9 cm distance from center of oil/sand cylinder in plan view.

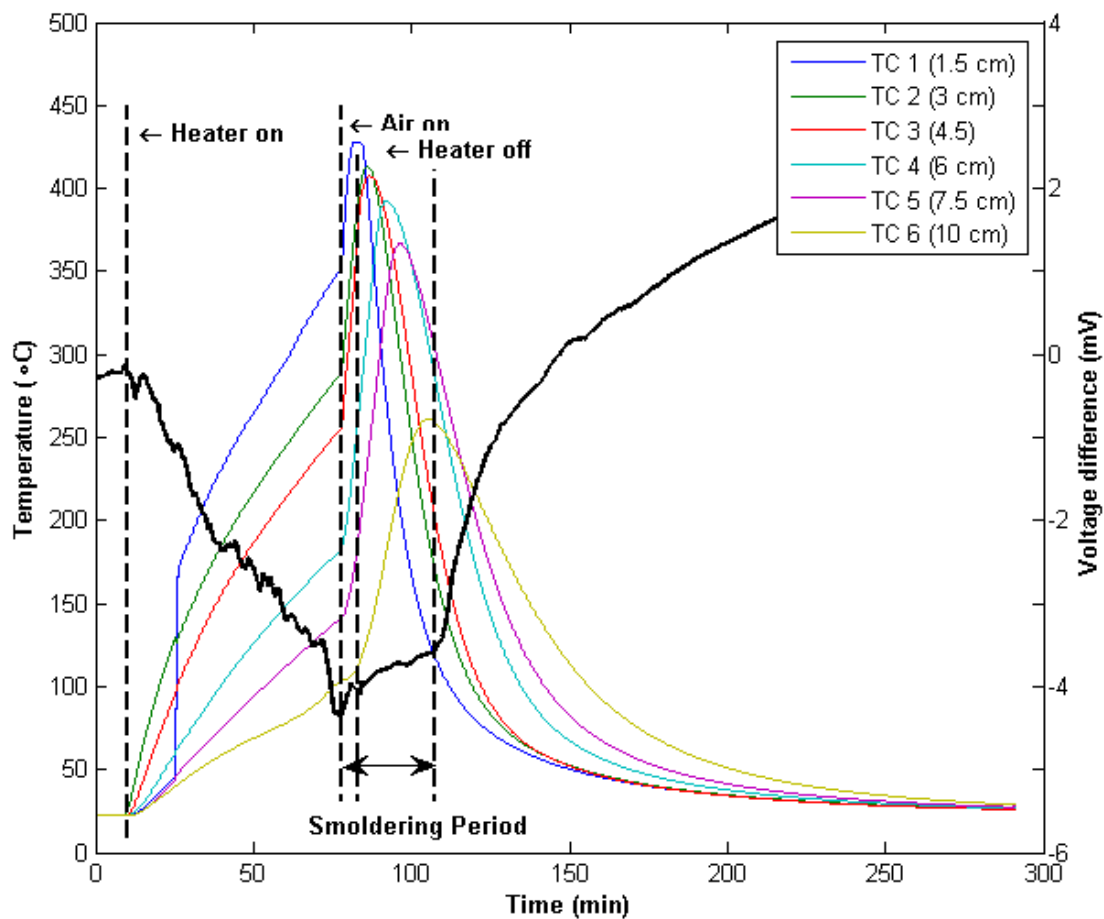


Figure F.2. SP data (not corrected for the temperature effect) over time vs temperature histories for TC1-TC15 in Smoldering3; Electrode position is corresponded to 9 cm distance from center of oil/sand cylinder in plan view.

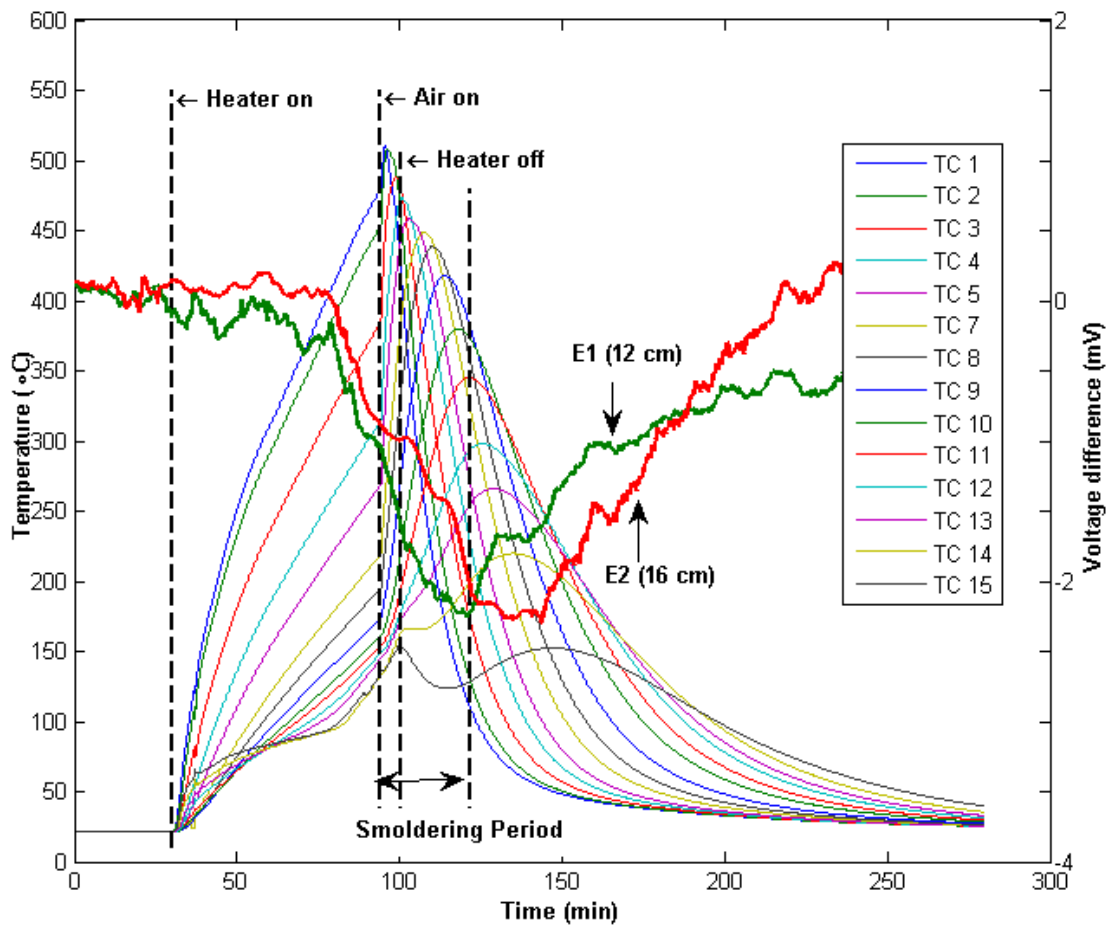


Figure F.3. SP data (not corrected for the temperature effect) over time for E1 and E2 vs temperature histories for TC1-TC15 in Smoldering4; E1 is corresponded to 12 cm and E2 to 16 cm distance from center of oil/sand cylinder in plan view.

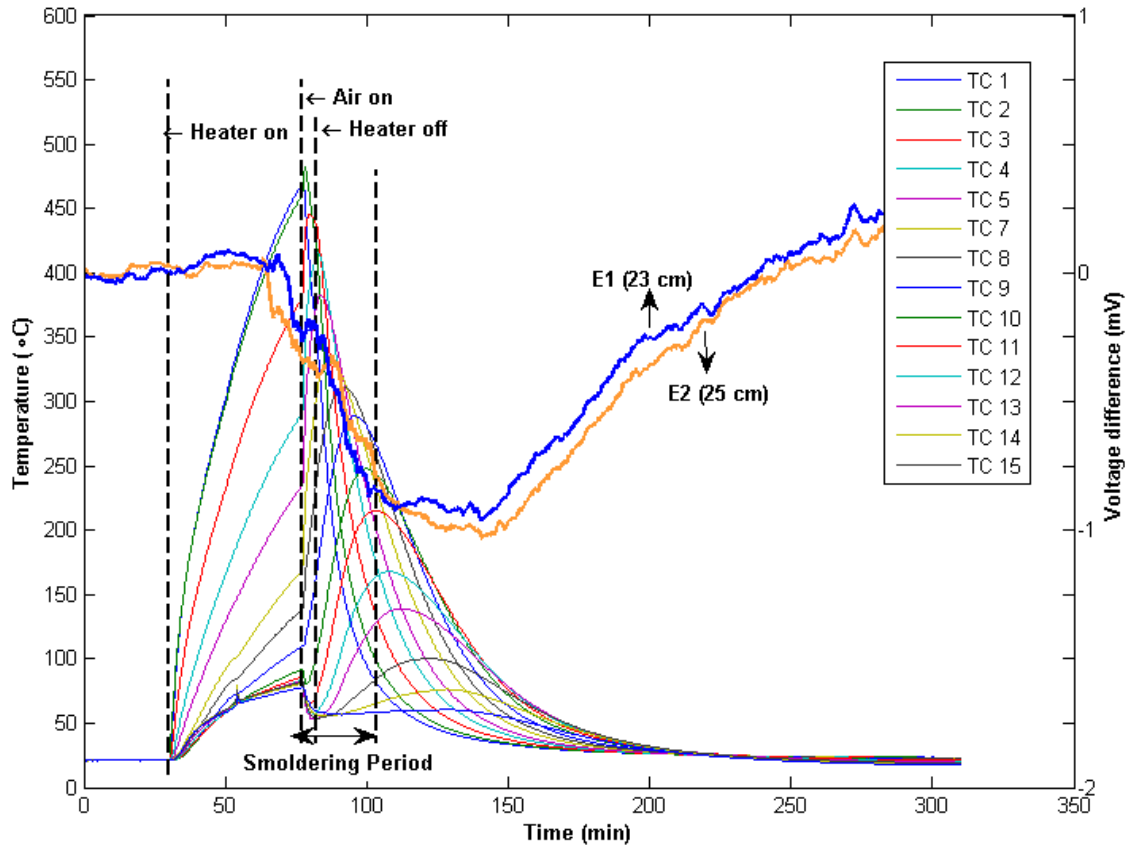


Figure F.4. SP data (not corrected for the temperature effect) over time for E1 and E2 vs temperature histories for TC1-TC15 in Smoldering5; E1 is corresponded to 23 cm and E2 to 25 cm distance from center of oil/sand cylinder in plan view.

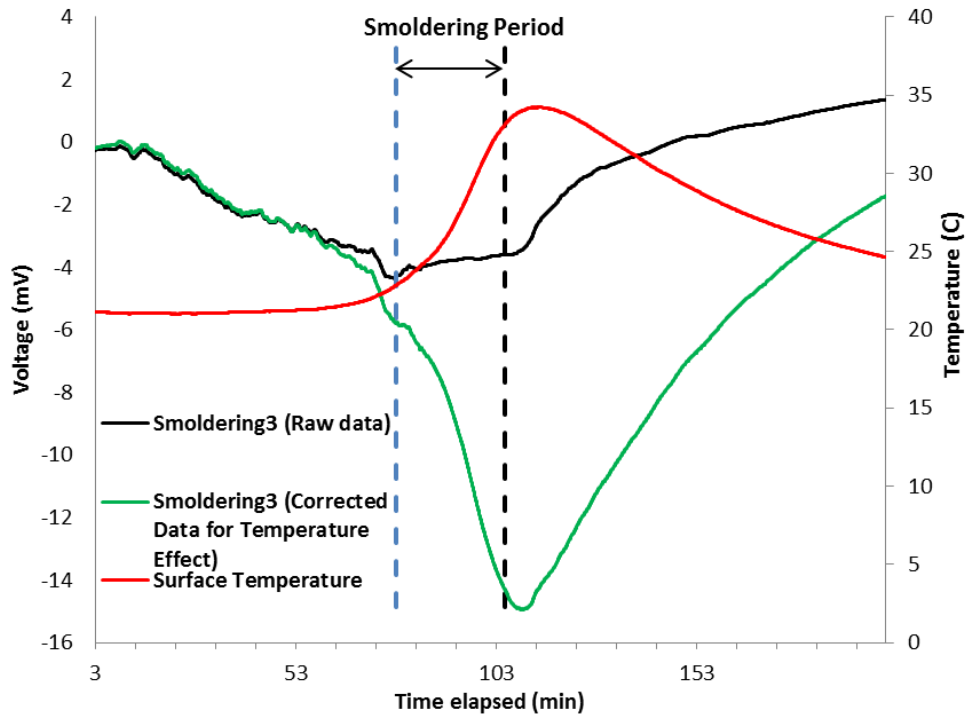


Figure F.5. Surface temperature and corrected SP data for temperature effect over time for smoldering3.

Appendix G. Self–Potential Anomaly Associated with Heating

In this experiment fine sand was saturated by deionized water and the heater was used as heat source (same experimental setup as Heating1). SP was measured at the surface at three stations; E1, E2 and E3. E1 was located above the heater at the surface and E2 and E3 distances from heat source in plan view were 5 and 10 cm. SP measurements over time for three stations and temperature of the heat source over time are illustrated in Figure G.1. In the SP anomalies associated with heating, recovery phase started just after terminating the heater; however, in SP associated with smoldering SP anomaly showed different patterns after terminating heater in smoldering period. The observed pattern in SP data associated with smoldering experiments was function of straight line distance between smoldering position and SP measuring stations. Therefore, two different patterns were observed in data associated with heating and smoldering reaction.

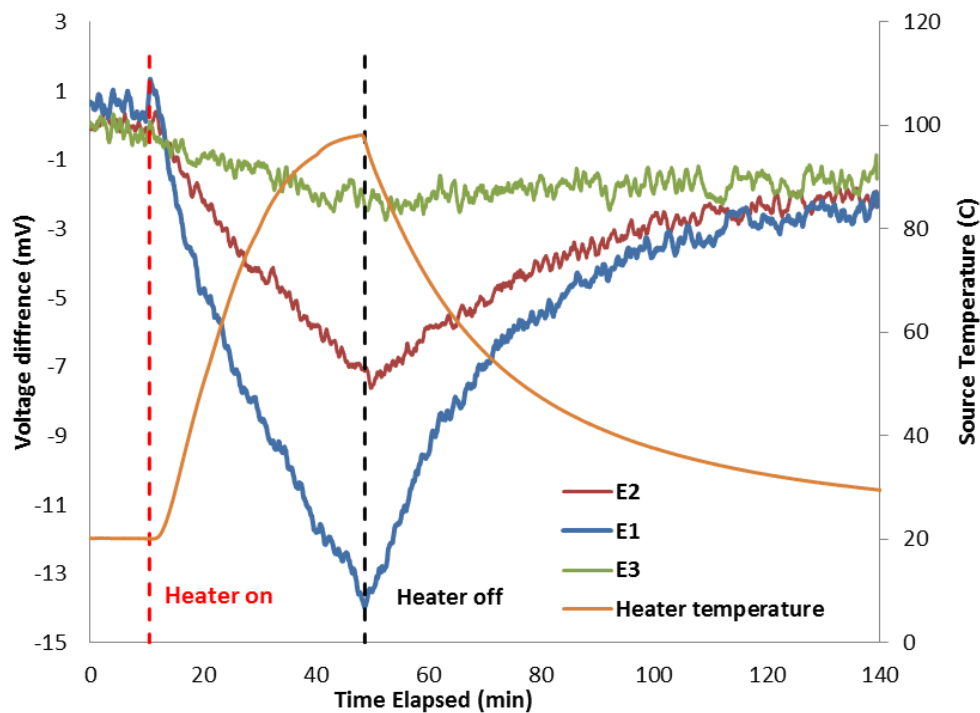


Figure G.1. SP data over time associated with heating for E1, E2 and E3 vs. temperature of the heat source over time.

Appendix H. Self-potential Anomaly Associated with Smoldering Using Convective Heater

The experiment had the identical experimental setup as smoldering2 with two differences; oil/sand cylinder had 6 cm height and in this experiment electrical heater and air diffuser was replaced by a conductive heater. Temperature histories over time and measured voltage differences over time at the surface are illustrated in Figure H.1. In Figure H.2 corrected SP data for temperature effect over time is illustrated.

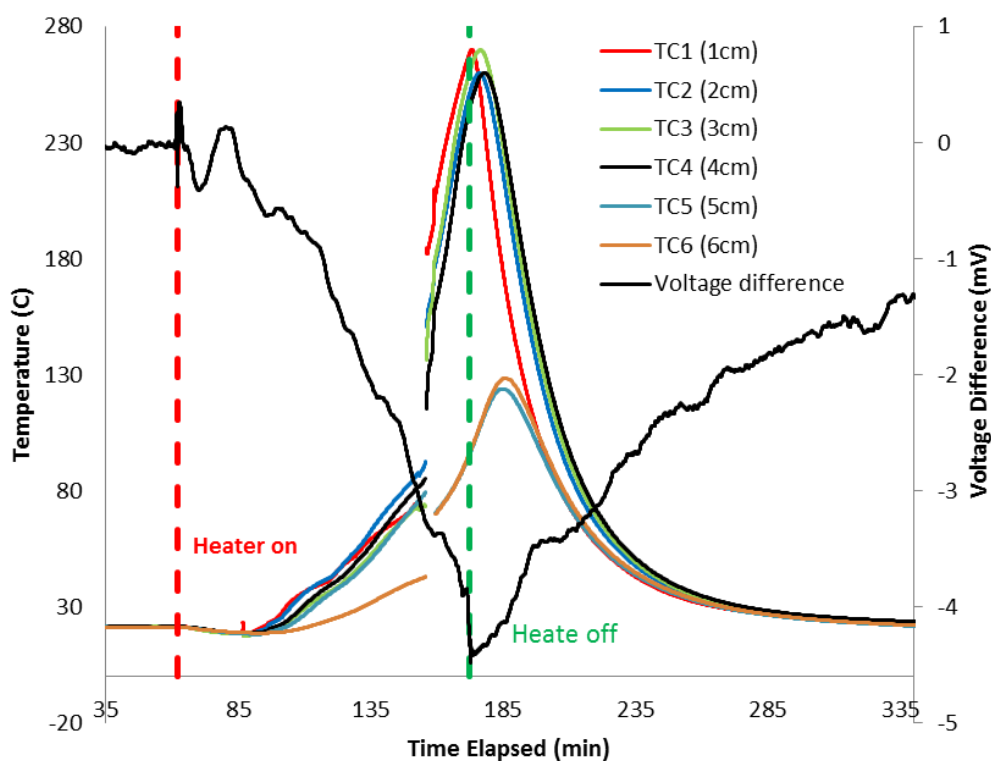


Figure H.1. SP data over time vs temperature histories over time for TC1-TC6.

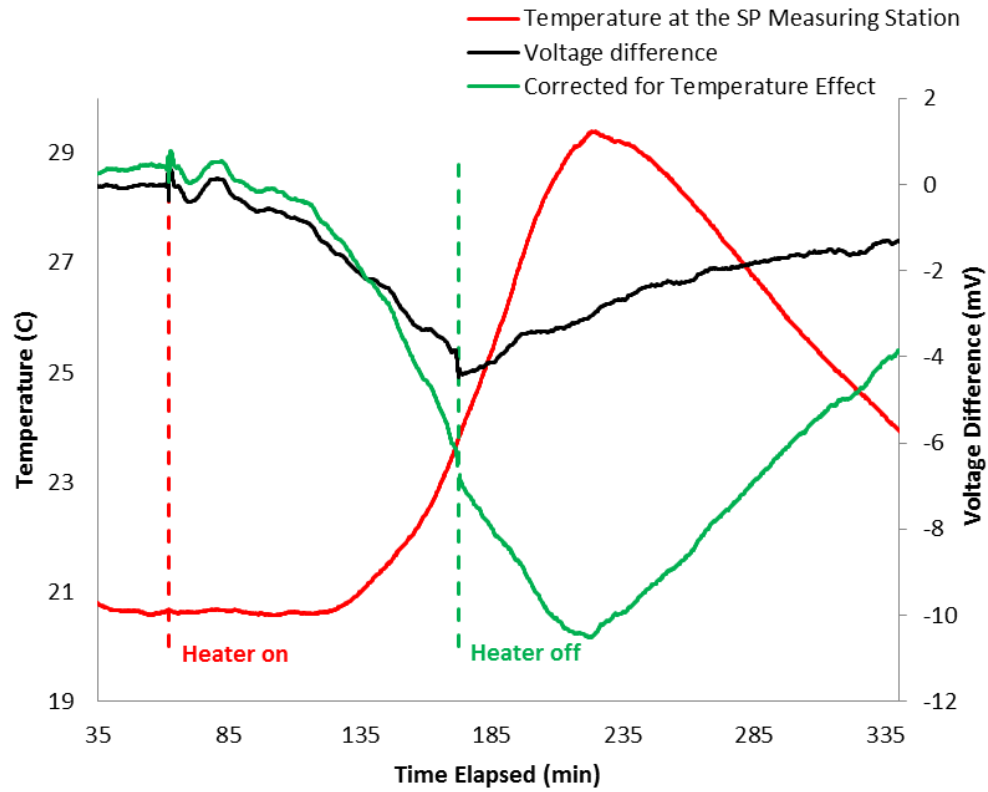


Figure H.2. SP over time vs. SP corrected for temperature effect over time.

Curriculum Vitae

Name: Mehrnoosh Ebrahimzadeh

Post-secondary Education and Degrees: University of Tehran
Tehran, Iran
2003-2007 B.Sc. (Mining Engineering)

University of Tehran
Tehran, Iran
2008-2011 M.Sc. (Mining Engineering)

The University of Western Ontario
London, Ontario, Canada
2012-2015 M.Sc. (Civil and Environmental Engineering)

Related Work Experience: Teaching and Research Assistant
The University of Western Ontario
2012-2015

Publications and Conferences:

Alimoradi, A., Angorani, S., Ebrahimzadeh, M., Shariat Panahi, M., "Magnetic inverse modeling of a dike using the artificial neural network approach", *Near Surface Geophysics*, 2011, Vol.,9, 339-347.

Ebrahimzadeh, M., Memarian, H., Tokhmechi, B., " Porosity Estimation By Wavenet In Oil Reservoir", 29th Conference of Earth science , Geological Survey Of Iran,15-16 Feb. 2011, Tehran, Iran.

Khorram, F., Ebrahimzadeh, M., Memarian, H., " Comparison between Kriging and neural network in geoelectric parameters estimation", 29th Conference of Earth science , Geological Survey Of Iran,15-16 Feb. 2011, Tehran, Iran.